UNIVERSITAT ROVIRA I VIRGILI

ANALYSIS OF WIRELESS BODY-CENTRIC MEDICAL SENSORS FOR REMOTE HEALTHCARE

Stefano Milici

ADVERTIMENT. L'accés als continguts d'aquesta tesi doctoral i la seva utilització ha de respectar els drets de la persona autora. Pot ser utilitzada per a consulta o estudi personal, així com en activitats o materials d'investigació i docència en els termes establerts a l'art. 32 del Text Refós de la Llei de Propietat Intel·lectual (RDL 1/1996). Per altres utilitzacions es requereix l'autorització prèvia i expressa de la persona autora. En qualsevol cas, en la utilització dels seus continguts caldrà indicar de forma clara el nom i cognoms de la persona autora i el títol de la tesi doctoral. No s'autoritza la seva reproducció o altres formes d'explotació efectuades amb finalitats de lucre ni la seva comunicació pública des d'un lloc aliè al servei TDX. Tampoc s'autoritza la presentació del seu contingut en una finestra o marc aliè a TDX (framing). Aquesta reserva de drets afecta tant als continguts de la tesi com als seus resums i índexs.

ADVERTENCIA. El acceso a los contenidos de esta tesis doctoral y su utilización debe respetar los derechos de la persona autora. Puede ser utilizada para consulta o estudio personal, así como en actividades o materiales de investigación y docencia en los términos establecidos en el art. 32 del Texto Refundido de la Ley de Propiedad Intelectual (RDL 1/1996). Para otros usos se requiere la autorización previa y expresa de la persona autora. En cualquier caso, en la utilización de sus contenidos se deberá indicar de forma clara el nombre y apellidos de la persona autora y el título de la tesis doctoral. No se autoriza su reproducción u otras formas de explotación efectuadas con fines lucrativos ni su comunicación pública desde un sitio ajeno al servicio TDR. Tampoco se autoriza la presentación de su contenido en una ventana o marco ajeno a TDR (framing). Esta reserva de derechos afecta tanto al contenido de la tesis como a sus resúmenes e índices.

WARNING. Access to the contents of this doctoral thesis and its use must respect the rights of the author. It can be used for reference or private study, as well as research and learning activities or materials in the terms established by the 32nd article of the Spanish Consolidated Copyright Act (RDL 1/1996). Express and previous authorization of the author is required for any other uses. In any case, when using its content, full name of the author and title of the thesis must be clearly indicated. Reproduction or other forms of for profit use or public communication from outside TDX service is not allowed. Presentation of its content in a window or frame external to TDX (framing) is not authorized either. These rights affect both the content of the thesis and its abstracts and indexes.

UNIVERSITAT
ROVIRA i VIRGILI

Analysis of Wireless Body-Centric Medical Applications for Remote Healthcare

---

STEFANO MILICI

DOCTORAL THESIS
2018

Stefano Milici

Analysis of Wireless Body-Centric Medical Applications for Remote Healthcare

DOCTORAL THESIS

Supervised by: Prof. Antonio Ramón Lázaro Guillén, Prof. David Girbau Sala, and Prof. Gaetano Marrocco

Department of Electrical, Electronic Engineering, and Automation

UNIVERSITAT
ROVIRA i VIRGILI

Tarragona **May, 2018**

Statement of supervision

UNIVERSITAT
ROVIRA i VIRGILI

Departement of Electronic, Electrinc, and Automatic Engineering (DEEEA)
Av. Paisos Catalans 26, campus Sescelades
43007,Tarragona, Spain
Phone: +34 977 558524
Fax: +34 977 55 9605

WE STATE that the present study, entitled Analysis of Wireless Body-Centric Medical Applications for Remote Healthcare, presented by Stefano Milici for the award of the degree of Doctor, has been carried out under our supervision at the Department of Electrical, Electronic Engineering, and Automation of this university.

Tarragona (Spain), May 2018

Doctoral Thesis Supervisors

Prof. Antonio Ramón Lázaro Guillén Antonio Lázaro

Prof. David Girbau Sala

Prof. Gaetano Marrocco

Gaetano Marrocco

Acknowledgements

I would like to express my sincere gratitude to prof. Antonio Lázaro, prof. David Girbau and prof. Gaetano Marrocco, my research supervisors, for their patient guidance, enthusiastic encouragement and useful critiques of this research work. I would also like to thank CUBIT consortium that offers to me the possibility to spend the time of my research in the company, and the staff of Ardeje that also has given me technical support.

I would also like to thank Dr Javier Lorenzo, for her advice and assistance in keeping my progress on schedule. My thanks are also extended to prof. Ramon Villarino in offering me his help for technical resources, to Dr Sara Amendola, who helped me to follow my research persistently.

I would also like to extend my thanks to prof. Enrico Maria Staderini for his profound learning.

Finally, I wish to thank my parents for their support and encouragement throughout my study.

Abstract

The exponential growth of a worldwide electronic trend over the last few years, the so-called Internet of Things (IoT) has inspired an influential, enthusiastic interest in healthcare and medical applications. Traditional medicine can get extraordinary advantages from the spread of individual information to rapidly make people part of a global, colossal network. These data will be instantly accessible from anywhere, making the diagnosis and medical treatments highly specialistic and successful. Consequently, by optimising time in recollecting information and in data analysis, cost of the healthcare would drastically drop down. A first example of sharing personal data has been introduced by the wearable technology, which has the aim to inform users about own vital parameters, that can improve quality of life. This market has become promising, as the number of connected wearable devices worldwide is expected to jump from an estimate of 325 million in 2016 to over 830 million in 2020. In any case, the complete integration of electronic circuits in the human body is considered one of the essential characteristics of a wearable medical device. Over the last few years, there has been enormous progress in materials, designs, and manufacturing processes for flexible and stretchable systems to fill the gap between a rigid and planar electronics, and the curvilinear and flexible biological tissues, fostering the well-known new branch of Electronics, called epidermal electronics. Despite the extraordinary effort to make the electronic circuit utterly transparent to the body, these newly redesigned electronics are still suffering the necessity of a stable telecommunication system able to connect the body with the rest of the

world. Uncomfortable cables are still commonly used to connect sensors to the body and, despite several wireless methods have been developed and tested, the communication method remains the highest challenge. New electronic circuits have been designed to reduce power consumption to limit the space for battery and investigate other harvesting methods. Embedding ultralow power sources, energy storage units and wireless modules in a minimally invasive form is hence an essential prerequisite for the acceptance of bio-integrated devices in daily life. This thesis aims to investigate a variety of different technologies to demonstrate the feasibility of using a low cost and low power device to detect vital parameters and power a robust and low-power communication method. Many different technologies can be employed to tackle the weaknesses of these innovations. With that background, a radiofrequency identification technology (RFID) would be considered a perfect compromise between power consumption and a minimal amount of space occupied. The communication through electromagnetic backscattering requires just a small low-power IC transponder, which is wirelessly powered-up and remotely accessed by a processing unit. Indeed, the intrinsically passive nature of the RFID technology allows to actively reduce energy for operations, avoiding using a large battery to feed transmitting and computational processes, encouraging the miniaturization of sensors. Among many RFID standards, the UHF RFID (860-960 MHz) is most promising in the field of sensing for human body parameters due to the possibility to reach reading ranges up to three meters. Although this technology could pave the way to a board range of pervasive application, it hits with many limitations that practically bounds many expectations. The presence of the body, indeed, absorbing a significant amount of electromagnetic power, reduces the performances of tags, which in turn decrease the reading distance. Furthermore, by adding sensing capability to a UHF RFID transponder, consequently, the required energy to power sensors raises, which need to be gathered by the electromagnetic fields. Therefore, for a reliable sensing capability, the RFID technology cannot be considered the most reliable option. Moreover, in medical use, very often, the sensors need to deliver data when an anomaly in the sensing is detected, nevertheless, since the RFID technology is fully passive, it cannot autonomously transmit, so it would not be able to send information if a remote controller didn't ask for it. Many other solutions can overcome that shortcoming. These standalone devices are regularly used when the monitored parameters evolve slowly. In these cases, a fully autonomous technology is an efficient alternative. Bluetooth low energy (BLE) or Smart Bluetooth, which is considered a new paradigm of the IoT, has reached an enormous success thanks to its very low power consumption and the capability to handle such different fields of application. BLE is currently the most used technology for wearable devices, boasting the highest growth in the "portable consumer electronics". BLE standard appears mature enough to address lacks of the RFID adequately; furthermore, it exhibits a significant advantage in term of data spreading because it doesn't need a dedicated processing unit to decode data, since, nowadays each commercial mobile phone integrates a Bluetooth communication module. Although the BLE technology is considered ultra-low-power compared to the other digital solutions, in the case it would be necessary to monitor parameters with high sample rate for an extended time, BLE doesn't have the necessaries requirements. The amount of energy to power a device would require batteries that are usually out of size for a comfortable, wearable application. A simple method to avoid an overmuch power consumption is to reduce the number of electronic circuits. In both of case above described, communication is entirely digital. Digital communication requires a considerable amount of energy (as it needs to establish a protocol) that is necessary to maintain the connection. On the other hand, analog communication would allow reducing power used for communication, optimizing energy resource to feed the sensors. The frequency selective surfaces (FSS) based sensors are a reliable option for addressing this limitaion. An FSS is any repetitive surface designed to reflect, transmit or absorb the electromagnetic fields. The FSS is well known in the field of microwave systems, antenna radomes and metamaterial, for its filtering properties. Many different reasons make the FSS useful in the communication for wearable devices. Analog devices could perform a long lifetime, cutting out the power consumption, being autonomous in term of energy. In fact, many harvesting methods could be investigated to turn a medical device into a standalone, self-powered, integrated part of the body.

Agreements

This research work has been conducted in the context of scientific collaboration between the Department of Infomation Engineering (Università di Roma “Tor Vergata”, Italy) and the Department of Electrical, Electronic, Engineering, and Automation (University of Tarragona “Rovira I Virgili”, Spain) under the *agreement of cotutela* signed by both Unversities.

Nomenclature

BLE	Bluetooth Low Energy
CZT	Chirp Z-transform
EDA	Electrodermal Activity
FFT	Fast Fourier Trasform
FSS	Frequency Selective Surfaces
GSR	galvanic skin response
IoT	Internet of things
NTC	Negative Thermistor Coefficient
OSA	Obstructive sleep apnea
RCS	Radar Cross Section
SoC	System on chip
UHF	Ultra high frequency

WHD	Wearable Health Device

Contents

1

Introduction

1.1 Wearable Internet of Things (wIoT)

The combination of a fast increase in elderly population, rising cost of healthcare, and the prevalence of chronic diseases paves the way for a new shape of healthcare systems, migrating from an hospital-centered system to a futuristic user-centered environment, improving citizen's life quality and wellbeing. A wearable health device is any portable sensor able to measure body-centric parameters to refine diagnosis and medical therapies [1, 2, 3]. Many of the common diseases develop from a lousy day-life behavior, which gradually degenerates in a certain degree of a significant pathology. Monitoring daily parameters and connecting them to a remote infrastructure some bad patient's habit can be avoided, allowing a substantial increase in treatment outcomes' efficacy and effectiveness. It has been demonstrated that a huge amount of chronic disease can be monitored by measuring skin characteristics. The epidermis is indeed a complex, time-evolving interface that provides a valuable insight into people's health wellbeing. The skin can reflect significant physiological changes earlier than central parameters, which are protected by homeostatic feedback. It is also the primary perceptual interface towards the surrounding environment, and it is continuously "sampled" by the central nervous system concerning tactile cues. With the new generation of connectivity technology, likewise, the IoT, body parameters measured from the skin can be easily shared on an extraordinary expanded network. Indeed, the concept of Internet-of-things (IoT) provides a robust framework for interconnecting edge computing devices, wearable sensors and smartphones and cloud computing platforms for seamless interactions. Therefore, these improvements are going to generate a high demand for creating a wearable IoT technologies (wIoT) to deploy large-scale wearable sensors networked with remote medical infrastructure.

Nevertheless, a substantial changing in electronics, materials and telecommunications methodology has to be done to achieve such a futuristic goal. Three essential concepts must be taken into account to design new wearable IoT: Mimetism, robustness, and connectivity. First, planar and rigid electronics does not fit requirements for medical on body device, which need to be soft, flexible and biocompatible to shape the body with comfort for the users. In addition, usability studies have changed the design of new wearable devices making them always invisible in day life (e.g., wrist accelerometer in the form of jewelry) allowing to create integrated and hidden sensors [4, 5, 6]. Second, robustness. As the information managed by wIoT is directly related to the users' life, any mistake caused for a weak measurement or an incorrect calculation must be remarkably reduced to accept wIoT technology as an alternative to the traditional medicine approach [4, 7, 8]. Third, connectivity, which is the basement for the wearable systems. A reliable network allows to quickly deliver data to health care centers, elaborate them and realize new aggregative analysis to boost the quality of diagnosis and therapies. Finally, three factors in particular have contributed to these advances: 1) increased data processing power, 2) faster wireless communications with higher bandwidth, and 3) improved design of microelectronics and sensor devices [9].

This chapter introduces technological improvements, which has been allowed a big step forward for healthcare body-centric systems [10, 3].

1.2 Sensors for body-centric applications

A variety of precise and reliable body sensors are currently employed to measure different key indicators of the health state. Electrocardiogram (ECG), heart rate, blood pressure, body and skin temperature, posture and physical activity are examples of commercial sensors for on body applications. Unfortunately, most of the developed medical devices are heavy, complicated, and out of size to be attached onto the body for a long time. In the last few years, a significant amount of wearable devices have been extensively studied to increase personal healthcare therapies and wellbeing. Activity detectors [9], security trackers [11, 12], ambient assistant living (AAL) device, home rehabilitation trackers [13], seizure alert as well as sleep monitoring devices [14, 15, 16, 17, 18], have already been developed and tested (Fig. 1.1) to overcome typical problems of the medical instrumentation. Thanks to the emerging low power microcontrollers and new communication technics, which are able of guarantee reliability, long lifetime, and accurate results, those devices can evolve from simple activity tracker to personal medical devices [19]. Continuous health and wellbeing data can be similarly monitored and seamlessly tracked, providing an excellent boost for remote healthcare. In fact, it can enable fast and safe diagnosis, reducing health care costs and morbidity of lifestyle-induced poor health. Nevertheless, this class of wearable devices need to satisfy specific medical criteria while operating under several ergonomic constraints and significant hardware resource limitations. Therefore, the challenge on the wearable systems for health monitoring remains in the areas of long-term stability, power management, and biocompatibility of embodiment.

Regardless to healthcare applications, three different generations of development can be considered. The first generation is the current commercial state of medical sensors, which use data to improve personal healthcare by tracking the body activity. The second generation identifies a step forward, where continuous monitoring of patient data can be used to detect and analyze chronic disease. The second generation emerged as the result of advances in sensing technology that facilitate continuous monitoring with multiple sensors. This new generation of sensing introduces the concept of *agents*, which use *processing units* for taking the necessary actions towards an objective. These actions can be based on an autonomous interaction with the environment or cooperation with other agents allowing a refined diagnosis. Finally, the third generation is a future research area that aims to combine continuous health monitoring with other sources of medical knowledge (e.g., genomics, proteomics, metabonomics) to improve a personalized clinical care. The innovations in sensor area are improving quickly, becoming ready to satisfy most of the wearable medical devices requirements. In fact, modern generations of medical devices usually integrates MEMS-designed inertial sensors, including accelerometers, gyroscopes and compasses, which provide an inexpensive and low power manner to collect body-centric data. However, through the different generation of developed sensors, in the last decades only some of these sensors are able to match all of specific requirements for a realizable, wireless and wearable application in daily life.

1.3 Electronics for body-centric integrated systems

Wearable systems used for activity tracking, storing data and deliver feedback therapy, are considered for a first personalized medicine. However, multiple technical challenges such as the fabrication of high-performance, energy-efficient sensors and memory modules that are in mechanical contact with soft tissues, with controlled delivery of therapeutic agents, limit the wide-scale adoption. In these applications, the classical interpretation of the electronics is outshine, making hard silicon wafer obsolete, replaced with such a new paradigm of electronics well-known as the *flexible* and the *epidermal electronics*. Research on materials, mechanics, and designs for multifunctional, wearable-on-the-skin systems that address these challenges for a proper integration, stretchable electronics on a tissue-like polymeric substrate are going very fast across the last few years. New frontiers of flexible and biocompatible electronic make these applications genuinely possible in the closest future.

1.3.1 More than wearable: Flexible electronics, smart textile, and epidermal electronics

The *Flexible electronics* can be considered a first expedient to achieve optimal mimetism behaviour for a wearable electronic device. Nowadays, the flexible electronics offers a wide variety of novel applications such as flexible circuits [20], conformable RFID tags [21], flexible displays [22], electronic paper [23], implantable medical devices [24], and robotic systems with skin-like sensing capabilities [25, 20], allowing improvements in the wIoT eco-system. Integrated circuits on flexible substrates produce attributes in electronic devices that are impossible to achieve with standard technologies that use semiconductor wafers. Nearly all associated device technologies continue, however, to rely on conceptually old designs. Until now, all electronic circuits as electrodes or sensors were attached to the skin via adhesive tapes, uncomfortable mechanical clamps or straps, all connected to rigid circuit boards, power supplies, and communication components. The *epidermal electronic*s introduces a different

(a) New-born sensing **(b)** Stretchable properties

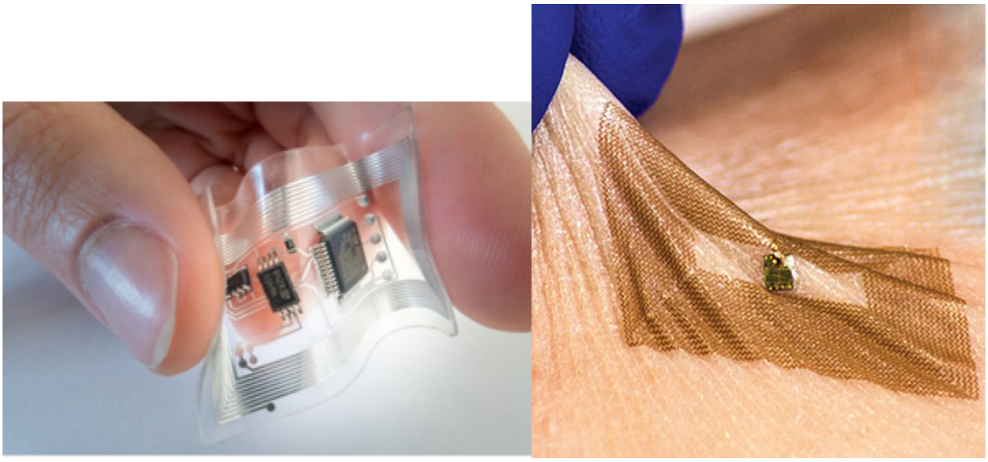

(c) Soldering capability **(d)** Skin-like sensors

Figure 1.1: Epidermal Electronics [23, 25]

approach, in which the sensors, micro-controllers, and the communication components are configured together into ultra-thin lightweight, stretchable "skin-like" substrate, invisible for the user, evolving much like a temporary transfer tattoos (Fig. 1.1)[26]. New materials [20, 27] based on organic structure, low power communication methods [28, 29, 30, 31, 32], and battery fabrication [33, 34] are, at the moment, extensively explored for flexible circuitry, even though that film-based or nano-structures of inorganic still show modest performance that might restrict the application possibilities.

1.4 Challenges and outlines of this thesis

Among the requirements and the technologies examined, appear essential to shaping the design on the precise target, avoiding a generic solution that considers a restricted option. For this reason, after having chosen a narrow range of medical application, to solve the problem by exploring different options can be more straightforward. After an introduction about the technologies that have been considered for addressing the requirements for wearable health devices (WHD), the first part of this thesis has the aim to analyze, modify and test a variety of sensors for specific WHD. This thesis discusses advantages and limitations of three different communication technologies for on body measurement and methods to choose and reshape sensors for optimum body-centric assessments. The RFID technology is considered one of the most influential solutions to overcome the limited power consumption due to the presence of many sensors connected. Further, the Bluetooth low energy has been studied to solve security problems and reading distance that overall represent the bottleneck of the RFID for the body-worn sensors. However, this technology is more complicated and, consequently, the battery life is sharply decreased. Analog devices can drastically reduce the energy needs due to the sensors and the communications, considering few elements and a simple transmitting method. An entirely passive communication method, based on FSS is studied, enabling a reasonable reading distance with precise and reliable sensing capabilities, which has been discussed in this thesis.

The objective of this thesis is to investigate multiple wireless technologies for wearable devices to identify suitable solutions for particular applications in the medical field. The first objective is to demonstrate the usability of the inexpensive battery-less technologies as a useful indicator of such a physio-pathological parameters by investigating the properties of the RFID tags. Furthermore, a more complex aspect regards the use of small passive components as wireless sensors for sleep diseases. Lastly, an outcome of the thesis is to develop an entirely autonomous system using the BLE technology to obtain advanced properties keeping low power and a low price.

Concretely, these are the primary goals of the thesis:

1. Desing, prototype and test an epidermal RFID tag, which can measure body temperature in order to demonstrate the employment of low-power, low cost and disposable technology for specific medical applications. Its

performances are explored considering the variability of the human body. Also, biocompatible materials are examined to identify their conformability with the human body. Finally, sensing capability are investigated to define a proper field of applications.

2. Analyse, prototyping and test a wearable and flexible breathing sensor based on the FSS transmitting method to demonstrate practical uses of this approach for a simple, low-power and reliable medical sensor. Its performance is investigated considering various frequency ranges, different substrate materials and different places on the body to validate its compatibility with the human body.

3. Investigate the use of the BLE as continuous monitoring of breathing to detect sleep disorder diseases by producing and test some prototypes. The primary goal is to study the trade-off between power consumption, data transmitted, conformability and reliability of the sensors.

The next Chapter provides an overview of the leading technologies used in telecommunications for medicine and to define the boundaries of the research, the outcome and the guidelines. Later, an introduction to the RF technology and its advantages in some application are discussed in Chapter 3. In the same chapter, a manipulation to develop an entirely passive, disposable and wireless radio-thermometer is explained. Chapter 4 clarify the semi-passive technique based on the frequency selective surfaces, which can increase reading distance and resolution to get more reliable measures. Here, a breathing sensor, based on temperature changes in the respiration airflow for assisting chronic sleep disease has been discussed as a proof of concept. After that, an introduction to the Bluetooth low energy (BLE) technology and a more complex form of data analysis is shown in Chapter 5, an application that makes use of the galvanic skin response sensor to detect sleep apneas and sleep arousals has been demostrated as a proof of concept. Chapter 5 also discuss a brief correlation between sleep monitoring sensors by using the BLE technology. Finally, Chapter 6 draws the conclusions.

2

Wireless technologies for wearable health devices (WHD)

2.1 Internet of Things (IoT): background for wearable communications

Healthcare applications in IoT systems are going to be part of that integrated network due to the ability of these systems to provide many useful features that facilitate remote monitoring of patients [35]. Thanks to the exponential production of wide variety of cheap, reliable sensors (wearable, implanted and environmental), the IoT has the potential to put in place personal *Smart-Health* systems as a part of the improvement in medical treatment and diagnosis. A pervasive interconnection with things requires a multitude of electronic objects and infrastructures able to manipulate data for secure remote control, especially for vital body parameters, where security, the integrity of data and privacy are the keys roles. The paradigm of *Cloud computing* [36, 2, 37] can provide facilities to access shared resources and infrastructure for aggregating data and analysis, offering services on-demand, over the worldwide network. Also, the advance of *machine-to-machine* communication (M2M) [35], which enables the direct interaction of pervasive healthcare sensors by extension with Cloud computing systems facilitates the data fusion and analysis. The perfect merge between cloud computing and M2M paradigm makes the IoT paradigm able to overcome issues due to critical information they carry on, by using specific protocols for inter-device and Internet communication, providing real-time access to device information and allowing the remote management of the devices with security privacy, and data integrity.

2.1.1 RFID approach for Health application

Radio frequency identification (RFID) can provide a reliable and inexpensive manner of measuring people wellbeing. Thanks to their natural thin shapes, RFID transponders (tags) can be easily worn as gadget, key-cards, and wristbands, or they can be integrated as part of clothing. A *passive RFID system* is a slim system, composed of a digital device called *tag*, embedding an antenna and an IC-chip with the unique identification code (ID), and a radio scanner device, called reader. Up to now, RFID technology is mostly applied to logistics of goods; nevertheless, the very recent research is exploring other paths, considering sensing applications in the field of healthcare and industrial sensing [5, 38, 39, 40, 41, 42]. RF identification (RFID) systems may represent the strategic alternative for not invasive and straightforward component due to the energy autonomy and their low cost, which is compatible with a widespread distribution and disposable applications. RFID systems could, therefore, permit to implement an efficient contribution to the wearable, implantable, and epidermal IoT concerning the pervasive quantification of the person's interaction with the environment. Passive and semi-passive (i.e., battery-less, battery assisted) devices in the band (860–960 MHz) are the best candidate for measuring body parameter in an indoor environment.

2.1.2 Bluetooth low energy (BLE)

One of the most exciting innovations on the IoT has been the advent of the new generation of Bluetooth. Announced at the beginning of 2011, the *Bluetooth Low Energy* (BLE) is an ad-hoc IoT implementation. Especially for healthcare application, it reveals excellent potentials due to various factors. Healthcare systems require dedicated technologies for handling the challenges of the growing population with chronic diseases [14, 43, 44, 45]. These medical conditions require continuous monitoring rather than episodic assessment and ubiquitous healthcare guarantee to make diagnosis and therapies more effective. BLE is an emerging new low power wireless technology that is developed for short-range monitoring and control applications, claims to offer many new features and is expected to get broad adoption by many mobile manufacturers around the world. In addition, it wants to be included in daily life mobile devices to be used in combination with dedicated chip able to measure the body-centric parameters and deliver data to the closer connected gateway. A typical BLE stack consists of two main parts, a *controller* and a *host*. The controller usually includes the *physical* and the *link layer* implemented in the form of a (System-On-Chip) with an integrated radio-transponder. Meanwhile, the host runs on an application processor and includes upper layer functionality: *Logical Link Control* and *Adaptation Protocol* (L2CAP), the Attribute control (ATT), the *Generic Attribute Profile* (GATT), the *Security Manager Protocol* and *Generic Access Profile* (GAP). The communication between the host and the controller is standardized as the *Host Controller Interface* (HCI). Such a complicated architecture furnishes a substantial interaction between the sensor, the host and the owner, the controller. BLE stack allows reducing the interaction between the sensor and the rest of the world thanks to its dedicated implementation, improving the battery life and reducing the size of the sensor on the body. It represents the best compromise between a powerful sensing capability and a light communication service.

2.1.3 Backscattering: Analog vs digital communications

Technologies above mentioned try to overcome the limitations of the power consumption in different manners; RFID avoids the use of the battery, taking advantage by the transmitting energy, the BLE technology tries to reduce power consumption reducing the operating time. In many cases, these solutions fail, and the results depend on the precise application. For these reasons, other technologies need to be considered. By reducing the number of the electronic component at the minimum value, a reduced amount of energy can be achieved. The aim of the technology based on *frequency selective surface* (FSS) is to define a minimum power consumption to use other harvesting methods for comformable, wearable, and long-life devices. The above mentioned techniques use sophisticated digital communication methods, which rise the power consumption. An alternative FSS based approach uses an analog communication, which reduces the number of components, computation time and then, the power consumption. Table 2.1 shows the main differences between the three categories of IoT telecommunication method commonly used.

	RFID	**Bluetooth low energy (BLE)**	**Analog backscattering (FSS)**
Average power consumption	<20 μA	7 μA - 15 mA	5-10μA
Max reading distance	1-5 m (with sensing capabilities)	10-15 m	3-5 m
Application	Disposable / Not Battery	long-range / asynchronous communication	long-range / not battery (harvesting)

Table 2.1: Comparing different wireless technologies

2.1.3.1 Frequency selective surfaces (FSS)

Daily applications such as respiration or heart rate detection, want to control vital parameters remotely by using a high sample rate and for an extended time. That drastically reduces the battery lifetime, and even the best RFID solution cannot afford such a long reading distance. Therefore, to decrease the power consumption the electronic components on the board can be minimized. FSS-based communication responds to the growing interest in the combination of wireless communication systems with wearable products. Advantages of textile antennas include, relatively lightweight, flexible substrates and simple integration into clothing, so that microwave devices, including antennas formed of unique fabrics, can be considered as a substitute for conventional printed circuit devices. In many cases, these flexible antennas are employed as a modulated surface that connects a modulator, which use a sensor to change parameters of the antenna [46, 33]. This approach allows saving much energy usually spent in transmitting process, increasing of more than a 100% the battery life.

2.2 Sensors requirements for wireless devices

Medical data are the most critical categories of personal information. That kind of data needs to be separately treated to be manipulated on a network and have to guarantee strong reliability. For this reason, the researchers are exposed to many different challenges to increase efficiency, safety, and security of wearable medical devices (WMD): First, there are different manufacturing and technological challenges, likewise;

- Improvements in sensor miniaturization and efficiency: Many sensors that are used for current wearable systems tend to be out of size and may require specific and often uncomfortable on-body placement to provide reliable measurements.

- Battery technologies and energy harvesting: Power consumption appears to be perhaps the most significant technical issue and the performance bottleneck in current implementations. Wearable sensor systems should be able to operate maintenance-free for an extended time. Further research in power harvesting techniques (e.g. through body heat or motion), low-power transceivers and improvements in battery technologies promise to solve this problem.

- Clinical validation: Developed systems must be exhaustively tested and validated by professional physicians.

- Standardization: The requirement for interoperability between different communication infrastructures and between various types of devices, sensors and actuators, addresses the need for homogeneity in communication interfaces and cooperation between experts, manufacturers, network providers, and health organizations.

The evaluation of the sensors for the WMD also involves different parties as manufacturers, doctors, and users. For this reason, the specific features have different significance levels for each interested side. In many cases, reliable medical instrumentations such as ECG or EEG are heavy, bulky and uncomfortable; often they do not meet the user's wishes and, consequently, their application is sharply limited. On the other hand, much of the activity tracker on the marketplace can be wear as gadgets, but they can not be employed as medical devices due to their reduced reliability. Therefore, the sensor features need to address an optimum compromise among requirements. Furthermore, a persuasive technology takes into account other significant improvements. A critical issue involves the manner to present the information to the users or professionals. Technologies that can successfully present long-term healthcare data could delay or even prevent the onset of medical problems. Nevertheless, to drive a significant behaviour change, an efficient strategy of four components have to be taken into account:

1) present a simple, tailored message that is easy to understand,

Property	**Description**
Wearability	The entire system have to overcame conformability issues, small size and light weight.
Aesthetic Issue	The system shouldn't not severely affect the user appearance
Lifetime	Low power consumption and long lifetime, small or not battery.
Real-time application	The system is usefull in real life scenario
Real-application	It can provide alert, or data in real-time, for a decision maker
Computational and storage requirements	Complex algorithm means high power consumption
Easy to use	Easy placement on the body
Reliability	Reliable and accurate result
Cost	Lower cost impact a spread distribution
Interference robustness	The system is not affected by the enviroment (little affected)
Fault tolerance	The user needs to feel free to do any movement
Scalability	Easy to upgrade
Decision support	The implementation can include some diagnosis/decision mechanism or a pattern recognition

Table 2.2: Requirements for wearable medical devices [48]

2) at an appropriate time,

3) at a proper place,

4) using a nonirritating strategy (even after possibly hundreds of presentations). Context detection algorithms provide information that can trigger messages at an appropriate time, and mobile computers allow message presentation at the right place. This class of device is called just-in-time persuasive interfaces [47], and it can be considered in the development of a WMD as a basement for a long-term monitoring process.

In Table 2.2, a list of requirement is described in order to address a general characteristic for body-centric measurements.

2.2.1 Sensors selection for medical applications

This research focuses on a limited range of sensors, which can meet most of the requirements. Table 2.3 resume a list of existing developed and tested sensor, which are considered for this research. Considering their properties, some of them are explored and discussed in this thesis.

2.2.1.1 Thermometers

Body core and skin temperature are good indicators of the health state. Many kinds of dull, small, and reliable temperature sensors are commercially available. Thermistors, and other integrated sensors can be used in many different manners to obtain an efficient wireless measurement. The modern commercial sensors hold compactness, high resolution, accuracy, versatility, and low price. Moreover, researchers are going to develop an entirely invisible elastomeric, transparent and stretchable sensor to ultimately meet the requirements of the compatibility with the human skin (Fig. 2.1). Furthermore, thermistor-based sensors are excellent examples of reliable and inexpensive sensors. Thermistors have been explored in a variety of industrial application, likewise; environmental sensors for monitoring temperate changing and for security systems. Depending on their resolution, thermal sensors can be used as an indicator of febrile states as an alert or, in case of more accurate measurement, for tracking the changing in the skin behavior to identify various pathologies. The wholly passive nature of the sensor minimizes the amount of energy employed, extending the battery lifetime. For these reasons, modern temperature sensors represent a low cost, low power consumption, and low-invasive solution.

2.2.1.2 Conductivity of the skin

The sweating is controlled by the sympathetic nervous system, while skin conductance is an indication of psychological or physiological arousal. Therefore, a minimally invasive measurement can give more data about significant parameters of the body. Improvements in materials and fabrication methods, as well as miniaturization of micro-controllers and conditioning circuits, has created new wearables, non-invasive applications. The conductance of the skin can be an important indicator of the sweating factor and the state of body hydration, enabling smart applications.

Type of bio-signal	**Type of sensor**	**Measured data**	**Low-Power sensor**	**Active/ Passive**	**Signal Elaboration**
Electrocardiogram (ECG)	Chemical electrodes (on Chest) Electrodes	Electrical activity of the cardiac cells	No	Passive	High
Respiration rate	Various (piezoelectric, resistive, thermistors, magnetometers)	Number of breathing act per minute BPM	Yes	Passive	Low
Oxygen saturation	Pulse oximeter	Oxygenation as % of oxygen carried in the finger cells	No	Active	Low
Body and skin temperature	Temperature probe or skin patch	Mesures the termoregulation of the body	Yes	Passive	Low
Perspiration or skin conductivity	Galvanic skin response (skin electrodes)	Electrodermal acrtiviy (activation of the sympatetic nerve)	Yes	Passive	Low
Heart rate (HR)	Skin electrodes	Frequency of cardiac cycle	Yes	A/P	Low
Blood glucose	Skin-based glucose meter	Amount of glucose in the vessels blood	No	Active	Low
Electromyogram (EMG)	Skin electrodes	Electrical activity of the skeletal muscle	No	Passive	High
Electroencefalogram (EEG)	Scalp-based electrodes	Electrical brain activity	No	Passive	High
Body movement	Accelerometer, gyroscope	Measurement of acceleration force in 3D space	Yes	A/P	Low
Blood pressure	Pulse oximpeter	Pressure caaused by the heart pulse and resistance of the vessels	Yes	Active	Low
Heart sounds	Microphone	Sound caused by the heart movements	No	Passive	High

Table 2.3: Bio-sensor for wearable devices [49]

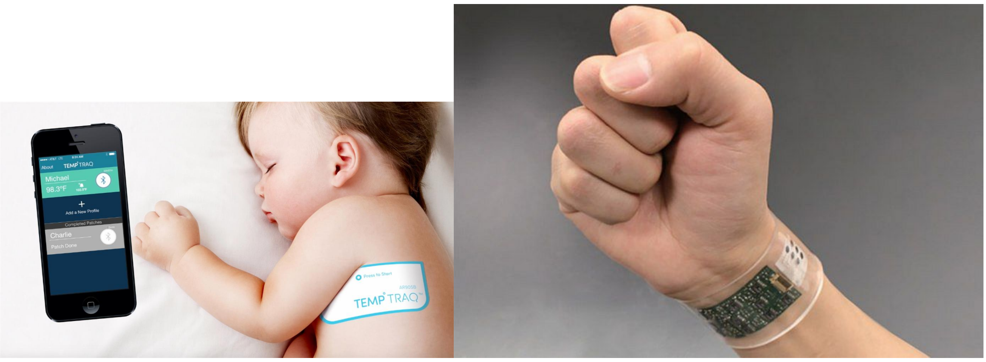

(a) wireless thermometer **(b)** Chemical sweat sensor

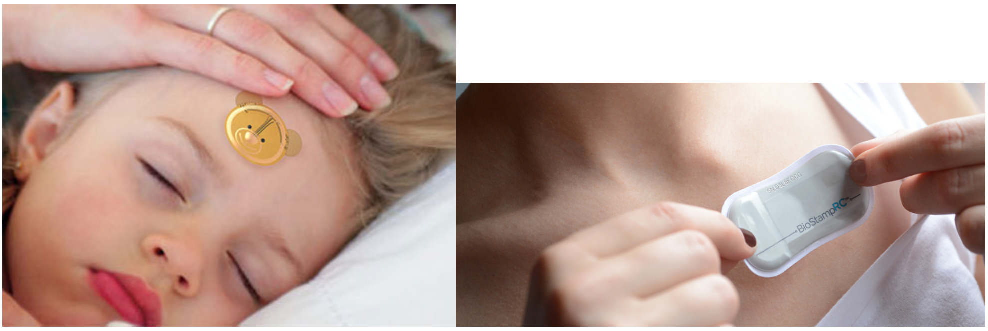

(c) Forehead wireless thermometer **(d)** Wireless flexible MC10® Sensor

Figure 2.1: Temperature sensors, examples. [50, 51, 52, 53]

Skin conductance can be easily measured by recording the resistance between two places on the skin by using an inexpensive metal-based electrodes. This is apparently easy method to measure skin properties. On the contrary, considering it relatively small variation, the signal needs to be processed, filtered and amplified to be efficacy used, which has limited its application in the field of portable medical devices. This parameter can be widely used in clinical setting.

2.2.1.3 Magnetometers, gyroscopes and accelerometers

Magnetometers, gyroscopes, and accelerometers are widely used as motion capture sensors and movement analysis. A magnetometer measures magnetic fields and the magnetization of materials. The simplest example for a magnetometer employment is the compass, which measures the direction of the environmental magnetic field; They are widely employed for measuring the Earth polarity. In recent years, magnetometers have been miniaturized to be incorporated in integrated circuits with a low cost, and improving their usage in portable devices. The magnetometer sensor is based on the modern solid-state technology to create a miniature Hall-effect sensor, which is able to detects magnetic field along the three geometric axes. The Hall-effect sensor produces the voltage which is proportional to the strength and polarity. Their voltage output is converted to digital signal representing the field intensity. The magnetometer is enclosed in a small electronic chip that often incorporates other sensors (typically a built-in accelerometer and gyroscope) that help to correct the raw measurements by data fusion (Fig. 2.3).

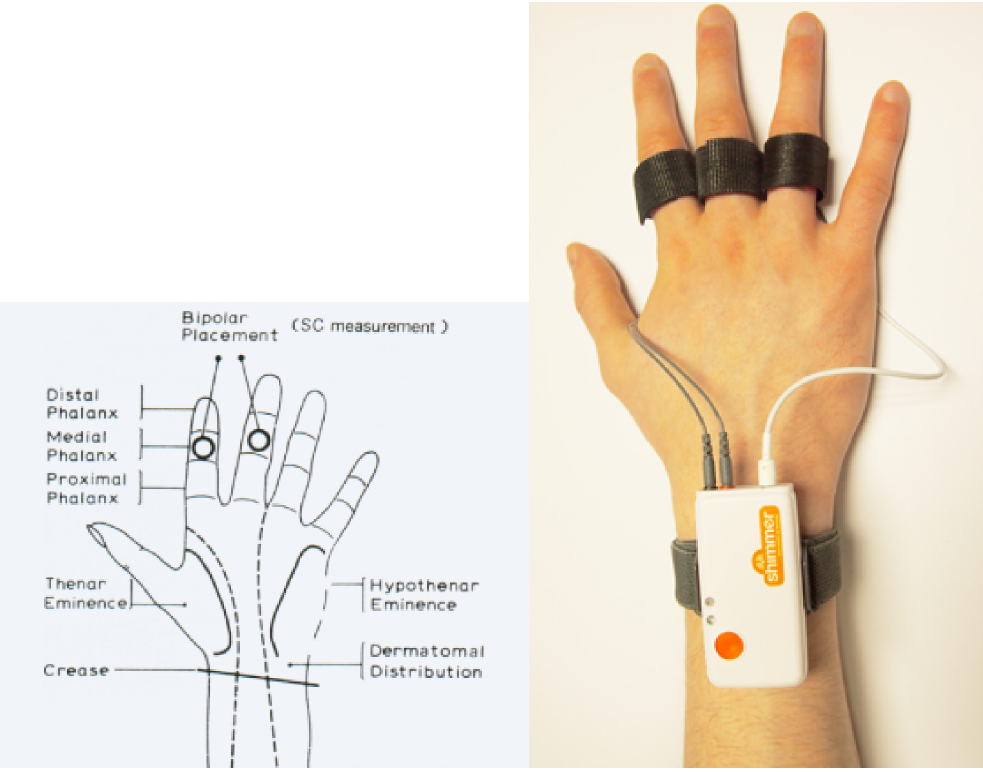

(a) GSR principle illustration

(b) Commercial GSR sensor for research studies

(c) wearable GSR sensor

(d) GSR embedded in a glove

Figure 2.2: Conductivity sensors, examples.[54, 55, 56]

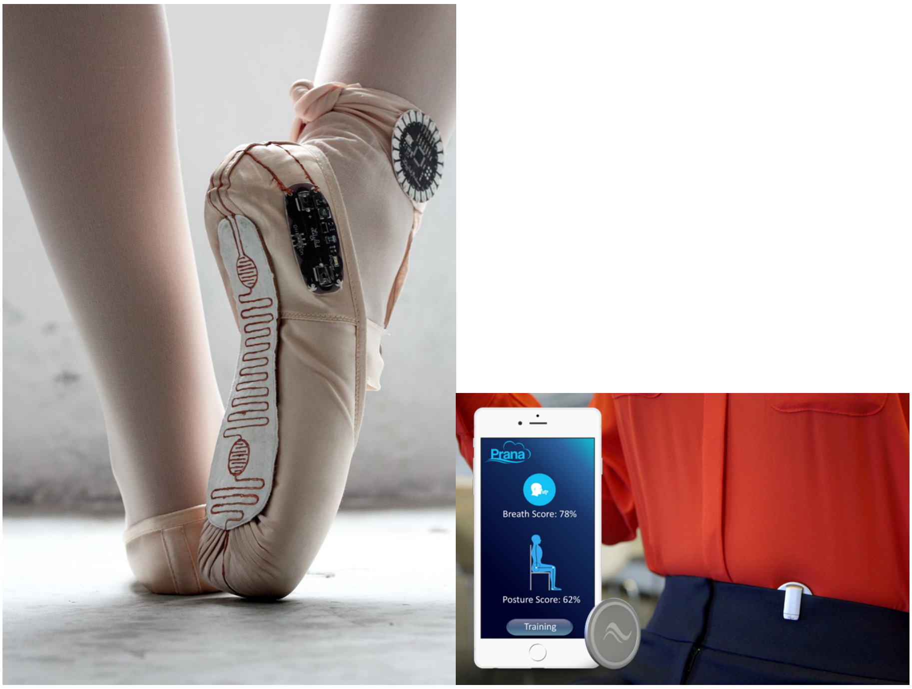

(a) Artistic painting, sensors are used to convert movement in art

(b) Posture sensor

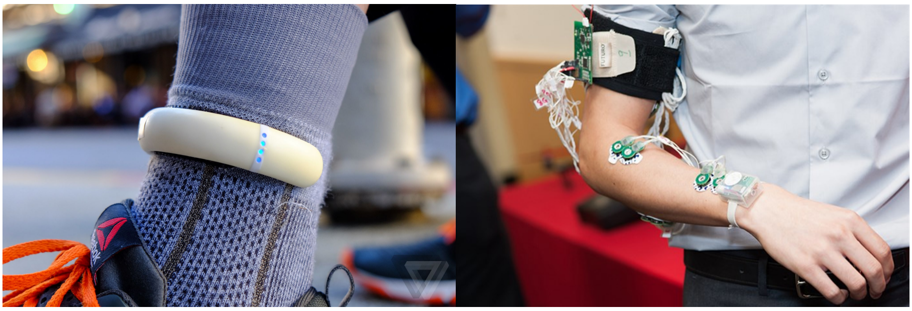

(c) Angle sensor

(d) orientation of the arm sensing

Figure 2.3: Sensors for body movements detection, examples [57, 55, 58, 59].

2.3 Applications for body sensing

2.3.1 Fever rush detector with RFID technology

The wireless and continuous measurement of human body temperature may open new frontiers in the monitoring and control of pathologies that involve fever rushes, such as epidemics or virus infection. It also takes care of the skin infection around wounds and lesions. Current technologies are mostly based on non-contacting infrared thermometers to quickly and non-invasively collect the body temperature. Those sensors, however, require instrument's probe very close to the body district and need the effort of an operator. Thus generate a massive workload for nurses and clinicians when concurs a fast sampling rate due to the number of patients. Automated wireless monitoring of temperature would instead enable data readings to be automatically stored, retrieved, and analyzed for trends and statistics. Battery-assisted temperature autonomous sensors for both clinical and personal use are nowadays commercially available, but the involved high costs and the not negligible volume (mainly due to the presence of battery) are currently an obstacle for their diffusion as disposable and nearly transparent devices able to conformally adhere to the human skin [21].

2.3.2 Body skin temperature

The skin temperature variation is a standard indicator of brain activity and particular psychological states. Long-term assessment of skin temperature can also provide accurate profiles of the circadian-system rhythm (for instance skin warming is functionally linked to sleep propensity) [60].

2.3.3 Breathing sensor and apnea detection

Breathing is a prominent indicator of several problems like allergies, asthma, but also more complex brain controlled breathing disorder, as well as many sleeping diseases. For example, the obstructive sleep apnea (OSA) is already considered the most common respiratory problem during sleep, which is characterized by cessations of airflow due to the collapsing soft walls at the throat. Nowadays, accelerometer-based sensors are designed to detect breathing and often share this information on the network, communicating through a gateway to a web service. Also, non-contact devices have been proposed to detect respiration. However, steps forward can be done to improve performance in battery lifetime, size, and comfort [61, 62, 63, 17, 64, 65, 66, 67].

2.3.4 Galvanic skin response (GSR) sensors for autonomous nervous system (ANS) activity

The sympathetic nervous system controls sweating, while skin conductance is an indication of psychological or physiological arousal. If the sympathetic branch of the autonomic nervous system is highly aroused, the sweat glands activity also increases, which in turn increases skin conductance. This parameter is strongly related to the healthy state of the body and if monitored continuously, can furnish a powerful help for diagnosis and therapies in many diseases like schizophrenia, insomnia, and brain disorders. GSR is widely studied in the forecasting of seizures in the epilepsy [64]. Galvanic skin response (GSR) adopts simple metal electrodes to measure the resistance between two positions on the skin. The density of the sweat glands changes along the skin, but thanks to the high density on the wrist as well as the fingertips, the electrodes can be displaced to provide more comfort to the user. This sensor can be also used in combination with other sensors to monitor the sleep, breathing and unexpected arousals.

2.4 Conclusions

This Chapter has presented technologies considered for analysis regarding body-worn sensors and communication methods. The overall aim of this introduction is to set up the boundaries of the research, reducing the investigation around three main examples to define their strengths and weakness for medical sensing. Next chapters describe the usability of three different technologies by introducing concrete cases of application and results.

3

Passive RFID for body sensing

The Radio-frequency identification (RFID) systems are mostly used in logistics and transportation, but in the last decades, have been successfully employed also in other, more complexes areas, such as the body-centric and environmental sensing. Born as a technology for simple identification of items, in the last years has developed various sensing capabilities, becoming an excellent choice for a disposable, wireless, and low price industrial applications. Furthermore, among the existing standards for BANs, the RFID appears as the most promising technology to interact with epidermal devices thanks to their thin shape and inexpensive price. A typical RFID architecture requires a small battery-less IC transponder (or tag), which is suited for integration within flexible, lightweight and ultra-thin membranes. RFID tags have therefore a great potential to be adequately reshaped in an entirely novel form of epidermal-like plasters that can be wirelessly powered-up and accessed by a remote reader. Especially in the UHF band (860-960 MHz), although strongly influenced by high dielectric materials like the human body, the RFIDs could provide in principle reading ranges up to one meter and more. The transponders comprise a miniaturized antenna for energy harvesting and communication with a remote interrogator, a microchip for data sampling modulation and several sensing elements connected to the IC or distributed over the radiator surface (e.g. sensitive coatings). New RFID transponders include sensing capabilities that give a very miniaturized dimension but force the communication unit to be laid directly on the skin. Therefore the performance of the tag decrease due to the presence of the body and a reshaping of the tag is necessary.

Also, the restrictions on the medical system force the classic RFID design to an entirely new shape. In this chapter, a temperature sensor based on the RFID technology has been thoroughly redesigned to meet the essential requirements for a wIoT application. A radio-thermometer is designed, modified to suit different body shape, and tested to study communication and sensing performance.

3.1 Challenges

The behaviour of the human body imposes severe limitations on the radiation performance achievable by UHF radiators. This problem has been widely discussed in the past by the research on wearable antennas. The main idea has been to decouple the antenna from the body as much as possible using ground planes (patch-like antennas) [68] or multilayer spacers placed between the body and dipole, slot, or a loop antenna [41, 69]. However, while wearable antennas are frequently integrated within clothes without any critical constraint of micro-metric thickness, epidermal ones are conceived to be attached directly over the skin by using at most sub-millimeter thick, soft membranes. As skin-mounted transponders must perform together communication and sensing, their presence must not interfere with the local metabolism of the epidermis such to not alter the measurements of bio-parameters over the skin surface. Accordingly, the substrates are required to be not only biocompatible but also breathable to ensure the preservation of the natural transpiration and the temperature of the skin. Shielding planes, as in the case of patch antennas, must be avoided and the amount of the metal conductor minimized. As a consequence, the antennas are expected to be affected by the inter-individual variability of human tissues as well as to the surface deformation due to the muscular contraction and body movements. Epidermal antennas are not an alternative technology aimed at replacing or outperforming the functionalities of conventional wearable antennas, while instead, they are the essential way to provide the emerging flexible/stretchable bioelectronics for medical devices and systems with communication capability. The following chapter introduces an original approach base yielding to the design and demonstration of real epidermal transponders having concrete applicability to the continuous and random monitoring of peoples health and wellness. The possibility to remotely access epidermal devices could permit to simultaneously interact with multiple skin devices to elaborate not only individual statistics but also cross-analysis patterns. The expected outcome of the work is to boost the usability of the epidermal electronics in the same way as the research on wearable antennas and body-centric communication. Also, the restrictions on the medical system force the classic RFID design to an entirely new shape. In this chapter, a temperature sensor based on the RFID technology has been thoroughly redesigned to meet the essential requirements for a wIoT application. A radio-thermometer is designed, modified to suit different body shape, and tested to study communication and sensing performance.

3.2 Background

An RFID system [70] is composed of two main components: the remote transponder or tag, including an antenna and a microchip transmitter (IC), and the local querying system or reader that collects and eventually processes the received data. Besides a unique identification code (ID), the data wirelessly transmitted back to the reader can include different sensing-related information that can also be stored in the IC memory. The tags could be *passive*, which are able to harvest the energy from the interrogating system, *semi-passive* when a battery is included only to feed embedded sensors or to increase the sensitivity of the receiver inside the microchip, or *active* where a local source directly feeds a micro-controller and the transmitting radio. Battery-less tags have an almost unlimited life, are low cost, lightweight, and need no maintenance. Because of the absence of a local power source, passive transponders provide a significant flexibility in seamlessly integrating the RF devices with the human skin. In passive and semi-passive technologies, at the beginning of the reader-to-tag communication protocol, the reader first activates the tag by transmitting a continuous wave that provides the required energy to perform actions. Usually, even if passive tags are chepeer then the active and semi-passive, the readers are more complicated and consequentely more expensive.

In passive and semiactive technology, at the beginning of the reader- to-tag communication protocol, the reader first activates the tag by sending a continuous wave that provides the required energy to perform actions. During this listening mode, the microchip exhibits an input impedance $Z_C = R_C + jX_C$, with X_C being capacitive reactance. The energy harvesting capability of the tag antenna with impedance $Z_A = R_A + jX_A$

is described by the power transfer coefficient:

$$\tau = \frac{4R_C R_A}{|Z_C + Z_A|^2} \leq 1 \tag{3.1}$$

which is maximum in case of conjugate impedance condition $Z_A = Z_C*$, i.e. when the chip can use the entire power available at the tag antenna. During the next steps of the communication, the activated tag receives commands from the reader, and finally sends back the data stored in the IC memory through a backscattered modulation of the continuous wave provided by the reader. In this case, the tag's IC acts as a programmable switching device between a low impedance and a high impedance states Z_C^{ON}, Z_C^{OFF} , thus modifying the reflectivity of the responding tag, and hence the strength of the reflected power. Under the simplifying hypothesis of free-space interactions, the power budget of the UHF-RFID radio channel, that is, the power $P_{R\rightarrow T}$ transmitted by the reader and collected by the tag (direct link), and the power $P_{R\leftarrow T}$ backscattered by the tag toward the reader (backward link), is characterized through the *Friis formula* and the radar equation:

$$P_{R\rightarrow T} = \left(\frac{\lambda_0}{4\pi d}\right)^2 P_{in} \cdot G_R(\theta,\phi) \cdot G_\tau(\theta,\phi) \cdot \eta(\theta,\phi) \tag{3.2}$$

$$P_{R\leftarrow T} = \left(\frac{\lambda_0}{4\pi d}\right)^4 P_{in} \cdot G_R^2(\theta,\phi) \cdot G_T^2(\theta,\phi) \cdot \eta^2(\theta,\phi) \cdot \tau \frac{4R_A}{|Z_C + Z_A|^2} \tag{3.3}$$

where λ_0 is the free-space wavelength of the carrier tone emitted by the reader; θ and ϕ are the angles of a spherical coordinate system centered at the tag; P$_{in}$ is the power entering the reader's antenna; $G_R(\theta,\phi)$ is the gain of the reader antenna; η is the polarization factor accounting for the mutual orientation reader-tag; $G_\tau(\theta,\phi) = G_T^2(\theta,\phi) \cdot \tau$ is the realized gain of the tag, i.e. the radiation gain $G_T^2(\theta,\phi)$ of the antenna corrected by the power transfer coefficient between tag's antenna and microchip.

At the reader side, various power-related parameters can be recorded besides the digital code of the tag. The first parameter obtainable from the forward link is the *turn-on power* P_{in}^{to}, that the minimum in input power P_{in} through the reader's antenna required to activate the tag integrated circuit (P_{chip}). From turn-on measurement it is possible to extract the realized gain of the tag G_τ , as follows:

$$G_\tau(\theta,\phi) = \left(\frac{4\pi d}{\lambda_0}\right)^2 \frac{P_{chip}}{G_R(\theta,\phi)\eta(\theta,\phi)\cdot P_{in}^{to}(\theta,\phi)} \tag{3.4}$$

that is a useful metric to experimentally evaluate the combined radiation and matching properties of a tag antenna independently of the connected IC. The backscattered power is also measurable by the reader in terms of the Received Signal Strength Indicator (RSSI) that is directly related to $P_{R\leftarrow T}$ through a reader-specific linear conversion formula.

The two main sensing paradigms for the RFID tags are based on two basic properties of the tags. In the analog tag with standard chips, the antenna itself plays as an electromagnetic transducer of some physical/chemical phenomenon under observation. On the other hand, digital transponders with sensor-oriented chips, encodes the sensed data at the chip level and transmit them in a digital form. This approach appear to be more stable, even if it needs more energy to power their sensors. The first approach exploits the intrinsic sensitivity of a bare tag to the time-variant boundary conditions. Although simple and powerful, such operation mode has the inherent disadvantage that the impedance mismatch caused by the evolution of the sensing process is damaging to the communication functionality. Finally, many issues limit the real-life use of the analog tag to an extensive application involving low-cost (<1€), eventually disposable, patches suitable only for a qualitative low-resolution [71] monitoring. The real added value for epidermal sensing will be probably raised by the new families of RFID ICs with augmented sensing capabilities [72, 73, 74]. They typically include an internal analog to digital converter (ADC), a high-speed non-volatile memory (EEPROM), an embedded temperature sensor, and a programmable front-end to connect general-purpose microcontrollers and sensor (thermoresistance, interdigital capacitors, strain gauge...). The physical information is sampled by the specific sensor, locally digitized and stored in the internal memory. The sensed data are then recovered by the reader straight away in a digital form, thus dropping out the source of errors due to the signal transmission. These chips can be used in both passive and battery-assisted mode. In the latter case, the tag can autonomously trigger measurements that are stored in the user memory and then retrieved asynchronously by the reader (log mode). The ultra-low power consumption of the IC circuitry (a few milliwatts) enables harvesting energy out of some cycles of the interrogation signal, as well as from piezo-electric, solar or thermal scavengers. These devices can be considered as a convergence point among fully passive tags and the autonomous sensor nodes with local computational capabilities that usually embed much more complex electronics. They could hence provide a possible tradeoff between superior sensing performance, immune to the environmental interactions and average cost. The price to pay for this exceptional capability is a higher cost of the chip (3 – 8 € versus a few cents for conventional RFID chips) and a slightly weak IC sensitivity (more than 10 dB lower than traditional chips), which significantly limits the read distance when used in full passive mode. Augmented IC are definitively appealing for quantitive monitoring of biometrics using tattoo-like sensors as well as for the multi-parameter accurate monitoring of environmental parameters in IoT healthcare scenarios, as will be shown in the following chapters.

The maximum distance at which the reader can detect a tag is a practical indicator of overall tag communication performance. In the case of epidermal antennas, the proximity with the lossy body induces a significant dissipation of electromagnetic power, extremely degrading the radiation gain. Consequently, much shorter reading distances must be expected for skin-mounted RFID sensors with the respect of free-space tag, with activation ranges intermediate between wearable and implantable systems. Moreover, as sensing functionalities provided by the new RFID ICs are achieved at the expense of a reduced power sensitivity ($P_{chip} >$ -10 dBm), the length of the communication link is further decreased. While extraordinarily low-profile and inexpensive epidermal sensors are mandatory in most of the cases (e.g. entirely passive disposable plasters), slightly complicated circuitry is acceptable as well when the improved reading performance and the reliable continuous monitoring are critical for the targeted application. Then, battery-assisted solutions may also be exploited, especially since flexible thin-film battery technologies[75, 76] still permit a certain degree of integration into soft skin-attachable patches.

3.3 Design of an RFID thermometer

Measuring temperature by an RFID tag attached to the body requires the tag itself not to modify the local temperature of the skin. In other words, the epidermal device should preserve the natural transpiration of the skin. At this purpose the substrate has to be not only bio-compatible but even transpiring and, for the same reason, the mass of antenna conductor has to be limited. Therefore, among various options for wearable antenna layouts, such as the dipole [41], the slotted patch [77, 78] and the loop [69], the latter configuration has been considered. This solution addresses the required small amount of conductor and for the known superior radiation performance close to lossy materials (as the human skin is). In particular, the sensor layout is derived from a one-wavelength rectangular-loop excited by a smaller inner loop whose shape factor is adequately selected to achieve conjugate impedance matching to the microchip (Fig. 3.1).

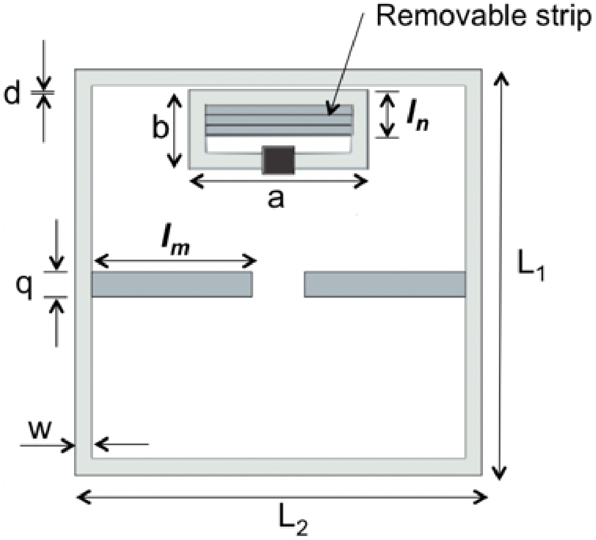

Figure 3.1: Layout of the epidermal tag

The external dimensions are fixed to $L_1 = L_2 = 50$ mm (to be on a medium-size plaster) in order to meet a possible trade-off between the antenna gain and the overall size of the sensor, that should be as low as possible for user's comfort. The two loops include additional elements (in darker grey) that permit to increase the antenna bandwidth and to modify the impedance matching of the tag slightly. To clarify this point, let assume the tag without the tuning elements (the only shape in dark grey in Fig. 3.1) to be connected to a microchip with impedance $Z_c = 23 - 145j\Omega$. Fig. 3.2 shows the simulated realized gain of the tag when it is attached over a layered model of the human body [77] simulating a thin and thick thorax.

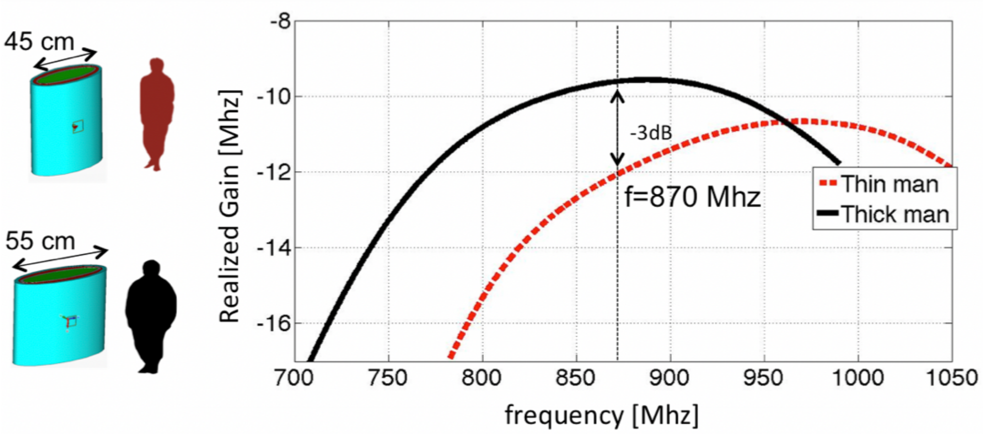

Figure 3.2: Realized gain, a comparison between the performance of the antenna that is laid on a slim and a thick person

There is a significant shift of the tag's response depending on the mass index of the phantom, and, accordingly, a considerable loss of reading performance will be expected when moving from a configuration to another. The width l_n of the longest segment of the loop can be indeed modified by removing strips of equal size to softly reshape the path of the excitation currents and hence to shift the resonance frequency of the device. In particular, the peak of the power transfer coefficient τ moves from right to left on removing one, two or three strips of conductors. It is moreover visible in the same Fig. 3.3 that there are two peaks of the power transfer coefficient: a significant band enhancement could be hence achieved by packing those peaks into the useful RFID band. This is obtained by adding two whiskers in Fig. 3.1: on increasing the length of the filaments, the two peaks get closer and closer (Fig. 3.3.), and a nearly unitary τ is obtained in the [780-950] MHz band for $l_m = 14$ mm. The resulting layout is hence potentially suitable for a worldwide application. Finally, the ratio between the total area of the conductor and the size of the tag is roughly 20%, with significant benefit to skin transpiration. The residual surface of the skin could be moreover used to host other devices, chemical sensors and even drug delivery mechanisms, for enhanced capabilities.

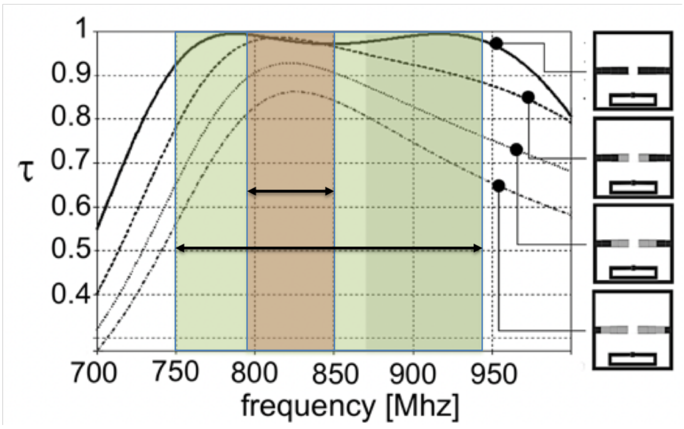

Figure 3.3: Tuning capability due to the internal stub

3.3.1 Substrates

A prototype of the epidermal RFID tag was fabricated onto a biocompatible material, a Poli(ε-caprolactone) (PCL) synthetic membrane [14]. PCL is a semicrystalline bio-reabsorbable poly α-hydroxyester with slow degrading rate due to its hydrophobic nature and high crystallinity degree. The membrane was produces by the electrospinning technique [79] by using PLC granules solved in CHCl3 and THF:DMF (1:1) solutions. Electrostatic fiber-spinning, also denoted as "electrospinning", is a straightforward, cost-effective methodology to produce non-woven micro and/or nano-fibrous fabrics for several biomedical applications, e.g. scaffolds for tissue engineering or wound dressings. The electrospinning process is activated by applying high voltages between a polymeric solution flowing through a capillary and a collector plate, in order to generate an electrically charged jet, as shown in Fig. 3.4a.

As the voltage is increased, the electric field intensifies hence causing a force to build up on the pendant drop of polymer solution at the tip of the needle. This force acts in a direction opposing the surface tension that holds the solution. When the electric field reaches the critical value, the electrostatic force overcomes the surface tension at the tip of the capillary and a continuos charged jet is ejected. When the energized suspension moves away from the needle toward the collector screen, the jet rapidly thins and dries as the solvent evaporates. At the end, the polymer is randomly deposited onto the grounded target forming a dense non woven membrane (see Fig. 3.4b) that is completely bio-compatible (free

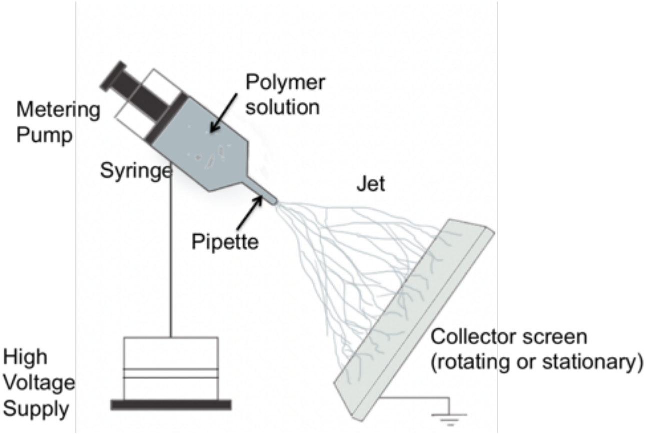

(a)

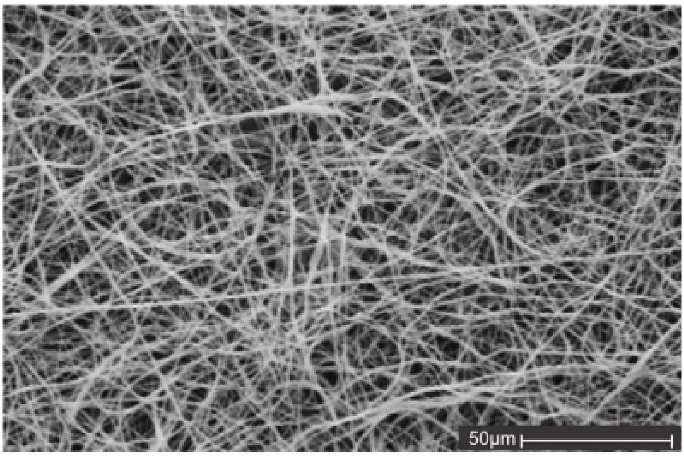

(b)

Figure 3.4: The poli ε-caprolactone membrane, a) fabrication technique b) texture of the electrospinend membrane

of toxic residues). PCL is moreover flexible and stretchable for a comfortable application over any body curvature and, thanks to its fibrous structure, the natural transpiration of the skin is preserved. The considered RFID microchip was the EM4325 IC [72] (impedance $Z_C = 23 - 145j\Omega$, power sensitivity ($P_{chip} = -4.5$dBm) able to work as conventional RFID transponder as well as to provide on-chip temperature measurements in the [-40°C, +64°C] range (in passive mode) with a resolution of 0.25°C. The antenna layout was fabricated on adhesive copper (conductive paints will be considered in the near future) carved by a two-axis digital-controlled cutter. The tuning elements on the inner loop were pre-cut in order to simplify the removal of the desired strips during the manual re-tuning of the antenna, if required. The RFID IC was hence soldered onto the antenna and the whole layout was finally transferred over the PCL membrane to give the prototype in Fig. 3.5.

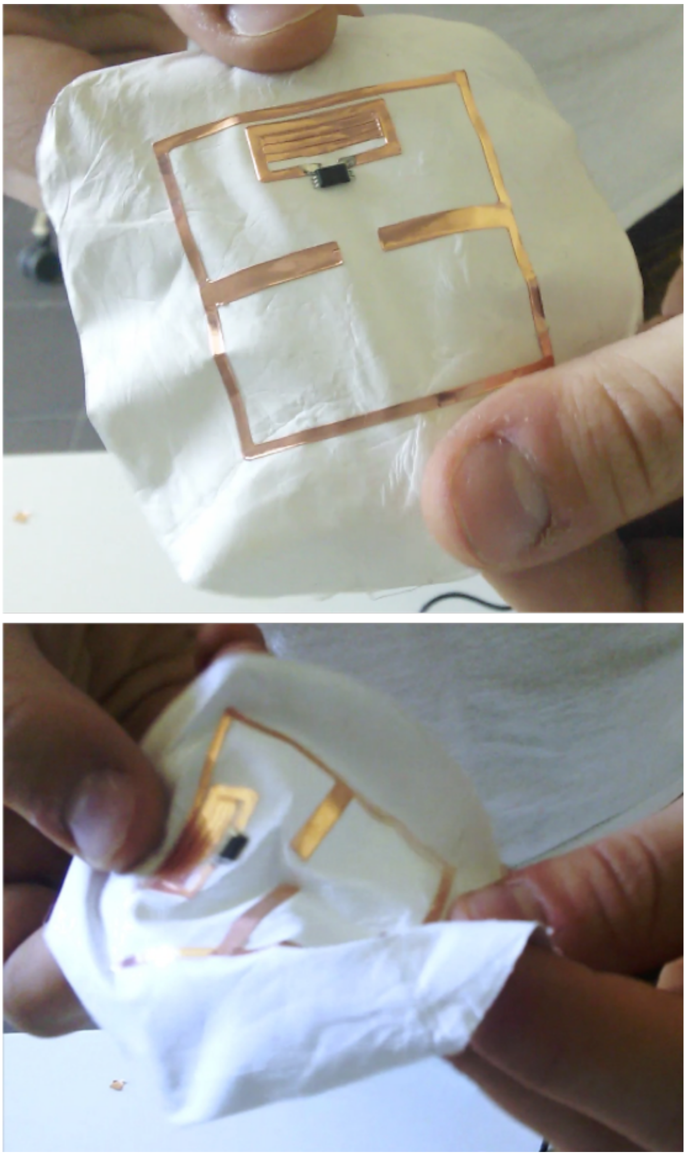

Figure 3.5: The flexibility texture of the electrospinend membrane loaded with the sensor

The communication performance were characterized by the measurement of the realized gain of the tag when it was attached onto the volunteer's arm by using a hypoallergenic cosmetic glue. The measurement set-up comprised a Thing-Magic M5 long-range reader, connected to a 5 dBi broadband PIFA antenna. The system is controlled by a custom software implementing the turn-on measurement procedure [80]. Results for the case of reader-tag alignment are shown in Fig. 3.6 in comparison with simulated data. The average antenna gain is of the order of -10dB in the [840-940] MHz band, in reasonable agreement with simulations. Accordingly, the maximum read range (by applying the simplified free-space Friis model) can be estimated as 80 cm and 30 cm in case of reader power emission of 3.2W EIRP (long-range reader) and 0.5 W EIRP (short-range reader), respectively. Such distances are computed by considering the low sensitivity of the microchip when the temperature data is read from the IC memory. Nevertheless these reading ranges could be fully compatible with a remote temperature monitoring.

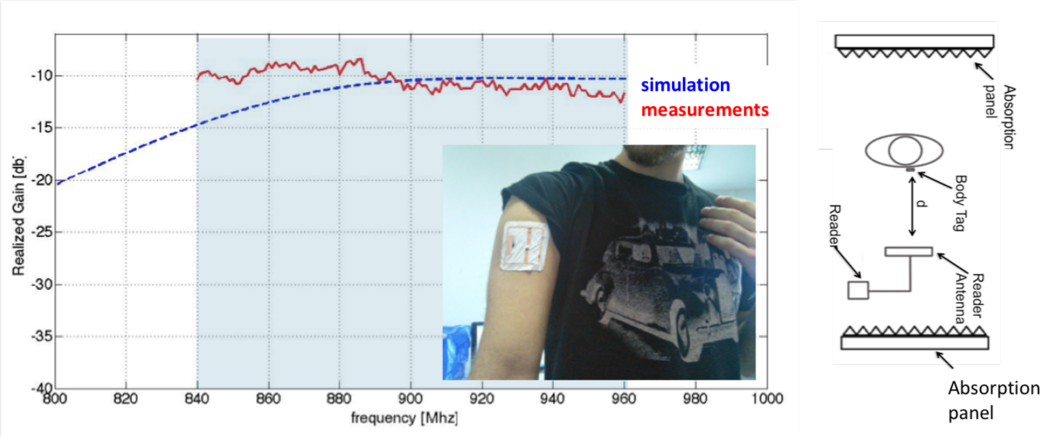

Figure 3.6: Exsperimental setup for the electromagnetic measurements

3.3.2 Thermal characterization

The interrogation of the EM4325 chip provides a thermal reading with an offset uncertainty to be determined by comparison with reference data. Thus, the thermal response and accuracy of the epidermal sensor were preliminarily evaluated by a reference test-case, wherein the RFID sensor outcome was compared with data provided by a thermocouple. The set-up comprised a water-filled plastic box (size 20 cm × 20 cm × 10 cm) wherein a heating electrode was inserted. The RFID sensor was attached onto the external surface of the container and interrogated by a CAEN-QUARK short-range reader (implementing the EM4325 non-standard reading protocol), emitting 0.25W and connected to a 3dB PIFA antenna, for an overall 0.5W EIRP. A PT104 thermocouple was placed close to the tag and connected to Picologic data- logger. The temperature of the water was increased up to 55°C; the heater was removed and the recovery curve was hence recorded by the two systems down to the ambient temperature. A 5.75°C temperature offset was estimated from the results of Fig. 3.7a and was then used for the calibration of the RFID sensor. Fig. 3.7b finally shows the true-measured temperature diagram derived from two further independent experiments. The resulting standard deviation of the calibrated system is lower than 0.25°C, which is comparable with the resolution of the temperature measurement of the EM4325 chip. The calibrated epidermal sensor was finally applied to the measurement of body temperature in both rest condition and under physical stress.

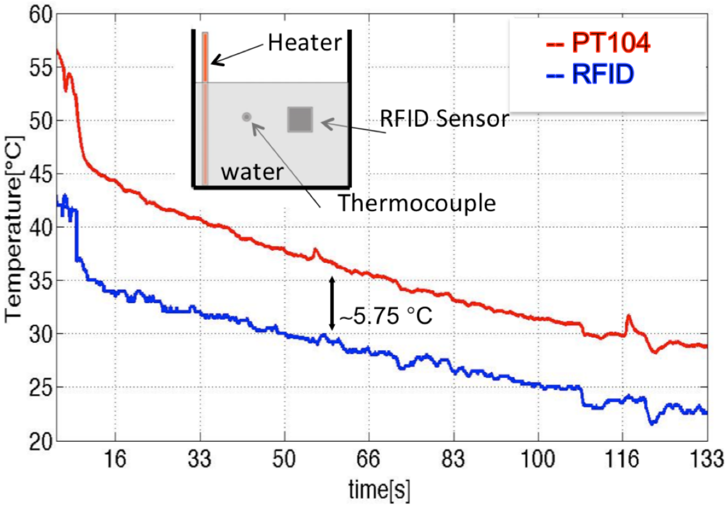

(a)

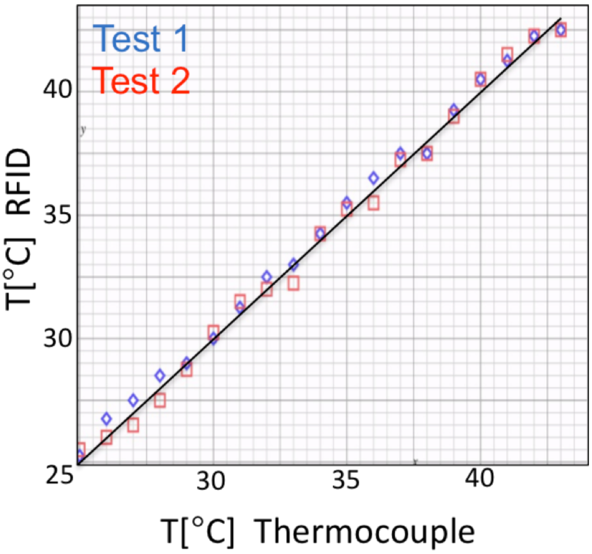

(b)

Figure 3.7: Thermal characterization (a) Calibration setup (b) calibration curve with a thermocouple

The sensor was attached onto the right side of the abdomen (Fig. 3.8) and again the thermocouple was placed at a close distance from it to provide reference data. The volunteer wore his usual fitness clothing. A first measurement was taken for 5min in rest condition and the detected temperature was 35°C. As expected, the measured values correspond to the superficial skin temperature which is lower than the core body temperature (about 37°C). Indeed, the surface temperature changes according to the different part of the body, even in the same subject, and is strongly affected by the blood flow at a particular time as well as by the surrounding ambient temperature . During the second experimental session the volunteer rode an exercise bike for about 1h. During the physical activity the temperature followed a slightly ciclic profile due to thermoregulation mechanisms (e.g. sweating changes in skin blood flow). A substantial agreement with the thermocouple data can be appreciated in both the experiments.

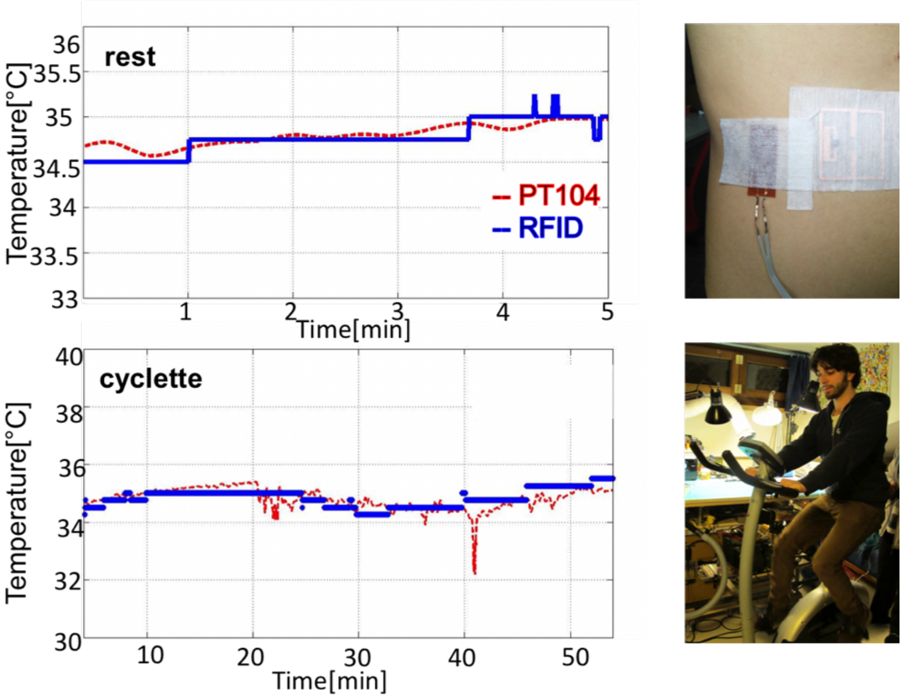

Figure 3.8: Thermal characterization

3.4 Modelling and testing of the body variabily

This section investigates the performance of the above-presented UHF RFID epidermal transponder in the form dual-loop tag depending on the specific placement over different parts of the human body and for a variety of volunteers.

The on-body tuning mechanism presented before is discussed and demonstrated in real applications at the purpose to improve the tag response for several placement loci and operating bands. Unlike wearable antennas, the unshielded and robust proximity between an epidermal antenna and the human body produces a significant sensitivity of the radiation performance of the tag versus the placement modalities. Although early evidence of the body dependent behaviour of the epidermal antennas in UHF RFID bands was already highlighted in [21], the effectiveness of such interaction is still mostly unexplored, and no mitigation method has been proposed so far. This section addresses in full details the characterization and optimization of the communication performance of the epidermal tag for placement over several regions of the human body with the following goals:

i) to evaluate the possible variability of the tag's realized gain depending on the position over the body, but also on the users' body mass and gender;

ii) to introduce and to fully characterize by simulations and measurements a retuning mechanism tailored for loop layouts and consisting in removing pre-cut portions of the impedance transformer of the antenna;

iii) to demonstrate throughout real experimentations how the same tag can be retuned on-body directly to achieve the best performance for the specific placement and the particular frequency in the worldwide RFID band. A reference dual-square loop layout is introduced, and the expected performance is investigated by the help of numerical simulations over simplified canonical models of the human body. The real communication performances of a fabricated prototype attached over different regions of the body are experimentally quantified. An on-skin tuning mechanism is introduced and experimented to get rid of the variability of the tag responses with varying configurations of placement. Finally, some realistic examples of the tuning method are provided. Some early and pioneering cases of epidermal antennas for UHF-RFID applications consisted of tattoo-like RFID tags in the form of nested-slot dipoles [81]. The antenna was fabricated by conductive silver ink, which was profiled onto a Temporary Transfer Tattoo material using a stencil. The same authors proposed similar tag layouts acting as a tonguetouch controlled switch [82] or as a passive strain sensor [83] for assistive devices helping patients with severe movement impairments. The reported read distances were in the range of 80–120 cm depending on the position of the tag over the body. The performance of several types of thin single-layer antennas (e.g., slot, self-complementary, and wire antenna) plaster-like sensor application at 2.4 GHz study was extensively investigated in [84] to search for the antenna layout that is best suited to operate in the very close proximity of the human body. Very recently, we proposed [85] a preliminary idea for a passive RFID epidermal tag for the on-skin temperature measurement, with a specific focus to the use of a highly breathable membrane, such as the ε-polycaprolactone. The considered tag layout was a dual-loop antenna. The close interaction between RFID transponders and the body is moreover stimulating discussions about safety and detuning. The electromagnetic exposure of the human body to interrogating antennas placed nearby of the human skin was investigated in [86] for the even more challenging problem of implanted UHF-RFID devices. The specific absorption rate (SAR), estimated through a detailed model of the human body, resulted significantly below the limits imposed by regulations. Accordingly, the exposure concerns are not critical as regards the interrogation of epidermal RFID tags. The unshielded and robust proximity between the antenna and the body produces a significant sensitivity of the radiation performance of the tag versus the placement modalities. Although early evidence of the body-dependent behaviour of the epidermal antennas in UHF-RFID bands was already highlighted in [81] and then in [85], the effectiveness of such interaction is still mostly unexplored and no mitigation method has been proposed so far.

3.4.1 Tag layout

The tag geometry (Fig. 3.9) has been introduced in the previews section. It comprises a copper trace forming the dual-loop layout over a silicone layer (permittivity $\varepsilon_{si} = 2.5$, $\sigma_{si} = 0.005$ S/m, and thickness 600 µm) having the same shape of the antenna. The inner loop is connected to a NXP–G2X-TSSOP-8 microchip transponder, whose nominal RF input impedance and power threshold are $\text{Z}_{chip} = 16 - \text{j}148\ \Omega$ and $\text{P}_{chip} = -15$ dBm, respectively. The external sizes of the loop are 5 cm × 5 cm, so that the physical area of the tag can be compatible with that of a medical plaster. The size of the internal loop was instead designed by numerical simulations for optimal impedance tuning at 950 MHz, which is the upper bound of the worldwide UHF-RFID band. It is worth anticipating that an ad hoc retuning methodology permits to easily shift the tag response toward lower frequencies as desired (see Section IV). For the sake of the simulation speed, the tag was initially placed onto a reference model of the human body, which consists of infinite planar tissue layers (thickness as in Table I and frequency-dependent permittivity and conductivity as in [53]). Simulation results are shown in Fig. 3.10. The maximum value of the realized gain along the broadside (frontal) direction is -12.7 dBi around 940 MHz. The performance of the tag when it is placed over different regions of the body and for some body masses are now discussed by the help of some parametric simulations wherein simplified planar and cylindrical models of body parts are considered.

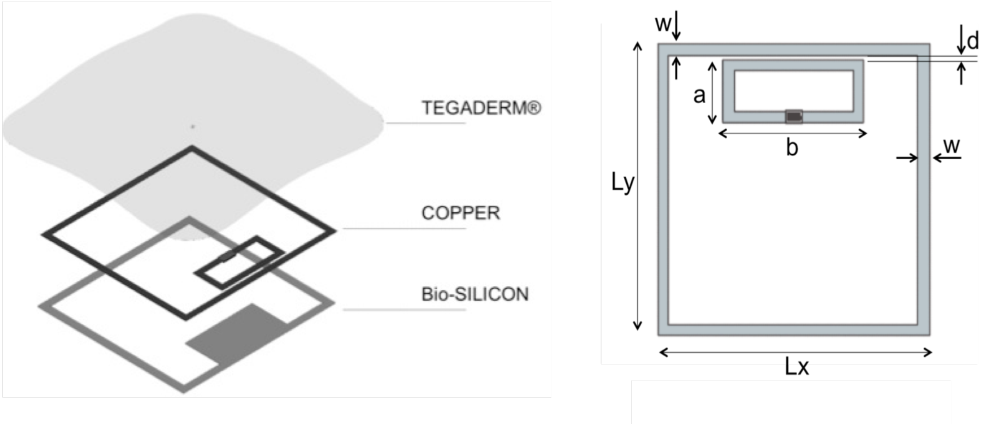

Figure 3.9: Layout of the epidermal tag. Size [mm]: $L_x = L_y = 50$, $w = 2$, $d = 0.5$, $a = 26$, $b = 10$.

3.4.2 Simulated performances compared with body regions

The first set of simulations focused on the sensitivity of the epidermal tag to the specific body parts where it could be placed in real applications. Four reference planar layerings were considered as in Fig. 3.10. They are representative of two regions with high water content, like limbs and abdomen, and of other two regions with a significant presence of bone, e.g. thorax and forehead. Fig. 3.1 shows the simulated gain of the epidermal tag in the four considered conditions. A difference up to 3-4 dB is visible between the two classes of layerings with better values in case of abdomen and limbs. Accordingly, the read distance, that is proportional to the square root of the the tag gain, could be reduced by more than one third when moving the tag from one region to another. The overall sensitivity of the realized gain versus the tag placement is hence a combination of an amplitude scaling and a frequency shift.

Table 3.1: Reference tissue Layer Thickness (in mm) of some body regions

Tissue	**Limb**	**Abdomen**	**Thorax**	**ForeHead**
Skin	2.5	2.5	2	2
Fat	8	10	-	2
Muscle	25	20	3	
Bone	-	-	10	7
Dura	-	-	-	1
CSF	-	-	-	2
Viscera (termination)	Bone	Intestines	Lung	Brain

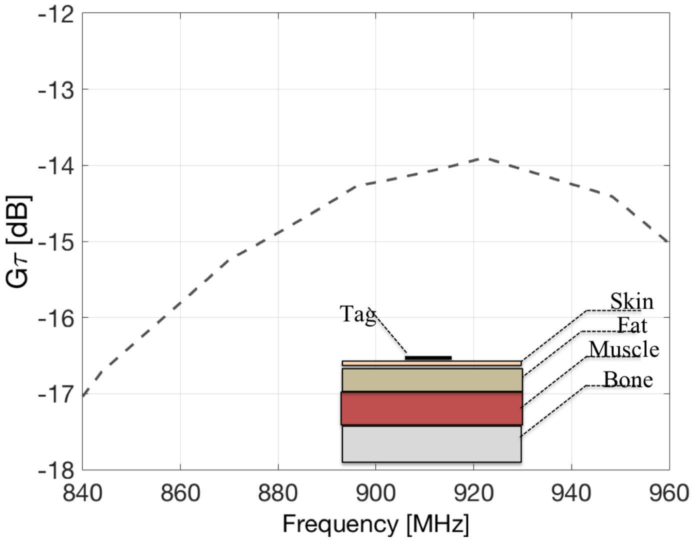

Figure 3.10: Simulated gain of the epidermal tag when it is placed onto four different planar layered models emulating typical body districts.

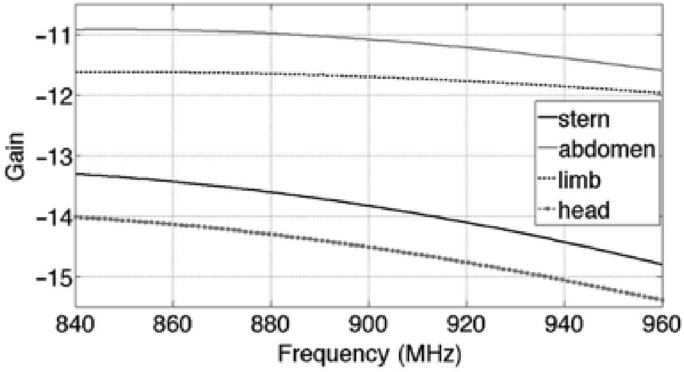

Figure 3.11: Maximum realized gain ($G\tau$) of the epidermal tag when placed onto four different planar layered models emulating typical body districts described in Fig. 3.1.

3.4.3 Simulated performances as function of body mass

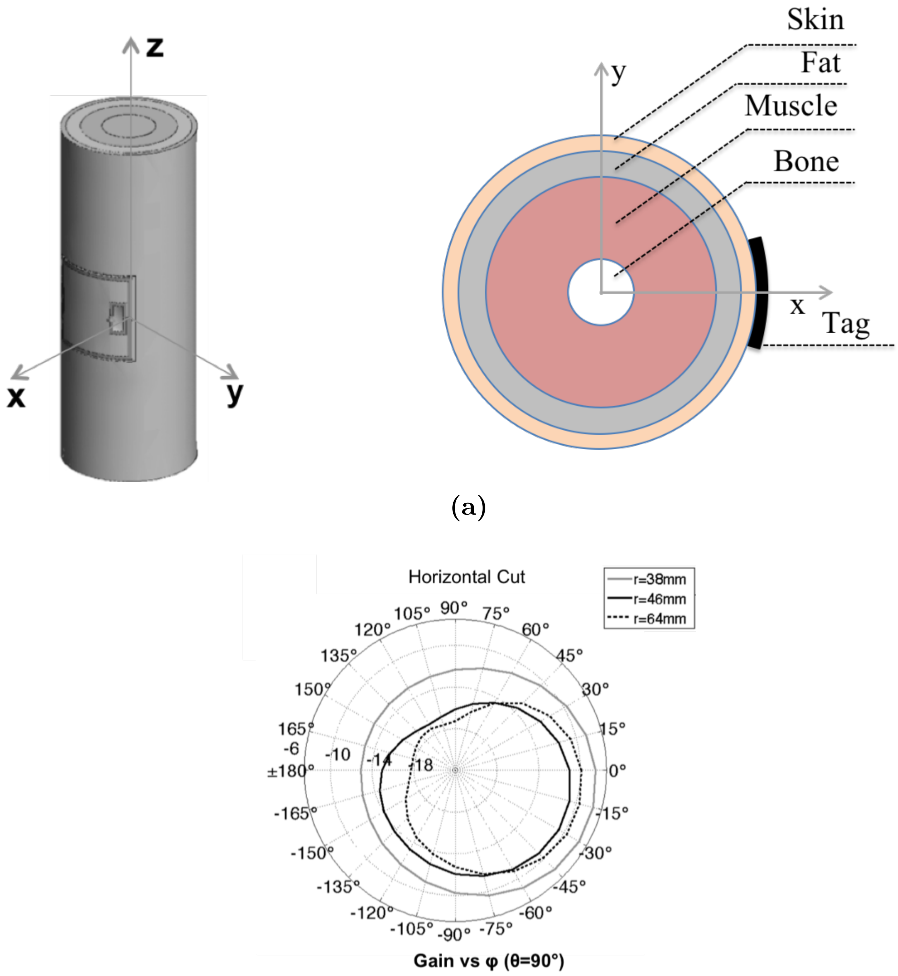

(a)

(b)

Figure 3.12: (a) Epidermal loop bent around the 4-layers cylindrical limb model of a human arm. (b) Radiation pattern of the conformal tag at 930 MHz for three different arm sizes. The grey area in the radiation pattern indicates the Half Power Beamwidth.

The epidermal tag was then simulated over a finite-size layered cylinder at the purpose to investigate the effects of the bending of the epidermal loop around a curved surface and the dependence of the tag's performance on the physical size of the underlaying body segment. A human arm was modeled by four concentric tissues layers (skin, fat, muscle and cortical bone, Fig. 3.12). Three geometries were considered in order to resemble different form-factors of the arms (see Tab. 3.2). The thickness of the skin and fat layers were kept constant in the models while only the muscular mass was changed.

Table 3.2: Radius (in mm) of the three cylindrical numerical phantoms

model	R_{skin}	R_{fat}	R_{muscle}	R_{bone}
A	38	35	27	15
B	48	45	37	15
C	64	61	53	15

Table 3.3: Radiation performances of the tag over the three cylindrical models.

model	G_{max} [dBi]	η_R [%]	FB [dB]
A	-8.2	6.6	5
B	-10.5	5.8	4
C	-9.6	4.5	8

Fig. 3.12 shows the simulated radiation pattern at 930 MHz in the horizontal plane ($\theta = 90^{\circ}$). The peak radiation occurs along the direction perpendicular to the tag and in all the cases there is a slight directionality effect. The radiation performance are resumed in the Tab. 3.3 where in the maximum gain, the radiation efficiency and the front/back (FB) ratio are reported. Differences are visible for both the peak gain and the efficiency and even more concerning the uniformity of the pattern. In particular the most affordable configuration to establish the RFID link is the smallest cylinder, while the largest one produces the least uniform pattern and a lower efficiency so that the interrogation of the tag may be more challenging. In all the cases, the Half Power Beamwidth is of the order of 130° - 175°. Therefore the expected read distance does not degrade below the 70% of the maximum value, which occurs in the optimum alignment, provided that the reader is placed reasonably in front of the tag. Even considering a few electromagnetic shadowing by the human body, the exact alignment between the epidermal tag and the reader's antenna is not expected to be a critical issue. It is worth

analyzing the near electric field pattern inside the cylinder close to the tag, which was simulated considering the tag antenna in radiating mode (Fig. 3.13). Two phenomena are clearly visible: a resonant-like behavior, especially in the smallest and medium cylinders and a back-reflecting effect in the large cylinder which forces the radiation pattern to be more directive. The efficiency loss and the different front/back ratios are hence the result of the two concurrent phenomena of strong energy dissipation inside the muscle and its reflector-like effect.

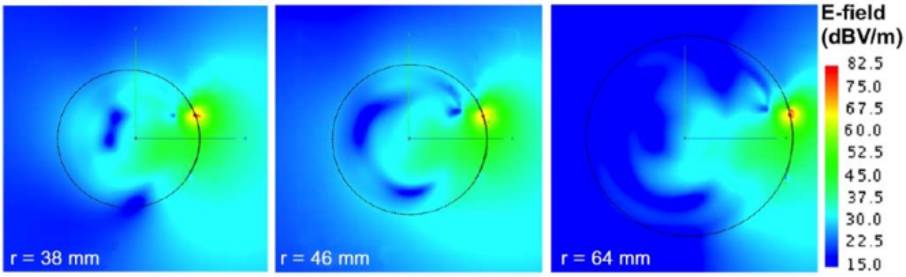

Figure 3.13: Electric near-field distribution (cross section, z=0) inside and outside the layered limb model at 930 MHz when the tag antenna was assumed as sourced by 1W.

3.5 Prototypes and on skin performances

A prototype of the epidermal tag (Fig. 3.14) was fabricated by adhesive copper (thickness 35 µm) which was carved by a two-axis digital-controlled cutter. The profiled tag was applied on a 600 µm-thick biocompatible silicone by means of an adhesive transfer tape. The biosilicone layer was shaped just around the conductors and the material in excess was remove out in order to improve transpiration. A commercial transparent and breathable adhesive film (Tegaderm^{TM}). was applied on top of gummy loop. The obtained plaster was hence still adhesive, with the copper placed between the two membranes, and suitable for a comfortable and nearly invisible placement over the skin. As the coating dressing is breathable, the tag can be worn by the user for many days without any discomfort. The ratio between the total area of the conductor and the size of the resulting tag is less that 10 %, with great benefit to skin transpiration. The residual internal surface of the skin could be moreover used to host other devices such as chemical sensors and even drug delivery mechanisms.

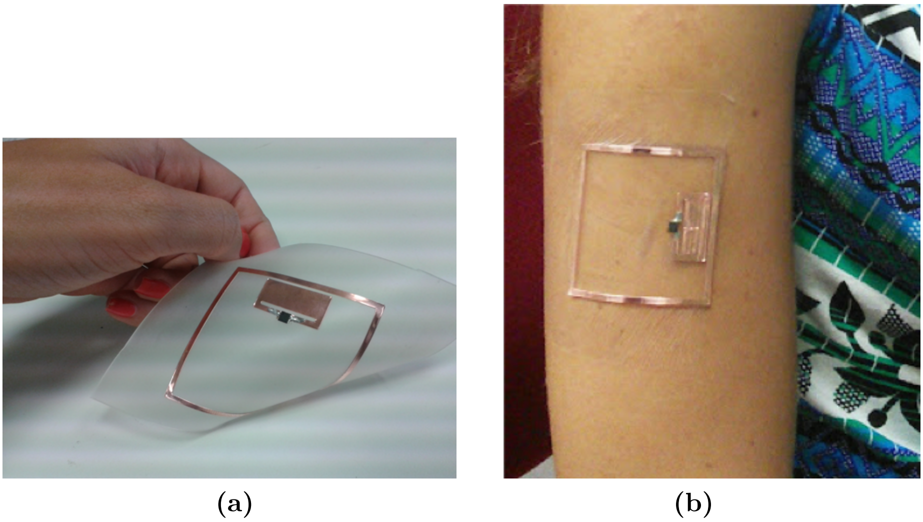
(a) (b)

Figure 3.14: (a) Prototype of the epidermal RFID tag sensor over biocompatible silicone shape and Tegaderm fixing. (b) Epidermal RFID tag transferred over an arm.

The communication performances of the prototype were characterized through the measurement of the realized gain of the tag attached onto a liquid phantom resembling the human body ($\epsilon_{phantom}$ =43, $\sigma_{phantom}$=0.33 S/m). The liquid was contained within a 13×13×20 cm^{3}parallelepiped box of PET ($\epsilon_{PET} = 2$, $tan\delta_{PET}$=0.005 S/m) having 1 mm thickness. The measurement set-up comprised a ThingMagic M5 long-range reader, connected to a 4 dBi broad-band PIFA antenna. The system was controlled by a custom software implementing the turn-on measurement procedure [87] for the estimation of the realized gain. The distance between the reader and the tag was kept fixed at 40 cm in all the experiments. The antenna of the reader and the epidermal tag (attached over the body or over the phantom) were mutually aligned in order to obtain the best polarization match.Results for the case of reader-tag alignment are shown in Fig. 3.15 together with simulated data. For comparison, the antenna was simulated over a parallelepiped box mimicking the measurements phantom. Measurement results follow the same profile as simulations with realized gain's peak around 940 MHz as expected[1]. The perfor-

---

[1] It is worth noting the many flat subsections occurring in the measured curves of the realized gain throughout the thesis are due to the poor resolution of the reader (±0.5 dB).

mance of the epidermal tag in real conditions are now discussed by the help of measurements over four volunteers: a *"normal" male*, a *"muscular" male* a *"thin" female* and *"robust" female*, whose height and weight are reported in Table 3.4. They were informed of the experimental procedures and of the goals of the research before the participation to the measurements. The experiments aimed at investigating the sensitivity of the epidermal tag to the specific locus of placement over the human body and on the user's body-mass, thus corroborating the results from previous numerical simulations.

Table 3.4: Data of the four volunteers for epidermal tag measurements

Volunteer	**height [cm]**	**weight [Kg]**	**Body mass Index**
thin female	155	45	18.7
robust female	178	75	23.7
normal male	174	64	21.4
muscular male	184	85	25.1

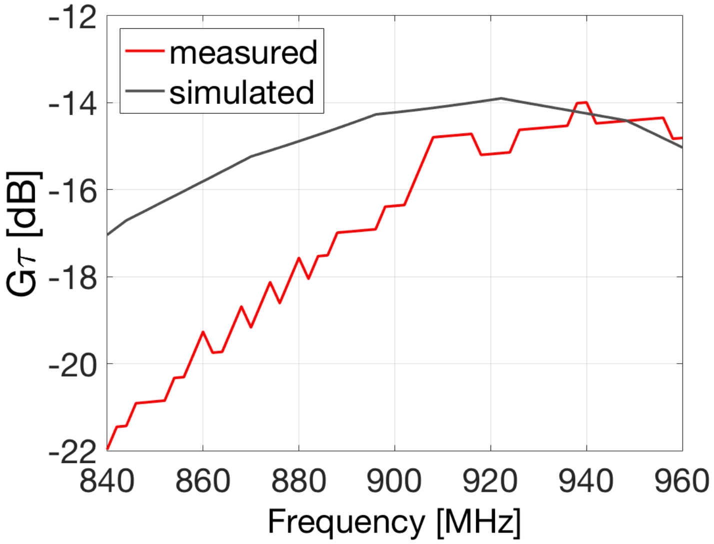

Figure 3.15: Measured realized gain along frontal (broadside) direction of the fabricated epidermal RFID sensor when applied onto a plastic box filled with a body-equivalent liquid phantom.

3.5.1 Measured performance considering body placement

In the first experiment, the tag was attached onto different body parts of the thin female volunteer such as arm, forearm abdomen, sternum, hand, neck, and forehead. Fig. 3.16 shows the measured realized gain for all the cases. As expected from simulations, the profiles are mutually scaled (due to change in the power absorption) and partially shifted by the effect of impedance detuning. The placement over the leg provides the highest realized gain, even better than what was predicted by simulations for the reference layered model (similar to the case of the former abdomen). In particular, the realized gain was higher than -10 dBi at 950 MHz and higher than -13 dBi in the whole UHF RFID band. The worst case was instead the stern position with a degradation of about 10 dB in the realized gain, which is even worse than the value predicted by simulations. In most of the cases, a successful communication link was correctly established at the distance of 40 cm by just 17-20 dBmW of power from reader that is much lower than the maximum available level.

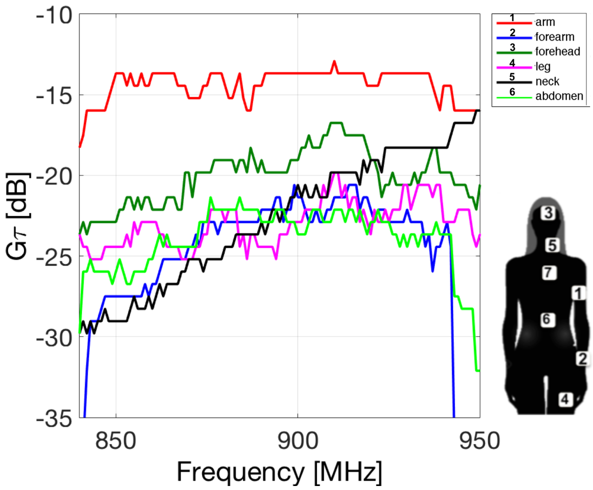

Figure 3.16: Variability of the measured realized gain of the epidermal tag when attached onto different body regions of a thin female volunteer.

3.5.2 Measured performance compared with body mass

The measurements were repeated for the four volunteers when the epidermal tag was attached onto arms, legs and abdomen. The resulting realized gains (Fig. 3.17) are sensibly different in scale and peak position, when varying both the placement of the tags as well as the body size of the user, as previously obtained in simulations. The tag placed onto the female and normal male volunteers exhibits, on average, better performance in comparison with the muscular man. The tag placed onto the two female volunteers provides comparable results in all the three configurations. Differences among male and female volunteers are particularly visible for arm and leg placement, in agreement with simulations. In case of abdomen there is instead no apparent difference since water-rich tissues dominate in both men and women. The placement over the leg provides instead the highest gain which approaches -9 dBi in the case of the thin woman because of the larger content of fat tissues. The maximum read distances, estimated in free space from the measured realized gains in Fig. 3.17 are summarized in Table. 3.5. We assumed the reader emitting 3.2 W EIRP, which is the maximum power allowed by the European regulation, and a polarization mismatch of 0.5. In all the cases the read distance is close to 1m and more, so that the UHF-RFID epidermal technology is suitable for comfortable and robust interrogation procedures.

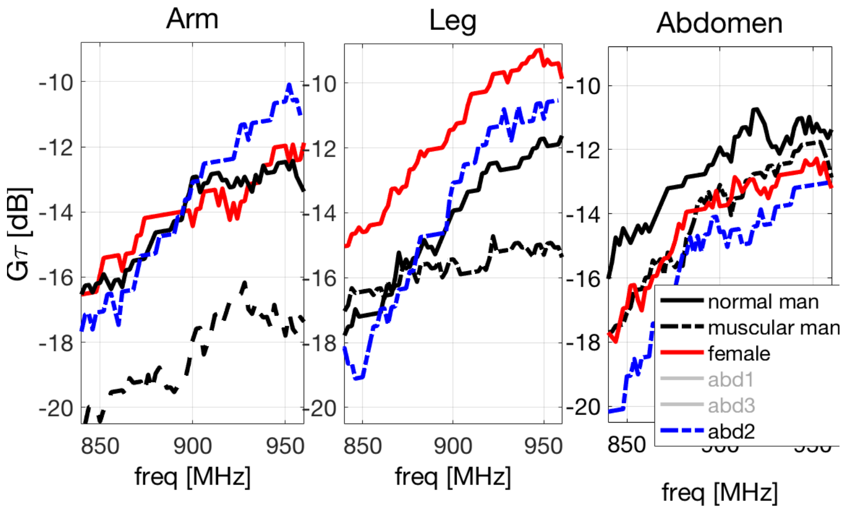

Figure 3.17: Variability of the measured realized gain of the epidermal tag when it is attached onto corresponding body regions of the four volunteers.

Table 3.5: Estimated maximum read distances (in meters) when the reader emits to 3.2 W EIRP

	arm	**leg**	**abdomen**
thin female	1.6	2.2	1.4
robust female	1.9	1.8	1.4
normal man	1.5	1.6	1.7
robust man	0.9	1.1	1.6

3.6 On-skin retuning

Previous simulations and experiments suggest the need to provide the antenna with some retuning capability in order to obtain a true communication-reliable epidermal device whose response is independent on the working frequency, on the specific position over the body and also on the user's mass. A new family of self-tuning UHF microchips is becoming available on the market. They have the capability to automatically adjust the chip capacitance in order to partially compensate for possible antenna mismatch. This emerging technology looks promising for epidermal devices. Anyway, epidermal tags are mostly envisaged for sensing applications besides the mere identification and the few RFID chips capable to handle sensors are not currently equipped with self-tuning. Therefore a more general-purpose tuning procedure needs to be developed. A post-fabrication and, possibly, post-placement retuning should be activated case by case, without removing the tag from the body. The considered tag consists of two loops and therefore the antenna impedance cannot be simply adjusted by trimming portion of the conductor length, as typically done with dipoles, since the galvanic continuity of the loop has to be preserved. Starting from the observation (Fig. 3.18) that the simulated surface currents flowing over the inner loop are more intense in the inner perimeter, a perturbation of such a profile is expected to change the equivalent self-impedance of the loop and of the mutual inductance between the two coupled loops. The input impedance of the epidermal tag will be modified accordingly. A practical way to implement this idea in a controllable manner is partitioning the segment of the inner coil, which is closely coupled with the external loop, into some equal-size pre-cut strips (Fig . 3.18). They could be easily removed, even after placement over the body, without affecting the tag integrity. Fig. 3.20 shows the simulated changes of the power transfer coefficient for the epidermal tag when the strongly coupled subregion of the inner loop (a=24 mm, b=12 mm) was enlarged and partitioned into six strips of size 20 mm x 1.9 mm and one strip was removed at time. The tag was again assumed as placed onto the layered geometry as in Table 3.1. The peak of the power transfer coefficient τ shifts toward the lower frequencies with even some improvement in the maximum value. As a result, the operating region of the tag may be freely modified within the whole UHF RFID band without changing the most part of the antenna and hence providing a viable means to achieve an inter-operable device. A detail of the prototype of the tunable tag is shown in Fig. 3.20.

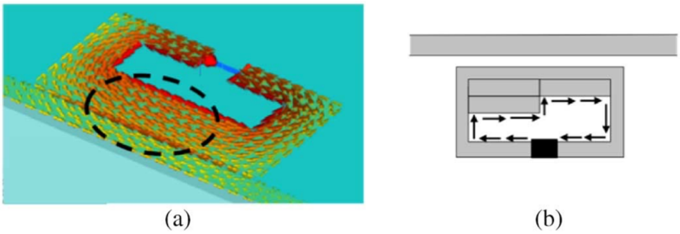
(a) (b)

Figure 3.18: (a) Zoomed view of the simulated current of the feeding loop. (b) The black arrows show how the path of the excitation currents can be modified by removing/adding equal sized strips made of conductor.

The pre-cutting of the inner loop is expected to produce a perturbation in the path of the surface currents since the galvanic integrity has been partially altered by discontinuities which are induced within the copper foil. Indeed, the tag performance, evaluated for application over the liquid body phantom as above, was different with respect to the continuous loop, as clearly visible in Fig. 3.19. In particular, the cuts produced a down-shift of the frequency response of the antenna, due to the increased current path around the strips, as in meandered antennas. This behavior can be however easily numerically modeled by including a 100 μm air gap among the strips and the results compare reasonably well with measurements. By removing the strips, the realized gain translates toward lower frequencies (Fig. 3.21) as expected from simulation in Fig. 3.21. Experiments started with the six-strips tag configuration, which theoretically peaks outside the frequency window of the measurement allowed by the considered reader. The realized gain is then gradually tuned to the Japanese band (952-956 MHz) by removing two strips, to the US band (902-928 MHz) by removing three strips and finally to the EU band (865.6 - 867.6 MHz) by removing four strips.

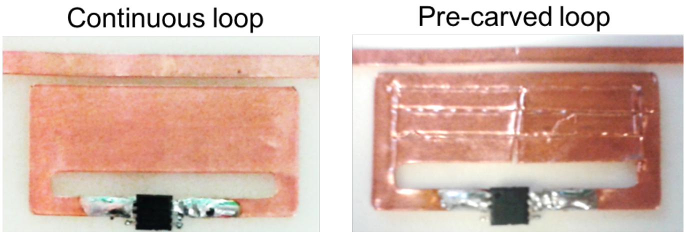

Figure 3.19: Measured realized gain of a double-loop epidermal tag with pre-cut inner loop in comparison with its continuous version. Tags were placed over the liquid phantom box as previously described, and three measurements were performed for each prototypes.

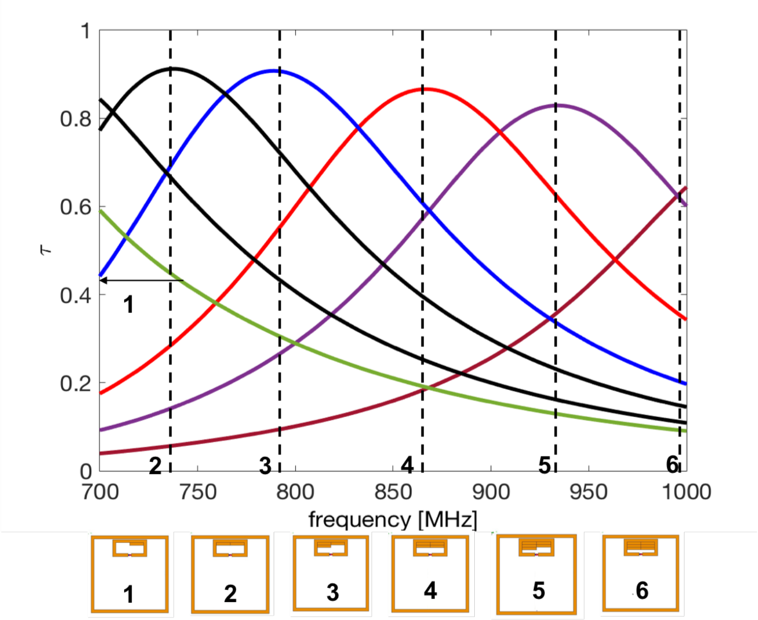

Figure 3.20: (a) Detail of the inner loop of the epidermal tag that has been pre-cut into six strips of size 20 mm × 1.8 mm and (b) its continuous version, used for comparison.

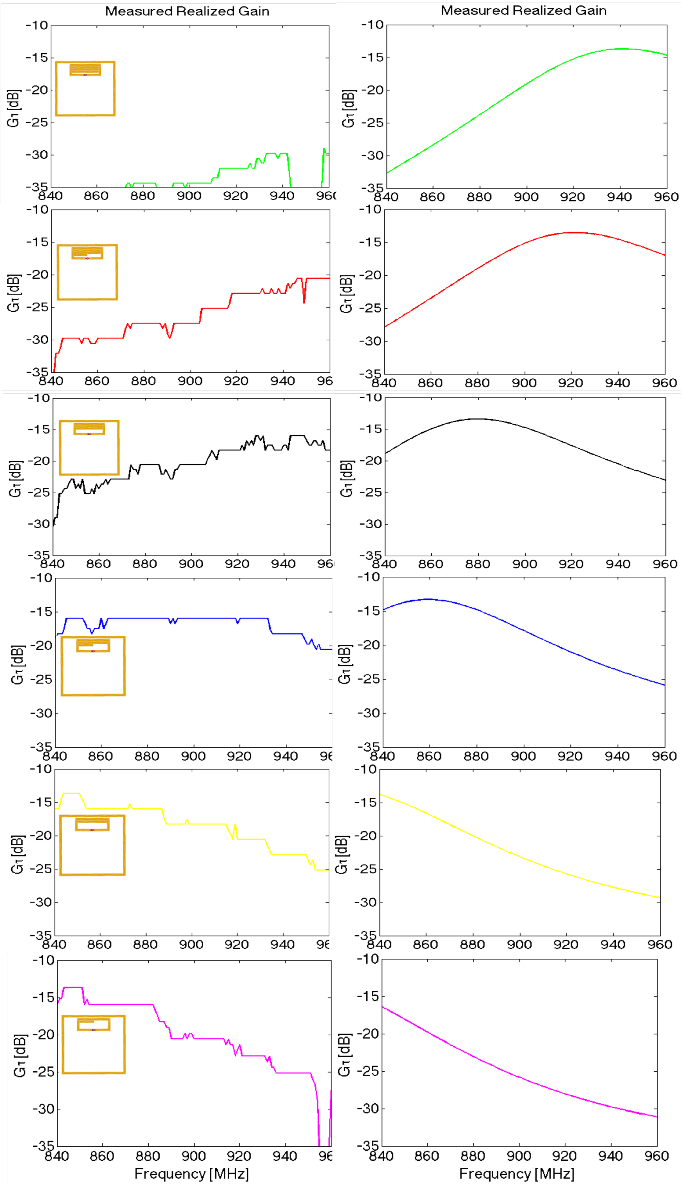

Figure 3.21: Characterization of the tuning method: measured realized gain of the epidermal tag placed over liquid phantom mimicking human tissues. From the top to the bottom and from the left to the right side the pre-carved strips are subsequently removed and, accordingly, the peak value of the $G \cdot \tau$ shifts downwards.

3.7 Examples

Some examples of frequency retuning are finally given for application of the epidermal tag onto the volunteers. Experiments considered the improvement of performance when

i) the realized gain of the tag placed at a given position is initially rather poor;

ii) the same tag needs to be used in different RFID band (USA or EU).

3.7.1 Tuning at a given position

The unperturbed tag (e.g. with all the six strips) was stuck onto the hip of the female volunteer. The peak of the realized gain occurred at 950 MHz, with a poor maximum value close to -20 dBi (a worse case than those experimented before)(Fig. 3.20. An improvement of more than 4 dB was achieved by removing only a single strip and the read distance is consequently increased of about 1.5 times.

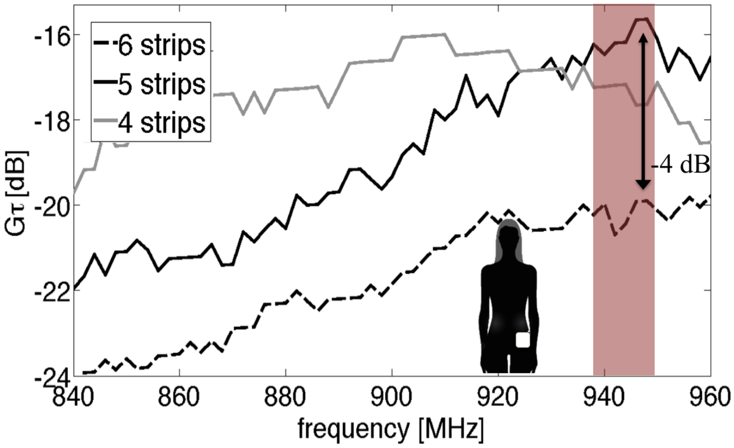

Figure 3.22: Example of on-skin retuning at 950 MHz when the epidermal tag in Fig. 3.20 was applied over the hip of the “woman” volunteer.

3.7.2 Change of the UHF band

A new tag in its initial full configuration was then attached onto the arm of the same volunteer and looks well matched in the US band (realized gain of -13 dBi). Three strips were removed (Fig. 3.23) in order to have the tag tuned in the EU band (realized gain at 870MHz equal to -13 dBi).

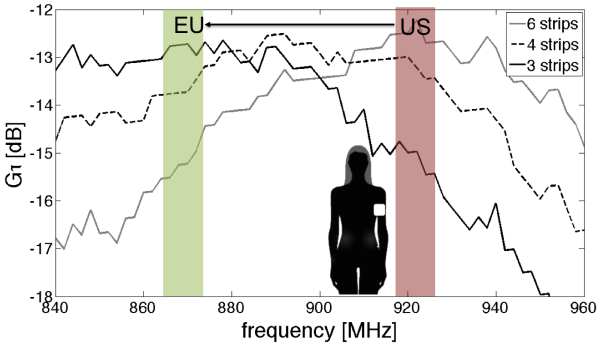

Figure 3.23: Example of on-skin retuning from US to EU band of the epidermal tag placed onto the arm of the woman volunteer.

Finally the tag was applied onto the leg of the *normal* male volunteer. Antenna tuning in the Japan and US bands (realized gain close to -12 dBi) was achieved by four strips and two strips configurations, respectively (Fig. 3.24).

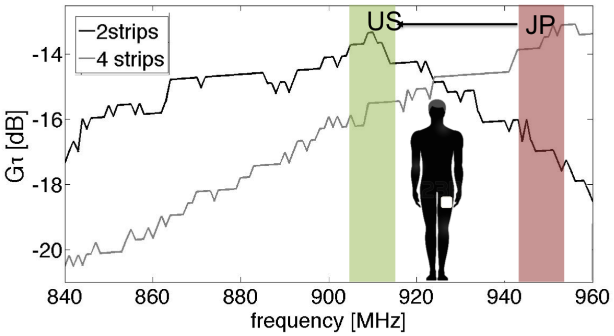

Figure 3.24: Example of on-skin retuning from 950 MHz to the US band when the epidermal tag in Fig. is applied over the "normal" man's leg

3.7.3 Overall analysis

The results of previous experiments can be summarized as in Tab. 3.6 to better highlight the effectiveness of the on-body retuning. The application of a same tag on different users and on different regions of the body (hip, arm, leg) really benefits at 950 MHz of the retuning (5, 6, 4 strips, respectively) with an overall nearly stable realized gain. The tag with 4 strips is suitable to multiple applications over hip and arm of the thin female volunteer at 870 MHz and at 900 MHz as well as to the leg of the normal man but at 950MHz. In all cases the read range performance will be reasonably similar.

Table 3.6: Summary of the strip numbers and (measured realized gain) for some placements and frequencies

Placement	870 MHz	900 MHz	950 MHz
thin female, hip	4 (-17 dBi)	4, (-16dBi)	5, (-16dBi)
thin female, arm	3 (-13 dBi)	4, (-14dBi)	6, (-14dBi)
norm. man, leg	2 (-15 dBi)	2, (-14dBi)	4, (-15dBi)

3.8 Conclusions

Unlike shielded wearable tags, epidermal antennas revealed as significantly sensitive to the placement conditions. Simulations and experiments demonstrated that loop-like epidermal tags, insulated from the human skin by just a thin membrane, provide a realized gain ranging between -17 dBi and -9 dBi depending on the body region where it is placed and on the body mass of the user. Limbs and arms are the most suitable targets for what concerns communication properties and the epidermal tag may be used for general purpose applications involving just identification or even for the wound monitoring or controlled transdermal drug-delivery. Placement over thorax, forearm and forehead, which could be relevant for instance at the purpose of temperature measurement, are more critical concerning the RFID link and may hence greatly benefit of on-body retuning. In real applications we may envisage an epidermal tag tuned by default at high frequencies (for example around 960 MHz). After the placement of the tag over a given body region the user will have a few degrees of freedom in sequentially removing some strips until the tag is read. This tool will adapt a unique epidermal tag to different kinds of placements and frequency bands thus making its mass production more affordable.

4

The FSS, a battery-assisted alternative for continuous monitoring systems

4.1 Introduction, background and related work

The methods of communication for medical sensors are habitually based on commercial Bluetooth, Wi-Fi, and Zigbee technology, which allows sending data to a gateway and storing them on databases, using a few amounts of energy. Often, a continuous transmitting is necessary to evaluate body parameters and then these technologies are not so adequate, since one of the most critical issues is a limited battery lifetime claimed by users, due to the power consumption of the micro-controller and the transceiver, especially in continuous long-term monitoring applications. Passive UHF RFID tags equipped with sensors have been proposed to bypass this constraint [42, 5, 38]. Although their performances are still limited in comparison with commercial sensors, the second important advantage of these devices consist of their lower cost and versatility.

One of the most significant challenges in wireless devices for wearable applications involves the effect of the body on electromagnetic propagation. This effect is particularly evident on the detuning of the antenna, which drastically reduces the antenna efficiency (for example in dipoles or monopoles) [88]. These effects produce a noticeable reduction in read range for the UHF tags. In some cases the RFID devices may not receive enough energy to wake up the internal integrated circuit [5, 89]. Passive UHF-RFID tags gather the power from the RF interrogating signal, which reduces the read range, and consequently, their applications are sharply limited. Some of those restrictions can be overcome by using semi-passive or battery-assisted tags (BAP). In general, RFID tags have two methods to increase the received power: by acting on the dimensions of the radiators or by using dielectric substrates that also improve the received power. Both the methods work on the radar cross section (RCS). However, it can reduce the bandwidth, and consequently reduced the sensing range.

Several types of antennas, which are compatible with wearable applications are specifically designed to prevent this condition. Little spacers, which are few millimeters thick can be located between the antenna and the body. They have been employed to reduce the losses caused by the body and thus increase the antenna efficiency. Furthermore, the thickness of these antennas and the multilayer designs bounds their uses as discussed in the previous chapter. Another method, which has been used in this work, is based on communication techniques that uses special structures called *frequency selective surfaces* (FSS). These structures can be engaged to avoid the power needs of the IC circuit in RFID tags. The FSSs are periodic structures in each direction of the plane, which act as filters [90]. This properties have been exploited in several applications [91, 92, 93]. FSS can be frequency tunable, introducing some switching (e.g. PIN diode) [94] or tuning elements (e.g. varactors) [95]. Recently, the FSS modulating properties are also proposed in millimeter-wave communications [96], terahertz applications [97] and radio Identification (RFID) tags design [98, 87]. In [99], FSSs are used to design FMCW radar transponders, where the bandwidth of the FSS is required to achieve high resolution. In recent works, FSS can also be used to modulate the amplitude of signals. Depending on the diodes state, the frequency response of the FSS is shifted. On the other hand, the FSS can increase the read range by modifying their RCS without acting on the substrate or their dimension. This property allows keeping a low profile on the tag. FSS can improve their performances by increasing its differential RCS. The differential RCS is the difference between the RCS of the radiators considering the two FSS states which are deteriorated by the diodes states. The price of this solution is an increase of the number of diodes. However, reasonable values of RCS can be accomplish with a few numbers of dipoles. Therefore, a large differential RCS can be carry out over a large frequency bandwidth. Since FSS based sensors can achieve a low power consumption for the reduced number of components, new energy harvesting methods can be engaged to power the sensor blocks. The FSS uses reverse-biased varactor diodes instead of PIN diodes to reduce the current consumption. A simple FSS tag consists of an array of dipoles loaded with reverse-biased varactor diodes connected to a low-frequency oscillator. Therefore, the communication is performed by modulating the radar cross section with backscattering. A semi-passive tag based on a modulated FSS is proposed for sensing [33] In previous works [98], it is demonstrated that FSS on contact with the body can achieve large bandwidth avoiding the typical detuning problem of narrow-band tags. Also, FSS can be printed on a flexible thin-film substrate that allows the integration of textile clothing, making it a flexible and comfortable option. The oscillation frequency of the oscillator, which modulates the FSS, may be used to sense various parameters.

This Chapter discusses two examples of FSS-based sensors for on-body sensing applications in order to increase the read distance and reliability, the most significant issue of the RFID tags. The first example involves a temperature sensor, which has been tested to be placed on the arm, making a comparison with the RFID technology. The second application regards the sensor for sleep disorders detection, which considers an FSS-based sensor to detect the respiration rate during sleep. The prototype has been fabricated and tested.

4.2 Design of sensors for FSSs communication

4.2.1 Operation principle

A generic system consists of a reader (details of the reader in section 4.3.1) and either one or more transponders (tags) based on FSS technology to be placed onto the skin. The reader produces a continuous wave (CW) that illuminates the tag with frequency f_c, which answers by modulating the backscatter of the FSS radar cross section (RCS).

The backscattered field (E_s) at the FSS can be expressed as a sum of two terms : a load-independent term (structural mode) E_{est}, and a load-dependent term (antenna mode), $E_m\Gamma$.

$$\overline{E}_s = \overline{E}_{est} + \overline{E}_m\Gamma \tag{4.1}$$

Where Γ is the complex power reflection coefficient of the diodes that load the dipoles of the FSS, which is modulated by switching the diodes using a low-frequency oscillator (with oscillation frequency f_m,). Varactor diodes in reverse bias are used as alternative to PIN diodes to reduce the current consumption. Then Γ changes between Γ_{ON} and Γ_{OFF} when the diodes are ON and OFF, respectively. The reflection coefficient can be approximated by a square waveform with amplitude $\Delta\Gamma = \Gamma_{ON} - \Gamma_{OFF}$ and frequency f_m and duty cycle δ. This reflection coefficient is a periodic function that can be decomposed in a Fourier series:

$$\Gamma(f) = \sum_{n=-\infty}^{+\infty} c_n \delta(f - (f_c - nf_m) \tag{4.2}$$

where c$_n$ are the Fourier coefficients. For a square waveform, the backscattered field can be written using 4.1-4.2 as [99]:

$$E_s = (E_{est} + E_m \Gamma_{avg})\delta(f - f_c) + Em \sum_{n \neq 0} \Delta\Gamma(\frac{\sin n\pi\delta}{n\pi\delta})\delta[f - (fc + nfm)]$$

where Γ_{avg}= $(\Gamma_{ON}+\Gamma_{OFF})/2$ are the average and difference in the power reflection coefficient between ON and OFF states, respectively.

Therefore, the spectrum of the backscattered field by the FSS is composed by several sidebands around the central frequency of the illuminating signal (Fig. 4.1). The frequency spacing between each sideband is f_m. The higher amplitude is produced in the first sideband. The received power at this frequency can be estimated as in conventional RFID systems using the radar equation and it is proportional to the differential radar cross section, RCS$_{dif}$. The differential radar cross section can be calculated using electromagnetic simulator from the difference between the backscattered fields for the two diodes states:

$$RCS_{dif} = \lim_{r \to \infty} 4\pi r^2 \frac{\left|\bar{E}_{S,ON} - \bar{E}_{S,OFF}\right|^2}{\left|E_{S,ON}\right|^2} \tag{4.3}$$

The modulation frequency depends directly on the backscattered signal, which is demodulated using a homodyne receiver, and then converted to baseband with a mixer and digitized using an A/D converter.

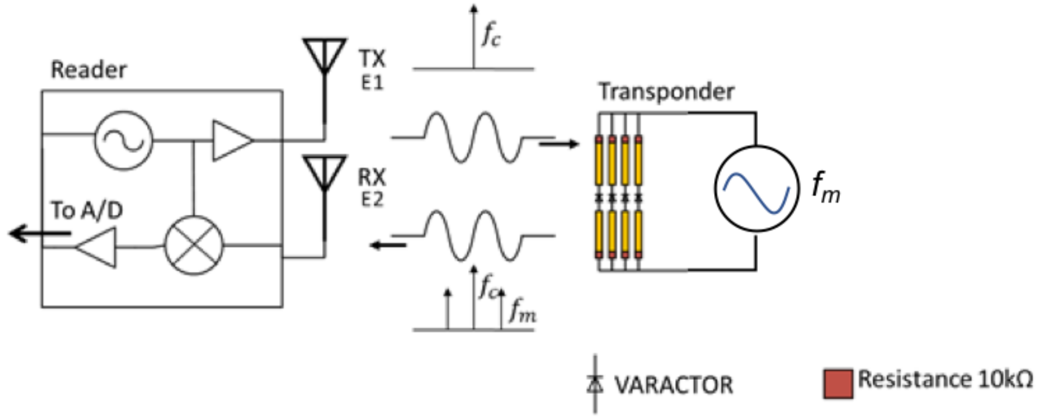

Figure 4.1: Block diagram of the system, including the reader and the FSS

4.2.1.1 Design and simulations of FSS at 2.4 GHz

In order to correctly design an FSS by using a numeric simulation, the diodes are inserted as a lumped elements whose component values change between the two diode states (ON and OFF). In the prototype, low-cost silicon varactors from Skyworks SMV1247-079LF are used. The diodes are taken into account as lumped RLC boundary conditions in the electromagnetic simulations. Their capacitance is 6.5 pF and 0.95 pF for V=0 (ON state) and V=-3V (OFF state), respectively. The parasitic inductance and resistance are 0.7 nH and 2 Ω. These values are obtained from the datasheet of the diode manufacturer. As a proof concept, an FSS has been implemented using a 100 µm thickness Ultralam® 3850 substrate and computer-simulated. 10kΩ 0605 SMD resistors are connected at the end of the arms of the dipole to feed the diodes and block the RF signal (Fig. 4.2). The feed line is orthogonal to the dipole direction to avoid interference in the backscattered field. The dipole length is adjusted to resonate at about 2.45 GHz. Its length (l) and width (w) are 25.6 mm and 2 mm respectively. The dipoles are spaced s=10.24 mm. Fig. 4.3 shows the design of the simulations about different FSS with different number of dipoles using a body representation. Body is simulated on HFSS using material properties in Table 4.1. It can be observed that the differential RCS increases with the number of elements and a small frequency shift is observed that can be compensated changing the dipole length (Fig. 4.5b). Fig. 4.4 show a consistent difference between total RCS and differential RCS. A large bandwidth is obtained. In this simulations, it was assumed that the surface over the FSS was laid, was a flat (or quasi flat) surface (Fig. 4.3).

Layer	**Thickness (mm)**	**Relative Permittivity (ϵ_r)**	**Dissipation loss tangent ($tan\delta$)**
Skin	1.5	42.8	0.27
Fat	1.5	5.3	0.14
Muscle	15	52.6	0.24

Table 4.1: Dielectric properties of arm used in simulations (around 2.45 GHz)

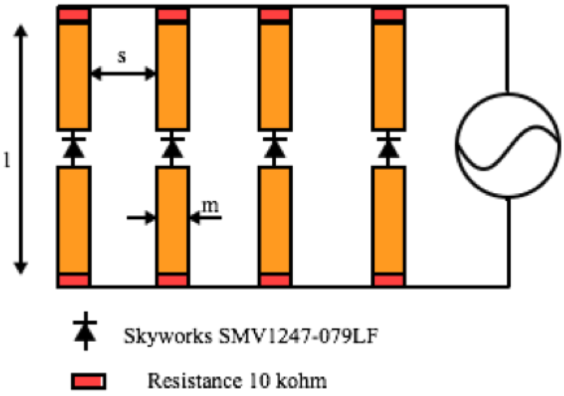

Figure 4.2: Layout and basic principles for the FSS-based sensor

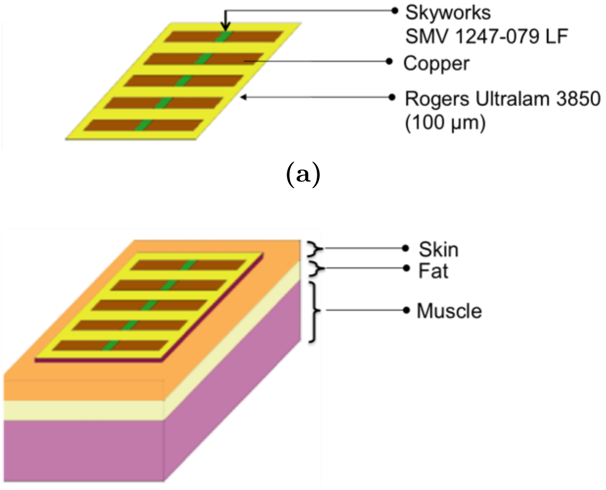

(a)

(b)

Figure 4.3: Structures simulated in HFSS: (a) dipoles on substrate in free space, (b) FSS transponder placed on body model with a different thickness of spacer.

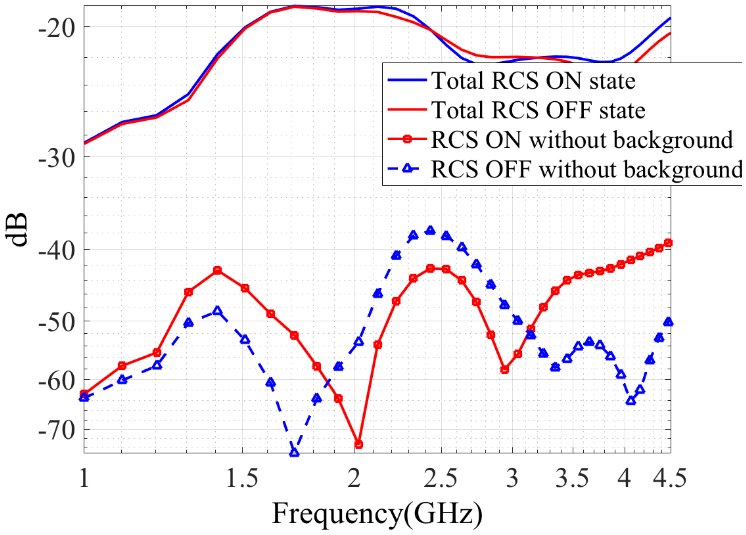

Figure 4.4: Total RCS and RCS after removing the background for the two diode states on/off

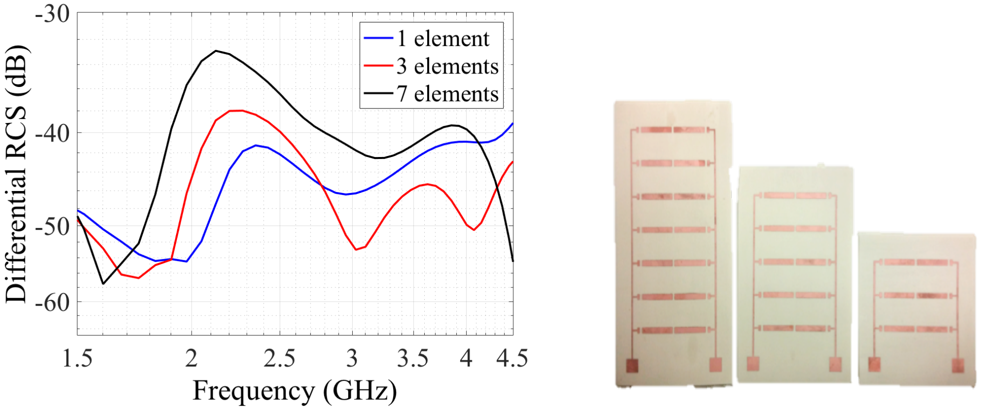

(a) **(b)**

Figure 4.5: Differential RCS as function of the frequency for different number of elements (a) Measurement for different number of dipoles (b) Tested prototypes

4.2.1.2 Simulation on curved body part

One of the most interesting locations for wearable devices is onto the arm, integrated into a belt or around the wrist. In order to study the performance of the FSS transponder in different curved parts of the body, various simulations on a cylindrical human model are performed. The body model (Fig. 4.6a) is simulated using a cylindrical multilayer shape surrounded by an FSS transponder composed by seven elements. The properties of the different tissues are specified in [98]. The incident plane wave illuminates the transponder around the model (it starts in front of the transponder, Fig. 4.6a.). The angular dependence obtained for different frequencies is presented in Fig. 4.6b. It is observed that, when the incident wave arrives from the front side, the power reflected is higher. On the other hand, when the incident wave arrives from the opposite side where the transponder is placed, the power reflected is minimum due, for the majority, to the absorption losses of the body. As a result, a power radiation of -3 dB beam width of 60° is observed.

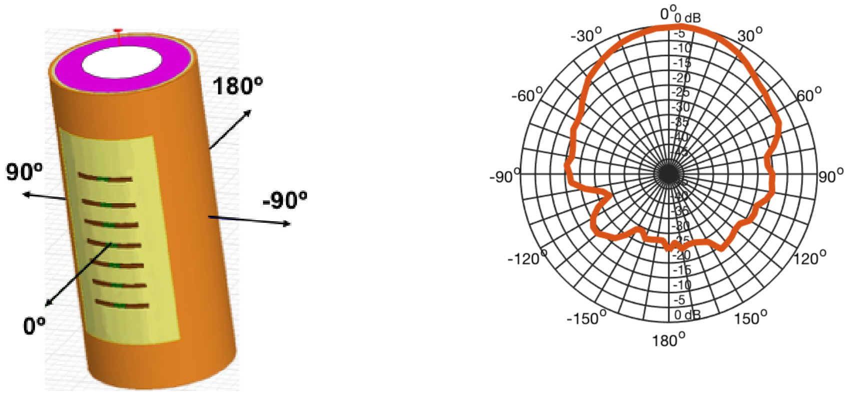

(a) **(b)**

Figure 4.6: (a) Model of the arm used in the simulations, (b) normalized differential RCS as function of the angle [98]

4.2.1.3 FSS Characterization

For the test, the FSS is fabricated on a flexible substates on Ultralam® (Fig. 4.8) and it is modulated with a low-frequency generator (Agilent 33521A) at f_m= 5 kHz, 3 Vpp. A CW generator that transmits a power of 10 dBm at 2.45 GHz using an 8 dB gain antenna illuminates a prototype with 7 dipoles. Fig. 4.7b shows the signal received at the spectrum analyzer (centered at 2.45 GHz) for two different distances of the reader-tag; 1.6 m and 4.8 m [98]. A strong central peak and two sideband peaks (spaced f_m) are observed. In order to characterize the frequency response of the modulated RCS, the FSS is illuminated in a range of frequencies that varies from 1 to 4.5 GHz. Two cases can be observed in Fig. 4.3: FSS directly in contact with the arm and the other one separated by a spacer of 2 mm from the arm (Fig. 4.9). The measurements are performed at a distance of 1 m between the reader and the transponder (Fig. 4.9). The measured power is similar in both cases, but when the FSS is in contact with the arm, its spectral response is shifted (the band pass is centered around 2 GHz) and the bandwidth is lower compared to the case where the FSS is separated by the spacer.

(a)

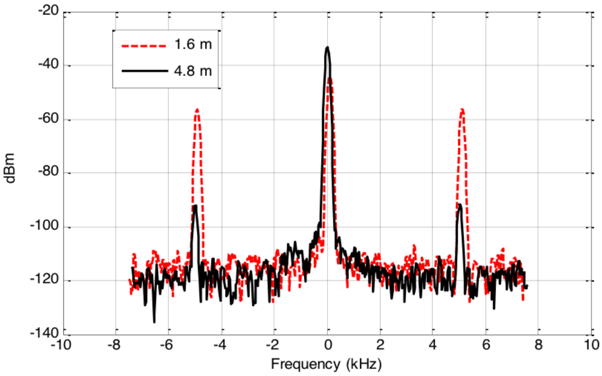

(b)

Figure 4.7: Measurement of the backscattering signal (a) Experimental setup (b) Signal Spectrum measured for different distances

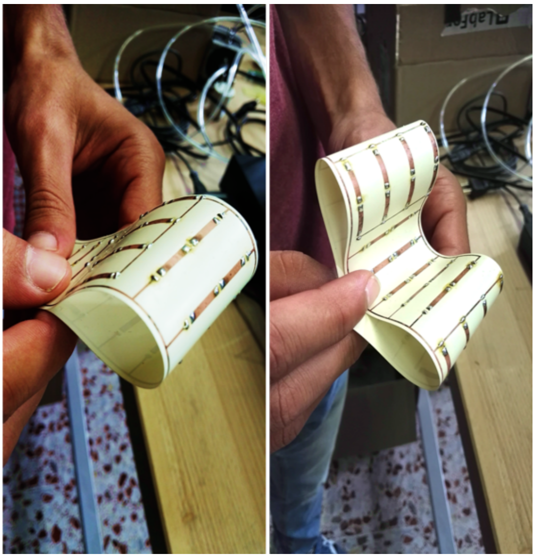

Figure 4.8: Photography of printed FSS on Ultralam®, flexible and solderable/weldable substrate

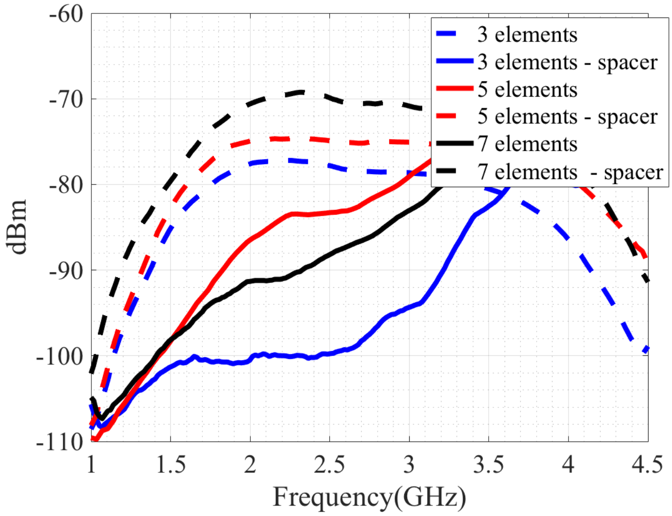

Figure 4.9: Comparison of FSS structure with spacer and without spacer considering different number of dipoles

4.2.2 FSS design for UHF RFID band

One of the most critical features of wearable devices is the capability to be placed on clothes or directly onto the skin. The FSS is a straightforward method to displace transmitting from sensing while still having a reasonable reading distance. Therefore, it can be used to communicate information about body parameters at a certain distance from the body. A good result has been achieved by using a 2.4 GHz ISM band. An FSS mounted on the arm, which is capable of measuring temperature variation has been already created. The advantage of using this band is the higher power allowed by the regulation compared with 2.4 GHz ISM band. To investigate the possibility to use the FSS in the RFID UHF band to sense body parameters, a modified FSS has been designed. The following steps are performed to test the design.

4.2.2.1 Electromagnetic simulations

Computer simulations and performance analysis of the backscattered field for UHF FSS have been performed in order to fabricate a suitable shape to be laid on the body. An FSS, which is built on a 100 µm thickness simulated layer of Ultralam® (ε_r =2.9, tanδ=0.0025 at 866 MHz) has been considered. In the implementation of the first prototype, which operate at 2.4 ISM GHz, the shape of the FSS is optimized, and calibrated to be placed in the air, and later, to be laid on a non-conducting surface (materials with inhomogeneous electromagnetic properties). A computer simulation of an FSS, which has been used for a UHF application, has been designed. In order to maintain a similar structure for operating around the UHF band, the proposed FSS need to have a bigger size, while the electromagnetic properties of the tissues (Tab. 4.2) to be placed with the characteristic at UHF Band. Electromagnetic simulation of five dipoles FSS printed on Ultralam® substrate and placed on a simulated planar multilayer body (Fig. 4.11) have been performed.

Table 4.2: Physical and geometrical parameters of the layered anatomical model at 870 MHz [5]

Layer	ε_r	tanδ	Thickness (cm)
Skin+fat	41	0.42	1.5
Fat	5.4	0.19	1.5
Muscle	55.1	0.44	15
Bone	20.8	0.33	15

Around these frequencies, the dimension and the shape of the radiators must be greater to achieve the same performance and consequently are more critical. A bigger surface, which is placed over the body can be uncomfortable for the user. By optimizing the dimension of the radiators, a tradeoff between performance and size can be obtained (Fig. 4.10). The method to analyze the electromagnetic simulation of an FSS and its modulation is entirely explained in [98]. Different simulations were run to examine the effect of the body on the FSS performances. A planar multilayer body model has been computer-generated. Considering few millimeters of distance between body and clothes, the FSS has been placed around 1 cm by the body (Fig. 4.11). The simulation demonstrates a reasonable RCS (Fig. 4.13), considering the same varactor model (Skyworks SMV1247-079LF) used for the simulations in the ISM 2.4 GHz band (Fig. 4.12). Therefore, a prototype has been fabricated and tested following the procedure used for the prototype at 2.45 GHz. From the scratch, the metallization was printed on a Ultralam® substrate, and then, the lumped components were soldered. Figure 4.16 shows the fabricated FSS.

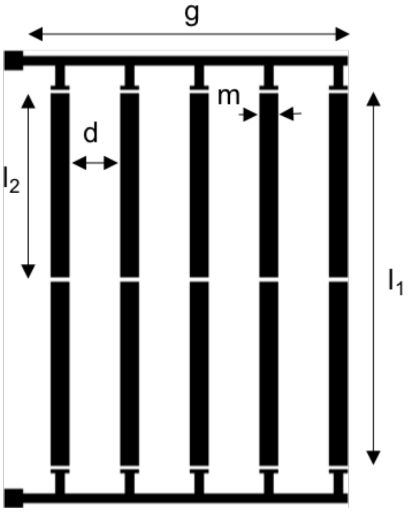

Figure 4.10: Layout of the tag. The dimension are: $L_1 = 83\,mm$, $L_2 = L_1/2$, $m = 9\,mm$, $d = 21\,mm$, $g = 93\,mm$.

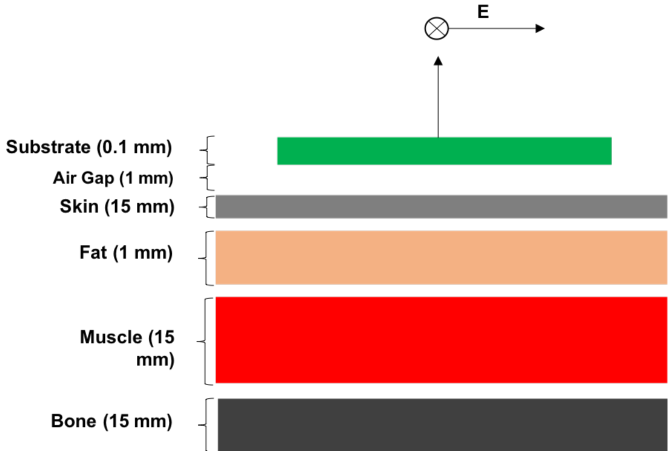

Figure 4.11: Model of the Body. Size [mm]: $Substrate = 0.1$, $Air\,Gap = 1$ $Skin = 15$, $Fat = 1$, $Muscle = 15$, $Bone = 15$.

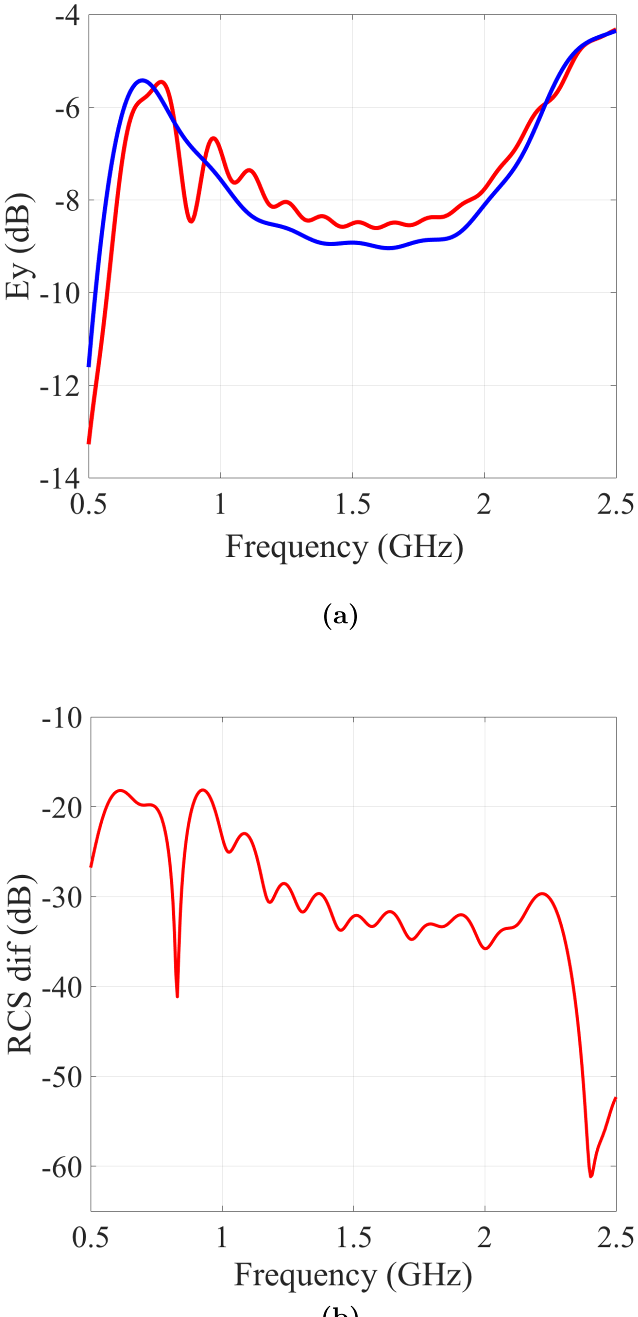

(a)

(b)

Figure 4.12: (a) Electric field without background. State ON (Blue), State OFF (RED) (b) Calculated Differential Radar cross section Of the model .

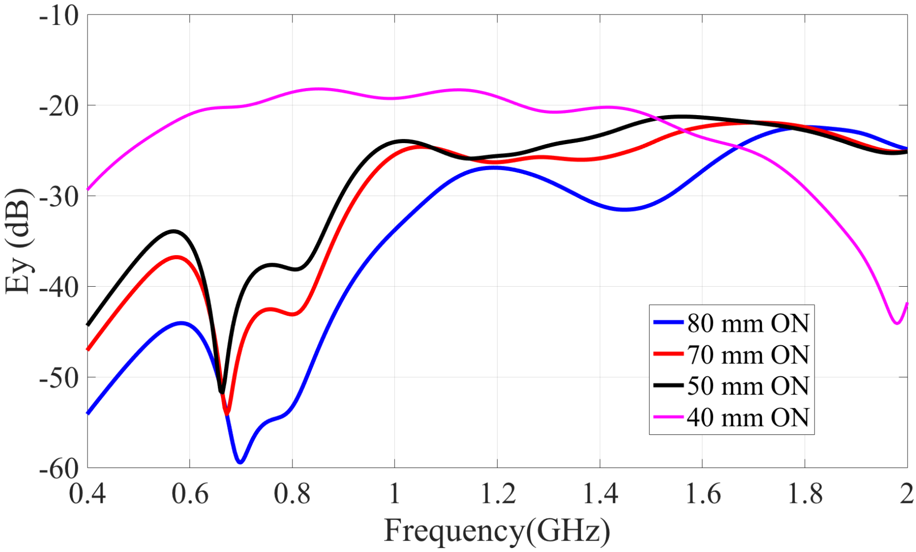

(a)

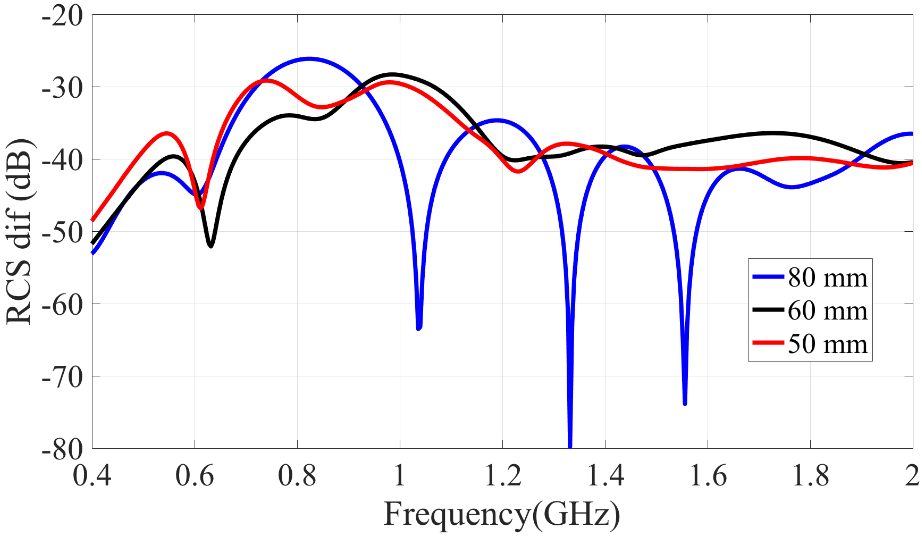

(b)

Figure 4.13: (a) Electric field after background subtraction. State ON and State OFF, for different length: black (40 mm), Red (50 mm), Blue (80 mm), Pink (25,6 mm) (b) Calculated Differential Radar cross section of the model.

4.2.2.2 Performances measurement

Figure 4.14 shows the scheme for the performed measurement. A sinusoidal wave signal generator is used to illuminate the FSS at UHF band by radiating power accordingly with the electromagnetic limitations, while a low-frequency signal generator (square form) modulates the FSS around 4 kHz. The backscattered signal is received by using a wide-band antenna and demodulated with a mixer. The signal is sampled by the spectrum analyzer and processed with MATLAB tools to obtain the modulation frequency. Two configurations are tested; bistatic and mono-static. A first configuration used a waveform generator to simulate the sensor modulation, a spectrum analyzer to demodulate the signal, two wide-band Vivaldi antenna for transmitting and for receiving, and a signal generator, which are used to receive, demodulate and process the data. The second configuration considers the mono-static case (Fig. 4.15).

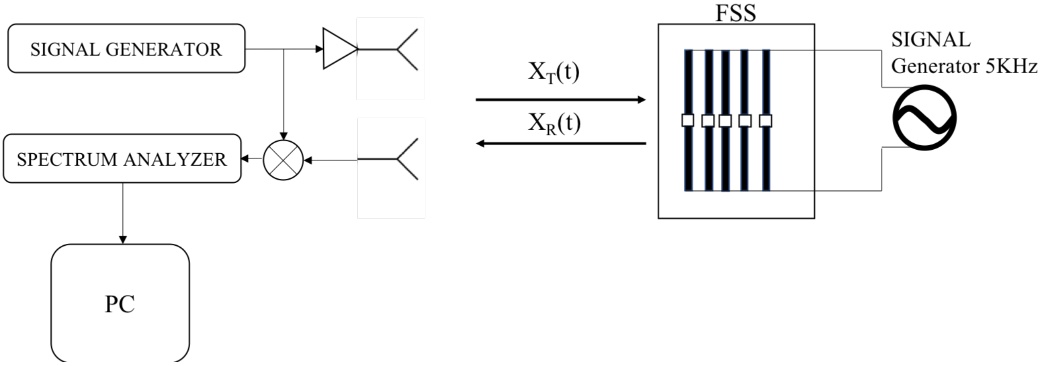

Figure 4.14: Measurement configuration 1

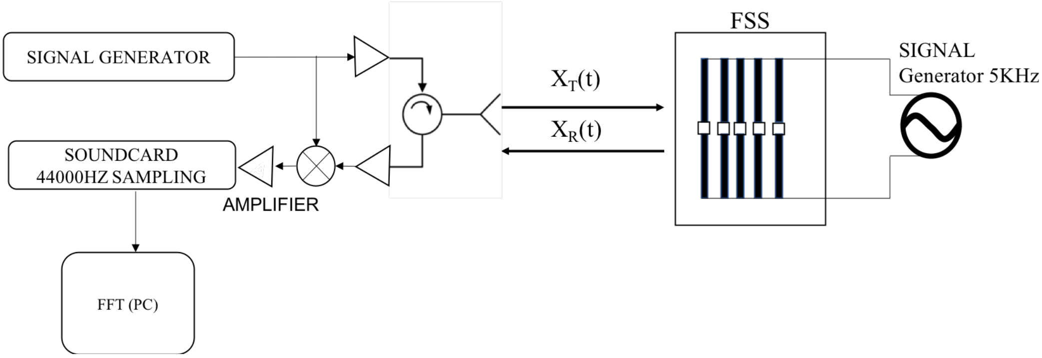

Figure 4.15: Measurement configuration 2

In this configuration the waveform generator (substituted with a PLL generator) is employed to illuminate the tag and the signal generator (square form) with an electric amplifier to modulate the FSS as explained in the first case. A circulator allows to use a single circular-polarized antenna at UHF band (around 865 MHz EU band) for transmitting and receiving. A soundcard is used for sampling, and MATLAB tools for the signal processing (FFT). In this configuration the use of a circular polarized antenna avoids the influence of tag orientation. A signal generator, which has been set up to oscillate at the frequency of 5 kHz is connected to the FSS by two wires driving a square wave voltage between 0 and -3 Volts. A waveform generator creates the signal for the transmitter antenna which radiates in the direction of the FSS. The FSS modulates the signal collected by a second receiver antenna oriented in the same direction with the same polarization angle of the first one. A parametric frequency sweep has been cacluated to evaluate the carrier frequency to characterize the behavior of the FSS.

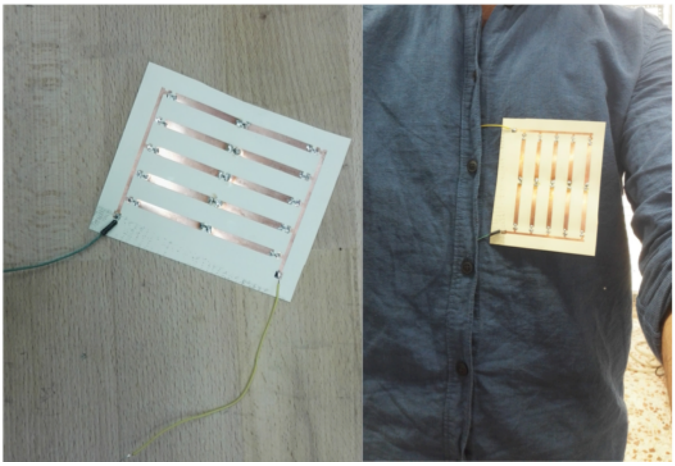

Figure 4.16: Photograph of the prototype

4.2.2.3 Experimental results

As Figure 4.17a demostrate, a wide-band is obtained when at least five dipoles are considered. Increased size of the FSS also improves the robustness of the signal allowing to achieve a reading distance of 4 m avoiding multi-path. The reading distance depends on the Signal/Noise factor, and it depends on the instrumentation used for measurement. Therefore, an improving of the receiver noise floor can be improved reducing the noise factor of the spectrum analyzer. In the second setup the noise factor is improved with respect the first configuration. The sound-card is faster than the instrumentation and it is also more accurate.

Another important fact is that the human body influences the backscattered signal absorbing most of the radiating energy. Usually, when a radiator is placed close to the human body, the radiation pattern is altered by the body due to its losses and the backscattered power is also reduced. Thanks to the increased dimension of the radiator, and the intrinsic nature of the FSS, which is very robust against the conductive and lossy material, the performances are increased. Figure 4.17b shows a comparison between the FSS placed in the air, and the same FSS placed onto the body. The presence of the body to the radiator, which is design to be in near vicinity to the skin, introduce a little frequency shift but it doesn't reduce the performance concerning the received backscattered power. Figure 4.18 shows the backscattering power for the FSS placed onto the body at 1 m.

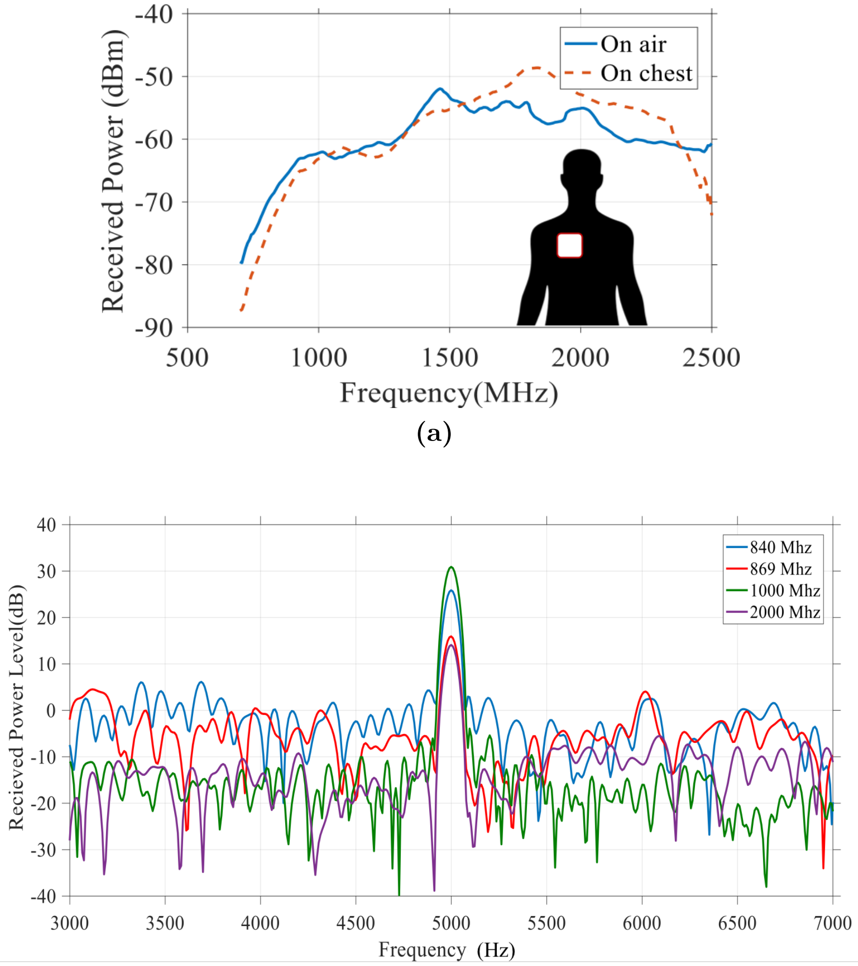

(a)

(b)

Figure 4.17: (a) Backscattering power measured with the spectrum analyzer as function of interrogating frequency, (b) Baseband spectrum at output of the mixer after Fourier transform of the recorded signal with the sound card.

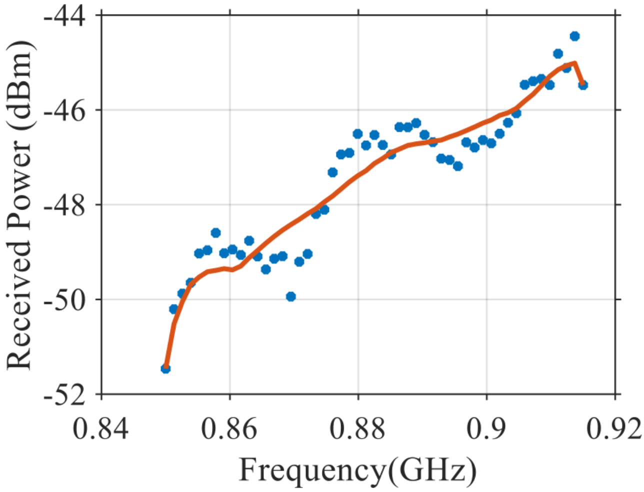

Figure 4.18: Received power in the second configuration in the range of UHF Band at 1.5 meters from the reader

4.2.3 FSS printed on clothes

Communication methods based on the FSS structure are versatile. Thanks to their simple shape and accessible design, the FSS can be easily included in textile materials. This feature can extend its range of application and their performance. To evaluate its achievements, a prototype of FSS has been designed and tested on a textile material for a wearable application. The textile substrate that has been used is DHJ PEARL with 110 µm thickness. The electrical properties have been measured using a cavity, the Damaskos Model 08 Thin Sheet Tester (Fig. 4.19), which measures the electrical parameters of low loss materials over the approximate band of 800-4000 MHz with a non-destructive practice. This technique is ordinarily used for thin dielectric sheets with thicknesses between 0.05 mm and 3 mm.

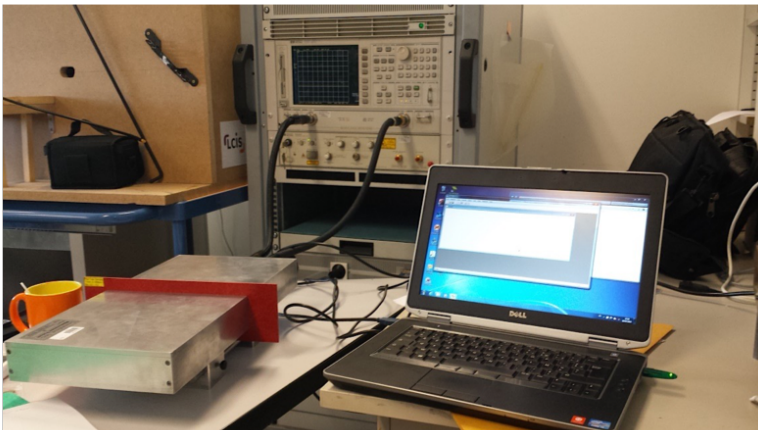

Figure 4.19: The Damaskos Model 08 Thin Sheet Tester

The followed procedure consists of taking three measures of each sample and perform an average of permittivity and loss tangent for each resonance. Table 4.3 shows the measured properties which are used of the electromagnetic simulation.

Table 4.3: Properties of the Textile Decoprint® *DHJ PEARL 110 μm*

Frequency $[GHz]$	ε_r	$tan\delta$
0,81	2,88	-0,0079
1,27	2,88	0,0231
1,89	2,88	0,0251
2,54	2,88	0,0206
3,22	2,87	0,0199
3,90	2,87	0,0194

4.2.3.1 Ink and Printing process

The FSS has been printed over the textile material with the facilities of the Ardeje® company, which has been involved in the consortium of the H2020 Emergent project. A customized printer, which can use a special conductive ink has been used for this purpose. The *Ardeje Origin D100®* (Fig. 4.20a) is an Hi-accuracy digital printing platform, which has been developed for R&D process development and prototyping. A dedicated GEN-4 printhead (Fig. 4.20b) can deliver approximately 7 pico-liter of a special conductive ink at 8m/s±15% velocity, with a Mechanical axis resolution (X/Y) around 0.5 µm, and Mechanical axis repeatability ±1 µm.

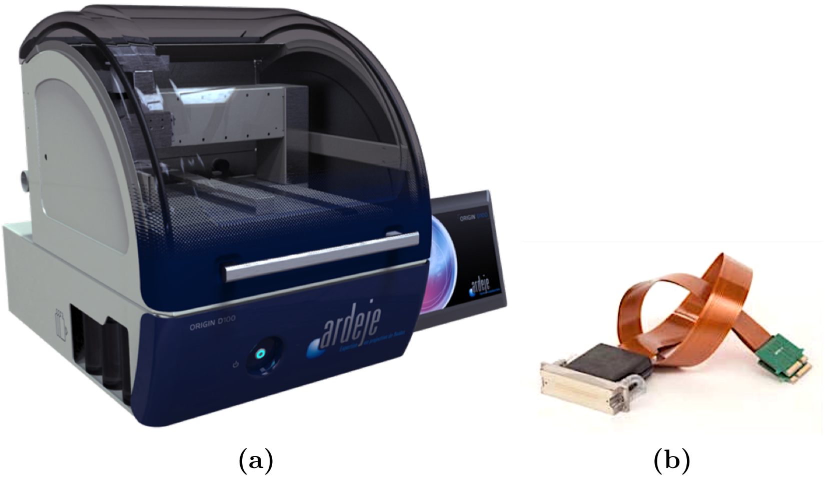

(a) **(b)**

Figure 4.20: (a) Printer *Origin D100®* (b) GEN-4 printhead

That properties allow a good performance for the FSS properties. The conductive ink is a *SicrysTM Silver Digital Conductive I50DM-106.* Its performance are described in Table 4.4. In order to obtain a continuous layer of ink the following two-steps process has been performed,

1. 2400x2400 dpi printing, first step
2. Sintering for 30 min with a temperature of 150 °C,
3. 2400x2400 dpi printing, second step,
4. Sintering for 30 min with a temperature of 150 °C.

Thickness of the metallization approximately 17 μm has been obtained.

Table 4.4: *Properties of the Solvent DGME and Ink used to print on textile materials*

I50DM-106		
Solvent	Solvent	DGME
	Viscosity	3.5
	Surface tension (dyne/cm)	34.6
	Evap. Rate @ 25C (nBuAc=1)	0.019
Ink	Solids (metal content)	40%
	Viscosity @ 25C (cP)	20
	Surface tension (dyne/cm)*	34
	Evaporation rate @ 50C (% solvent/time)**	50%/5 min 90%/20 min
	Sedimentation rate (µm/sec) (T=10%; Lumisizer®)	0.37
	Open time (min) jetting temperature(°C)	1.5 min (40 °C) 10 min (30 °C)
	Resistivity (µΩcm) (thermal sintering, C, min)	≤10 (150, 30) ≤12 (130, 30)
	Sheet resistance (mΩ/□) (thickness, µm)	10 (10μm) 102 (1.5μm)$*$
	Substrate adhesion tested***	ITO, Glass
	Compatible printheads	KM1024, KM1024i, Ricoh E3, DMC 11610, SapphireQS-10pl
Solvents: DGME - diethylene glycol monomethyl ether, Notes: * - Surface tension measured with Pendant Drop method; ** - Evaporation rate of ink estimated using internal procedure; # - Laser sintering; *** - Adhesion depends on substrate, sintering conditions, substrate pretreatment and pattern thickness (tested according to ASTM-3359-09 or ISO-2409)		

Fig. 4.23 shows a first prototype printed on the textile. After the entire process a test in DC current has been performed to check the conductivity at low frequency range. The conductivity changes with the direction of printing on the prototypes. The resistance on the metallization is higher in the direction of the source line (Fig. 4.21), while on the other direction is lower. This result depends on the printing method. By observing the metallization with a microscope (Fig. 4.22), it is easy to detect the direction of the printing. However, this effect is not drastically

influencing and the following experimentation evaluates the performance of the prototype.

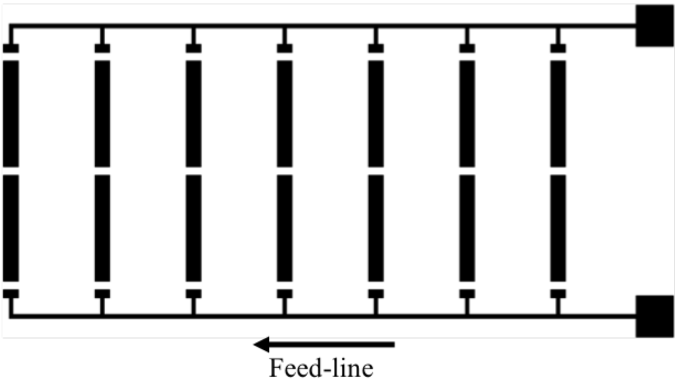

Figure 4.21: Layout of designed FSS for operating at 2.4 GHz

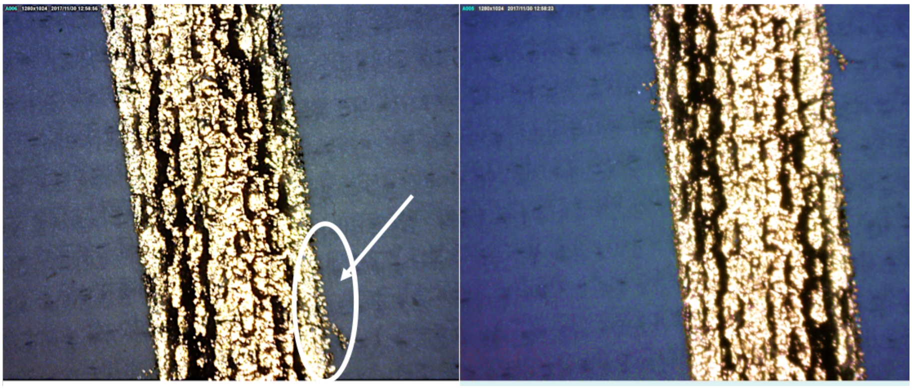

Figure 4.22: Prototypes printed on DHJ PEARL 110μm Microscope zoom

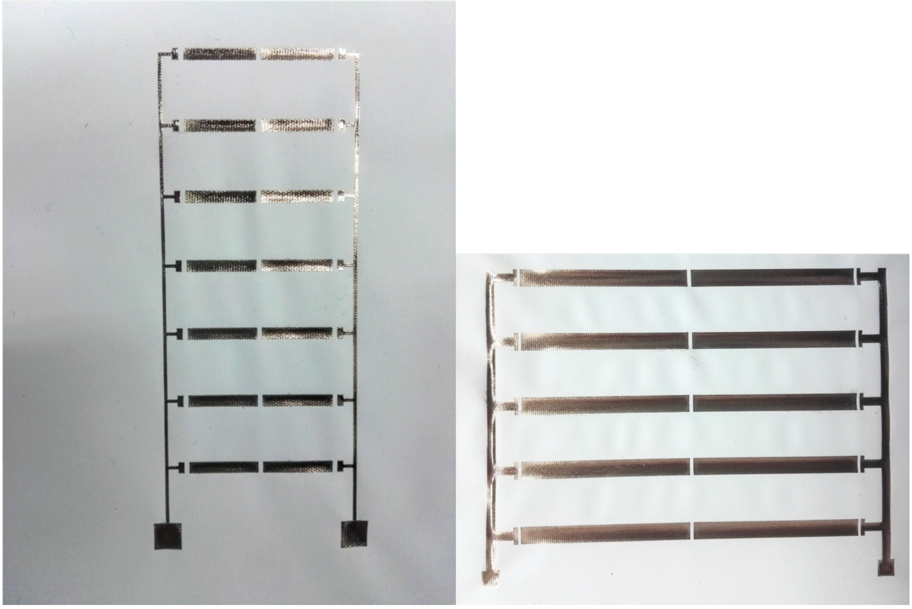

(a) **(b)**

Figure 4.23: Prototypes printed on DHJ PEARL 110 μm (a) Prototype for FSS at 2.4 GHz (b) at 866 MHz (RFID UHF-band)

4.2.4 Prototyping and testing

After having printed the FSS, the lumped elements were attached to the textile. Since the classic soldering was not possible, an alternative technique has been employed. The high temperature of the soldering would have burned the textile. Therefore, cold soldering has been performed using an epoxy paste. After applying the epoxy glue on the lumped element, the prototype has been put into the oven for 30 min at 150 °C. After that, the adhesive has become hard and more conductive. Later, a first test has been performed to control the conductivity of the track and components.After that, the printed FSS has been tested with the same setup of previous section. The following test have been performed.

1. Backscattered power with the FSS in the air,
2. Backscattering power with the FSS on the body,
3. Reading distance and robustness during a normal random and fixed walking.

Measurement in the air shows a wide broadband and a high backscattering power. That shows a high independence by the substrate material

(Fig. 4.24). Measurement on the body have been performed by posing the FSS attached to the chest.Fig. 4.25 demonstrates the wide-band achieved. However, a frequency shift can be notice, which is caused by the presence of the body. The same experiment has been conducted by adding a spacer in between.

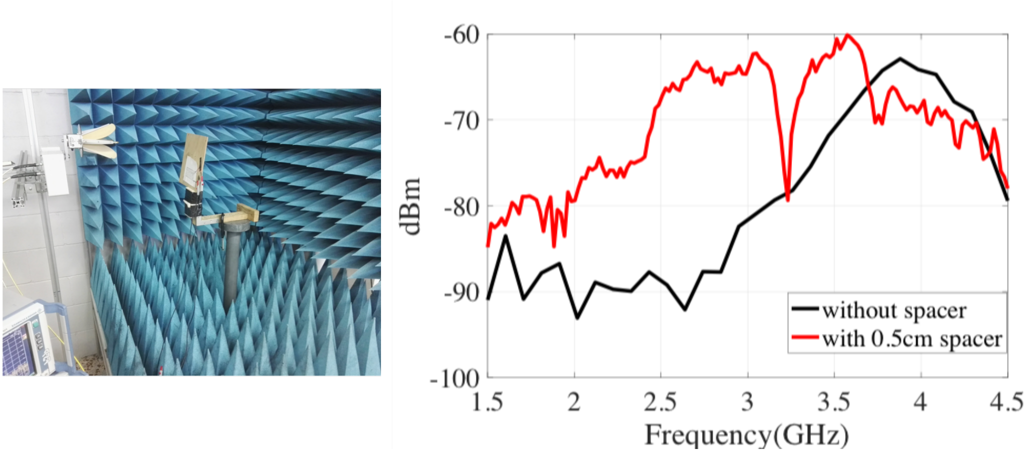

(a) **(b)**

Figure 4.24: Measurement of power received (a) Experimental setup, a spacer in between the body and the FSS (b) Backscatered power. The spacer mitigate the effect of the body.

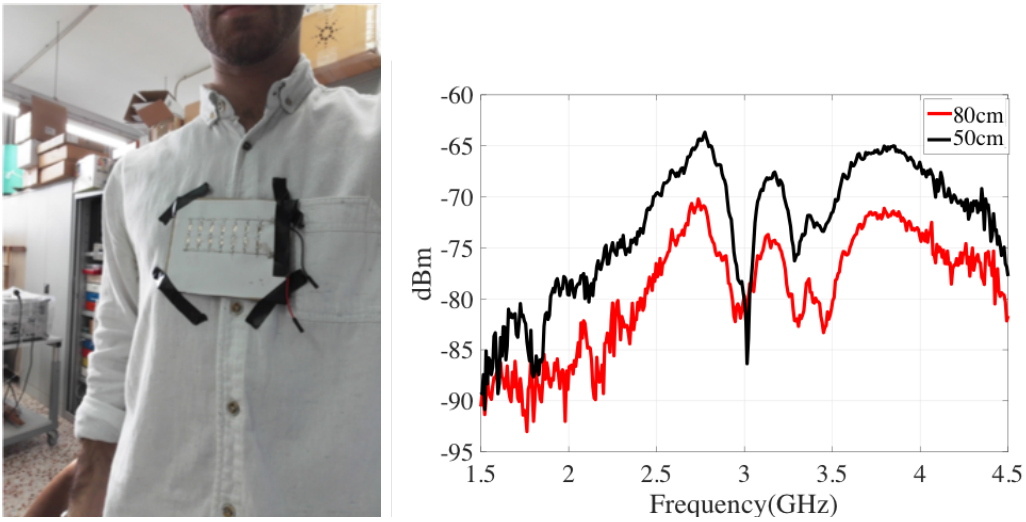

(a) **(b)**

Figure 4.25: Measurement of power received (a)Experimental setup, a spacer in between the body and the FSS (b) Backscatered power. The spacer mitigate the effect of the body.

This gap reduces the frequency shift with respect to the FSS in the air. In the last experiment, the user walk on a fixed path in order to evaluate its reliability during motion. Fig 4.26 shows the result walking in a 9 m^2 path. The measurement shows a strong reliability. During movement the sensor can detect the target continuously. Despite the signal strength is strongly dependent of the position of the user, the experiment demonstrate that there are no lack of signal thanks on the high sensibility of the reader and the properties of the FSS. Fig. 4.27 shows a cumulative distribution function (CDF). According to [100], CDF furnish information on the robustness of the entire system. The FSS demonstrate a good performance avoiding multi-path despite it is printed on the non-homogeneous material.

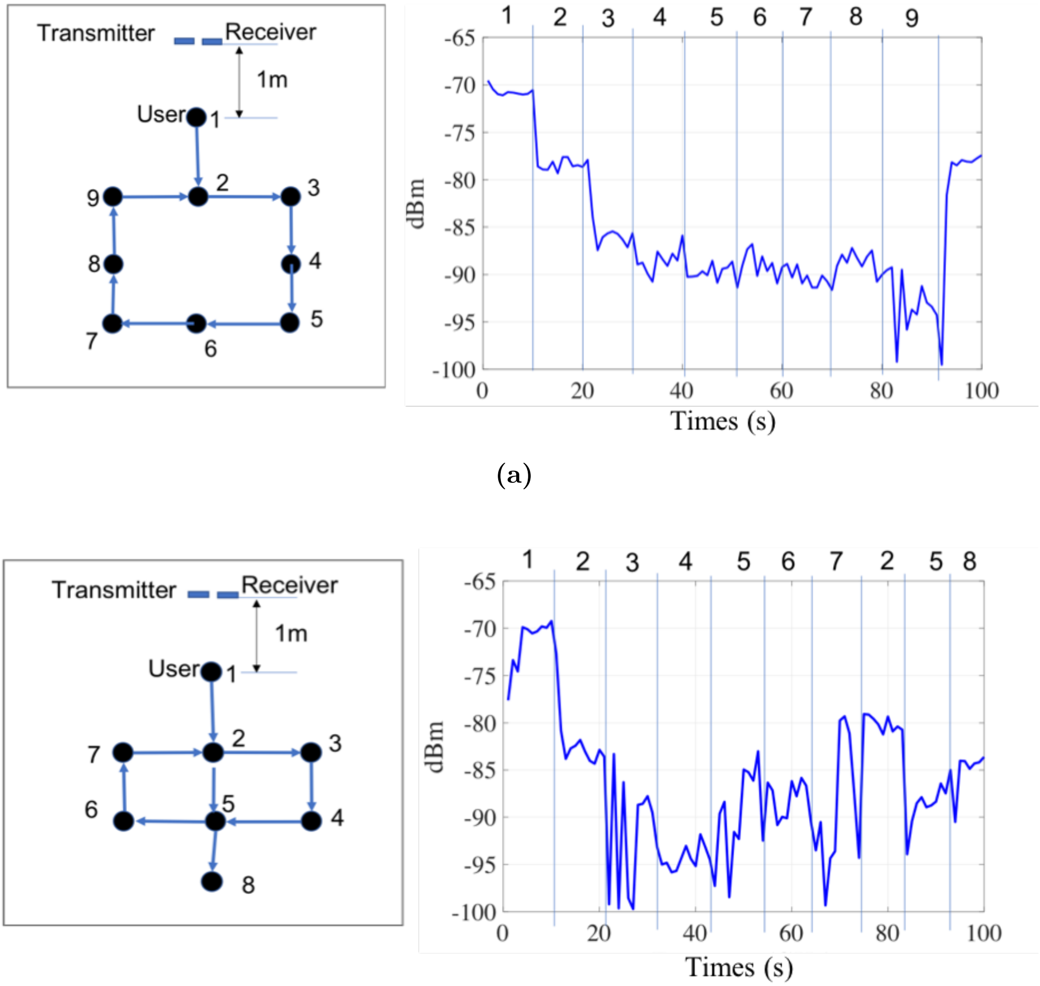

(a)

(b)

Figure 4.26: Power received during a fixed walking path (a) round path (b) cross path

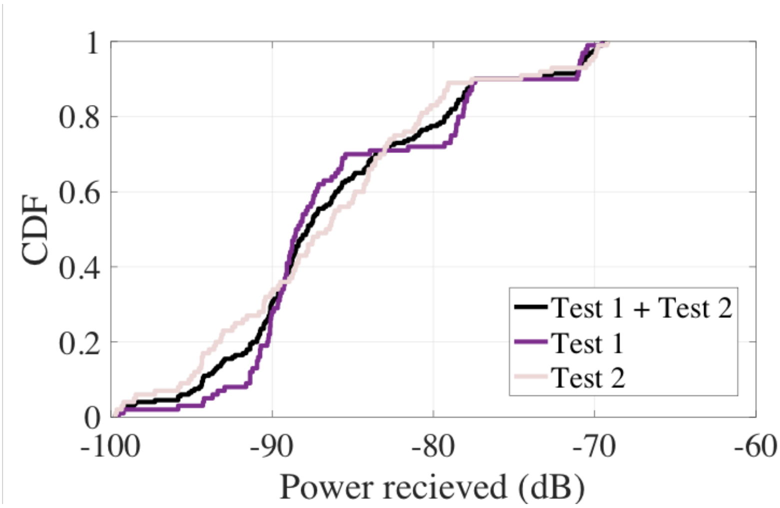

Figure 4.27: CDF measurement for two different random test

4.2.5 Temperature sensor

A negative temperature coefficient resistance (NTC) has been adopted as the temperature sensor. NTC is a low-priced sensor with high sensitivity in the range of the body temperature (35-41°C). A drawback of the NTC is that its resistance does not change linearly for the entire range of the measurement. However, for this application, the temperature range is relatively narrow, hence a linearization can be performed. In order to avoid the usage of complex electronic circuits such as analog-to-digital converters (ADC) and micro-controllers, as well as to reduce the power consumption, an analog approach is proposed. The oscillator is composed of two inverters based on low-voltage NANDs (SN74AUP1G00) and an RC network (see Fig. 4.28). The resistance changes produce a frequency variation at the oscillator's output that modulates the reverse-biased varactors of the FSS, which, in turn, modulates its backscattered field. The diodes are therefore switched between -3V when the output of the oscillator is in high state (3V), and 0V when the output of the oscillator is in low state (0V). The oscillation frequency can be estimated using the following expression :

$$f_m = \frac{1}{2\ln(3)RC} = \frac{0.455}{RC} \tag{4.4}$$

where, R is the resistance of the NTC (1 MΩ NTC from AVX NB20R00105JBA) connected according to the schema in Fig. 4.28.

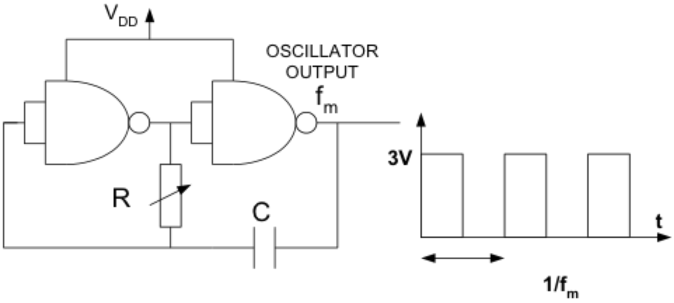

Figure 4.28: Oscillator scheme

The NTC is soldered to a thin strip of flexible PCB made with Ultralam 3850 substrate (from Rogers Corp.) and it located on the body to detect the temperature. The oscillation frequency depends on both the capacitance and the resistance values that are chosen in relation to the environmental temperature. In addition, these values must be adjusted taking into account both the desired frequency range allowed by the analog-to-digital converter of the reader and the Nyqvist criterion to avoid aliasing. Here C=330 pF produces a modulating frequency range between 2 kHz and 3 kHz around the body temperature. The Steinhart–Hart equation [101] is widely used to model the NTC resistance. The thermistor manufacturer uses the first-order approximation:

$$\frac{1}{T} \approx \frac{1}{T_0} + \frac{1}{\beta} \ln \frac{R}{R_0} \tag{4.5}$$

where T is the temperature in K, R0=1 MΩ is the nominal resistance at T0=298 K, and β=4400 K is the Steinhart–Hart parameter that is taken from the thermistor data-sheet. The resolution in the temperature measurement is limited by the frequency resolution. Combining the equation 4.4 and 4.5, deriving it as a function of the temperature, the frequency shift (Δf_m) due to the change in the temperature ΔT is obtained:

$$\frac{\Delta f_m}{f_m} \approx \frac{\beta}{T} \frac{\Delta T}{T} \tag{4.6}$$

It should be noted that the factor β/T is very large in 4.6, therefore the sensitivity in the measurement of the temperature is very high. Using signal processing techniques, a frequency resolution (Δf_m) better than 1 Hz can be achieved, as presented in section 4.3. Therefore, assuming a temperature value of T that is close to T_0, an oscillation frequency of 2 kHz, and a Steinhart–Hart parameter from the data-sheet, the temperature resolution from the equation 4.6 is calculated, which is at an order of 0.01 K. For that reason this sensor can be used in several medical applications.

4.3 Wireless breathing sensor based on modulated FSS

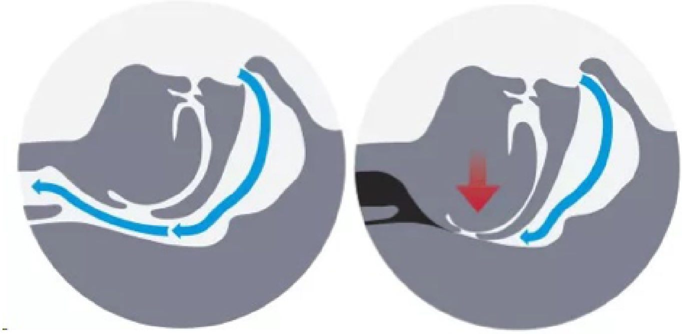

Figure 4.29: Obstructive sleep apnea

Breathing is one part of physiological respiration that is required to sustain life. Unconscious breathing is controlled by specialized centers in the brain, which automatically regulate the rate and depth of breathing depending on the body need [102][103]. The apnea is a term for suspension of the breath. The sleep apnea is a common respiratory disorder that occurs during sleep, which is characterized by cessations of airflow to the lungs [103][104]. Apnea is basically divided into two types: central and obstructive. Central apnea is due to some deficiency on the respiratory system development, whereas the obstructive apnea is due some type of obstruction in the airflow as shown in figure 4.29. This episode can occur many times during the sleep and this pathology is known as sleep-disorder breathing (SDB). The SDB is known as a relatively common condition, which can affect 24% and 9% of middle-aged men and women, respectively [102]. Apnea events can occur 5 to 30 times an hour. Many studies have indicated that SDB is highly related to various cardiovascular diseases in forms of hypertension and stroke [103][104]. It has also been linked to other conditions, such as: type 2 diabetes, obesity, and hypertension. The Central apnea can't be detected by acoustic methods because it is more complicated than obstructive apnea (OSA). In the clinical setting, the exact diagnosis is made by polysomnography (PSG). PSG measures a large number of parameters and it is made off different parts: an electroencephalogram, which records the sleep stages, a single-lead electrocardiogram, which monitors the heart rate, an electromyogram which records the leg movements, a thermal sensor and a nasal pressure transducer both of which measure the breathing rate, including airflow at the nose and at the mouth. Therefore, the PSG test is highly invasive, labor intensive, requires expensive instruments, is a time consuming process and hence is impractical to perform apart from a general population check-up. Consequently, many people with SDB, perhaps up to 93% of the population, remain undiagnosed [105]. An effective screening in the primary core setting could increase the number of patients identified. Thus, a new generation of technological tools is under development. The remote health monitoring can be acceptable in the case where the device fulfills all of the following requirements: comfortable, easy to use, and low cost. In order to detect apnea and calculate the respiration rate, there are many sensors that are commercial available. Various portable monitor devices, like sleep-stripes, already exist in the market. It is an at-home sleep test diagnostic device. This device has to be worn for a minimum of five hours during sleep. The device is placed on the individual's face where the two flow sensors (oral and nasal thermistors) are placed just below the nose and above the upper lip, in order to capture the patient's breath more effectively. Most of them are based on sound recording techniques [106] or on micro-controllers which are integrated inside a belt [107]. Unfortunately, however, these devices are noisy and often, neither easy to calibrate, nor suitable for long-term monitoring. In order to match the properties of comfortability, flexibility, and a long lifetime for the battery, a wireless breathing sensor that is based on a frequency selective surface (FSS) has been proposed. The novelty of this work is the application of these devices as a wireless interface of the breathing sensors.

4.3.1 Wireless measurement and experimental setup

The continuous monitoring is usually performed in the case of apnea diagnosis, where several days of analysis are required. The oscillator, based on the two-inverter that is introduced here, draws 40 µA at 3V; this leads to more than one year in the lifetime of a typical 330 man coin-battery. In addition, this solution allows a miniaturization of the device, as the number of parts in the system is decreased. The wireless measurement is carried out using a customized reader. The system uses the same mechanism of acquisition discussed in section 4.2. The transponder backscatters the electromagnetic signal and modulates the incoming signal at the frequency of the oscillator (see fig. 4.30), The FSS placed directly onto the body can achieve a large bandwidth, and the effect of losses in terms of performance, introduced by the body presence, can be compensated by increasing the number of radiating elements, as it has been shown in previous sections. The large bandwidth provides robustness to the system in front of the variation of permittivity between different bodies or the different FSS positions, considering the same body. Read ranges of around 3 m have been experimentally achieved [99, 98].

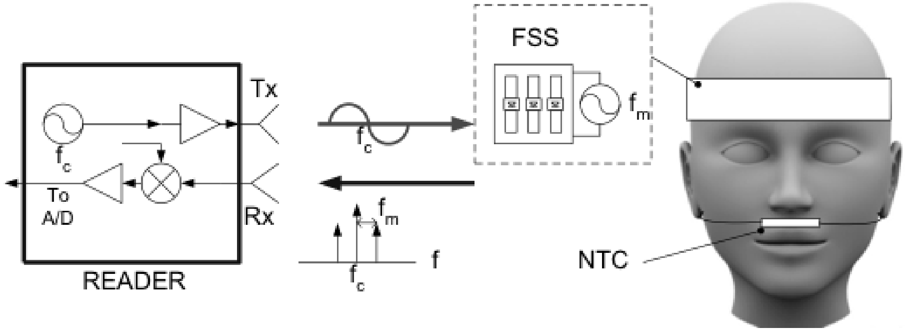

Figure 4.30: Block diagram of the system, including the reader and the transponder.

The varactor-loaded FSS is integrated in a headband along with the oscillator and the battery, as shown in Fig. 4.31. The NTC is connected with thin flexible wires to the oscillator to reduce the interaction with the skin, which would be more comfortable for the patient. Low-cost silicon varactors from Skyworks SMV1247-079LF are used as switching diodes. The FSS is manufactured over a 100 µm-thick Ultralam® 3850 substrate. Two 10 kΩ 0605 SMD resistors are connected at the end of the arms of each dipole to feed the diodes and to prevent the undesired

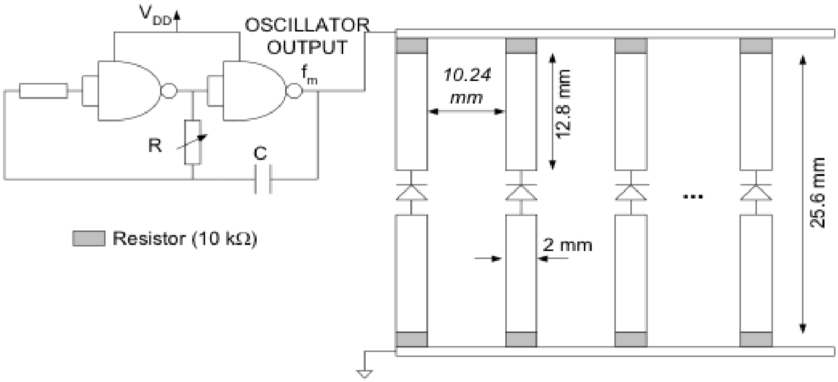

Figure 4.31: Schema of a FSS loaded with varactors connected to the two-inverter oscillator controlled by the NTC resistance (R).

flow of the RF signal on the feed line. The dimensions of the FSS are provided in Fig. 4.31. The headband is a FSS composed by four groups of 5 loaded dipoles each as shown in Fig. 4.32. To ensure the ability to read the backscattering signal, the FSS is designed to surround the entire head and then a reading of 360° is allowed. The dipoles are also orientated in a different manner to permit the reading independently of the rotation movement of the head.

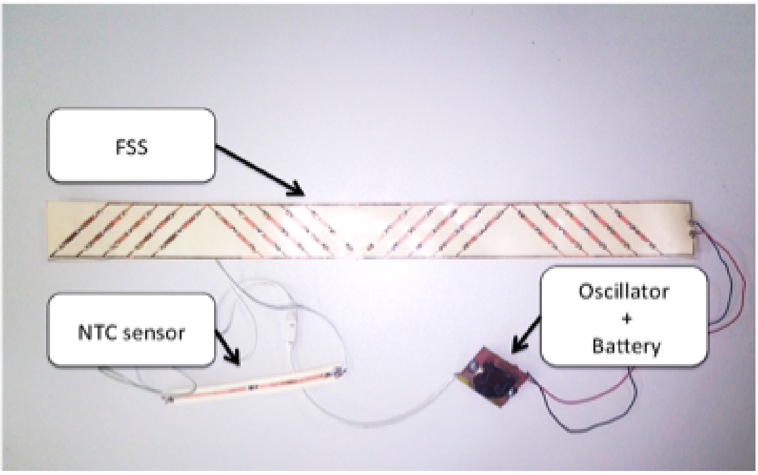

Figure 4.32: Photograph of the headband with the FSS and the NTC sensor and the oscillator.

4.3.2 Customized reader

The scheme of the reader prototype is shown in Fig. 4.33a. It has been designed using a custom software defined radio (SDR) module. The transmitter is composed by a frequency synthesizer (Minicircuits KSN-2450A-119+) that generates a signal, a Minicircuits GAL84+ to amplify it, and a linearly polarized antenna. The output power is 18 dBm. The interrogating frequency is programmed with a micro-controller (Arduino UNO board). The local oscillator for the mixer (Mini-circuits LRMS-30J) that down converts the signal detected from the receiver is obtained using a coupler. The intermediate frequency (IF) signal at the mixer's output is amplified using two operational amplifiers with an overall gain of 50 dB and an analog filter with a cut-off frequency of 20 kHz connected in cascade. The output is sampled using the analog-to-digital converter (ADC) integrated in the sound-card of the PC. Fig. 4.33b shows a photograph of the prototype. The sensor temperature can be determined from the modulation frequency (f_m) using the equation 4.4.

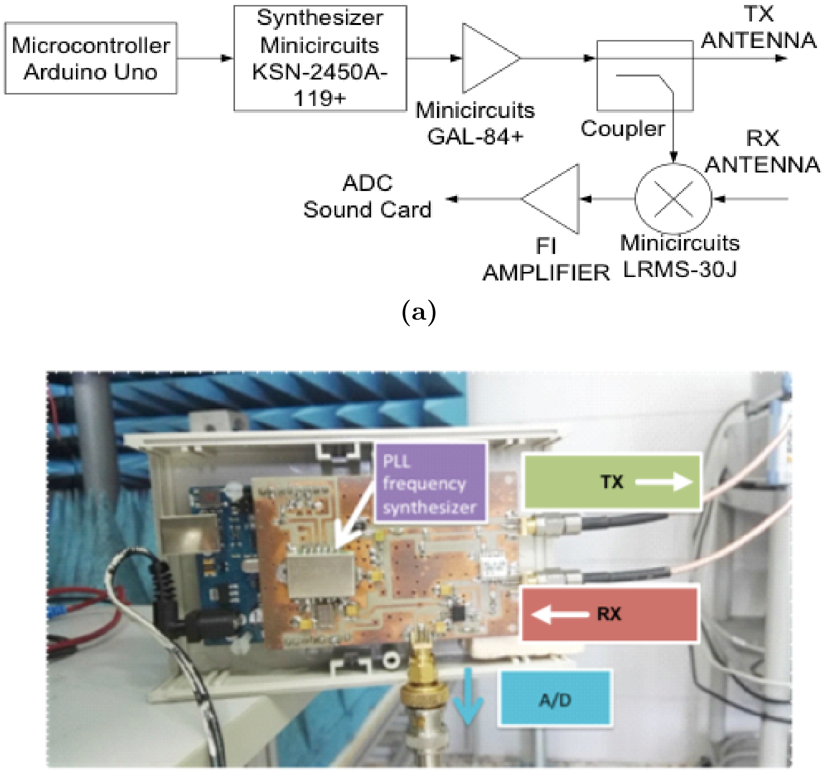

(a)

(b)

Figure 4.33: Customized reader at 2.45 GHz ISM. (a) Electric scheme and photograph (b).

The modulation frequency can be obtained from the spectrum of the base band signal at the output of the mixer. The chirp Z-transform (CZT) algorithm [108], and a Hamming window is used to achieve the appropriated frequency resolution. This transform can be efficiently implemented using Fast Fourier Transforms (FFT) and makes the frequency resolution independent from the number of samples. The modulation frequency f_m is estimated from the peak of CZT using 1000 samples taken with the ADC at 44000 Hz. This procedure (sampling plus CZT and Peak detection) needs approximately 63 milliseconds. As a result, the modulation frequency that is function of the breathing is sampled at approximately 15 Hz. This sampling frequency is enough, because a normal breathing rate is around 0.3 Hz. Fig. 4.34 shows a sample of 20 seconds of normal respiration, taken at 1 meter of distance between the head and the reader. The samples at the output of the ADC, along with the baseband spectrum from 1.5 KHz and 3 KHz that is computed with the CZT, are shown on Fig. 4.34a and Fig. 4.34b, respectively. A clear peak corresponding to the first side-band of the modulated signal can be observed. The modulating frequency f$_m$ can be easily obtained from the peak of the spectrum. In this case, the signal-to-noise ratio is more than 20 dB. measurements taken at room temperature (which is assumed to be constant). The measurements have been fitted using a gaussian distribution. Fig. 4.35 depicts the Gaussian probability distribution density overlapped to the histogram with a good agreement. The standard deviation is 1.7 Hz, which using the equation 4.6 corresponds to the standard temperature variation of 0.019 ºC. This small error due to random measurement noise does not affect this particular application.

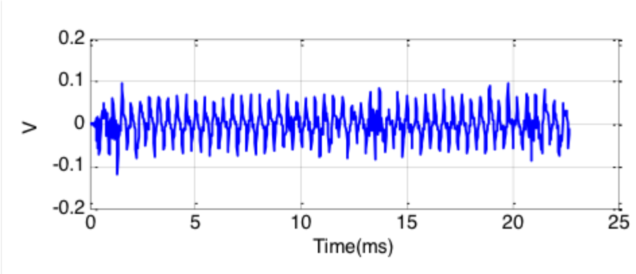

(a)

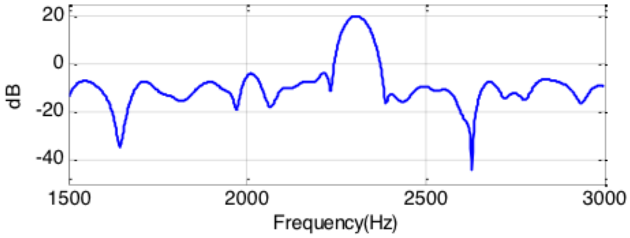

(b)

Figure 4.34: Example of measurement at 1 m of distance. (a) Baseband signal in time domain, (b) spectrum computed using CZT

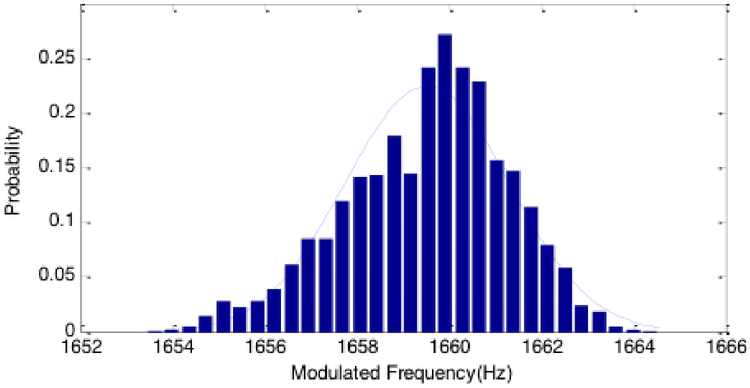

Figure 4.35: Histogram and fitted Gaussian distribution of the measured modulation frequency

4.4 Signal processing for a simple a robust breathing detection

The block diagram in Fig. 4.36 describes the algorithm implemented to calculate breathing rate and apnea time. As a first step the modulating frequency f$_m$ obtained from the spectrum of the signal, just at the output of the receiver mixer, considering it as a function of time is measured. This signal is referred to as the breathing signal. Fig. 4.38a shows an example of normal breathing just after installing the sensor close to the nose. It is possible to estimate the change of temperature, ΔT, in the thermistor using equation 4.6 from the modulated frequency shift. During the respiration cycle, the temperature variation is about 2 Kelvin when the NTC is in the vicinity of the nose. Fig. 4.38b shows the estimated temperature change as a function of time. It can be observed that the sensor is gradually warming due to the proximity of the body, while the ripple depends on the breathing. An increase in temperature is observed during the exhalation time, and a decrease during inhalation. The amplitude of the temperature ripple depends on the relative distance between the sensor and the nasal cavity. A real-time peak detection algorithm has been developed to obtain the peaks and troughs of the breathing signal. Then the breathing rate, usually expressed in breaths per minute (bpm) is estimated from the inverse of the interval between two consecutive peaks, 1/Δt (Fig. 4.38c). The algorithms to detect the

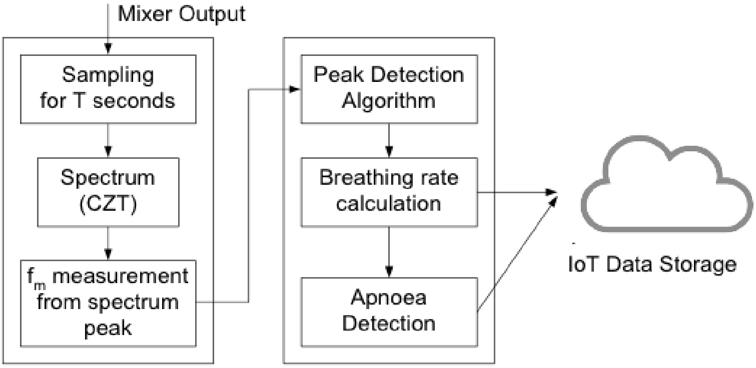

Figure 4.36: Block diagram of the algorithm for breathing rate and apnea detection.

local maximum (or minimum) usually present some problems in case of noisy data such as breathing data or ECG data. The well-known zero-derivative method often fails when the zero crossing of the first derivate occurs, due to noise. A typical solution consists of smoothing the curve by using different low-pass filters [109]. In this work, a robust peak detection algorithm is presented. The algorithm assumes that a peak occurs at its highest point between troughs and that there are lower points around it. The strategy is to look for the highest point and around it there are lower points shown by a Δ on both sides (see Fig. 4.37). The algorithm only needs the current sample and the last detected maximum (or minimum). Thus, it can be efficiently implemented on quasi-real-time for continuous breathing monitoring. The pseudo code is shown in Algorithm 4.1.

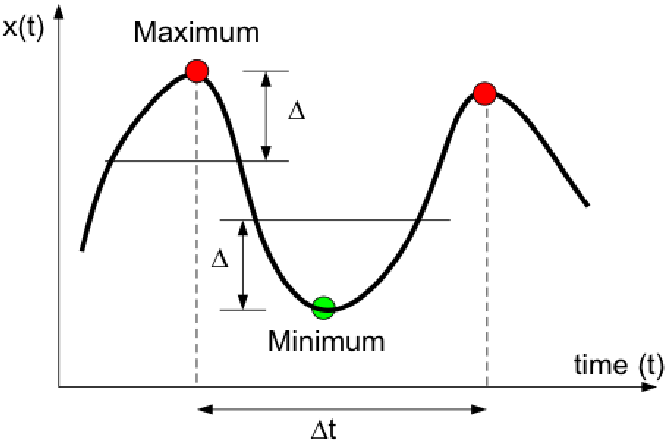

Figure 4.37: Strategy to find the local maximum and minimum of the data.

Algorithm 4.1 Algorithm for the peak detection

```
# Initialization of variables
maximum = Inf;
minimum = -Inf;
lookformax = 1
do for each measurement
{
    #Perform a measurement
    # t is the measurement instant
    # x is the measured sample
    if x > maximum
    {
        maximum = x
        maximumposition = t
    }
    if x < minimum
    {
        minimum = x
        minimumposition = t
    }
    if lookformax=1
    {
        if x < maximun-delta
        {
            save the maximun and maximum position
            minimun = x
            minimumposition = t
            lookformax = 0
        }
    }
    else
    {
        if x > minimun+delta
        {
            save the minim and minimum position
            maximun = x
            maximumposition = t
            lookformax = 1
}}}
```

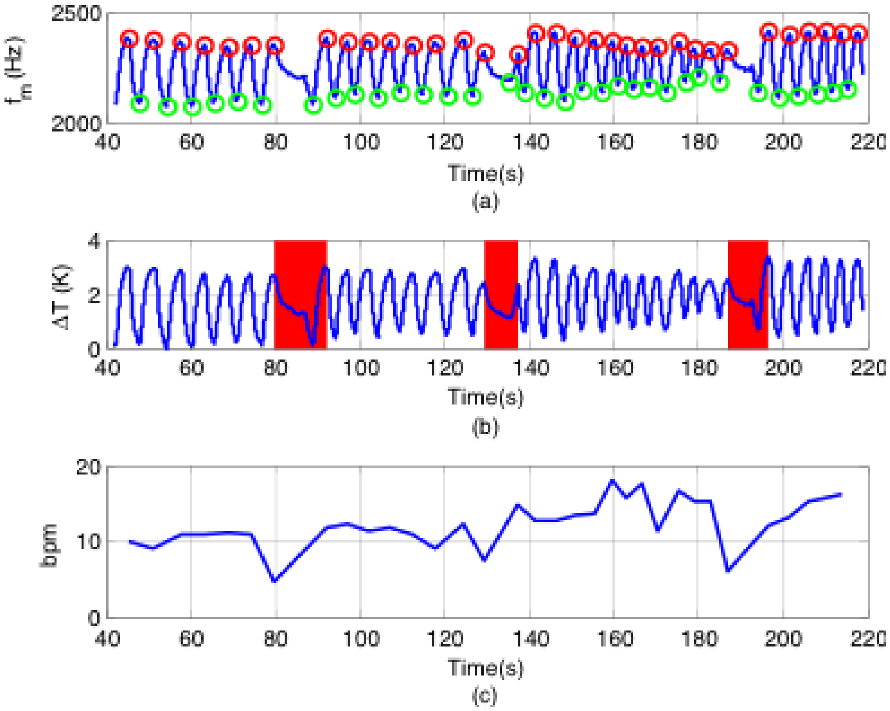

Figure 4.38: Example of measurement for a person with normal breathing: (a) measured modulation frequency, (b) temperature change and (c) breathing rate in bpm as function of the time

4.5 Experimental results

The prototype has been integrated into a flexible headband (see Fig. 4.39a) in order to test the algorithm, measure the reading distance, and assess the power consumption in a real situation. The headband is placed around the head of a volunteer and the sensor is placed under the nose, as shown in Fig. 4.39b. The reading distance is taken standing up, in front of the reader for a period of time of 100 seconds. The maximum reading distance measured is up to 3 meters (Fig. 4.40).

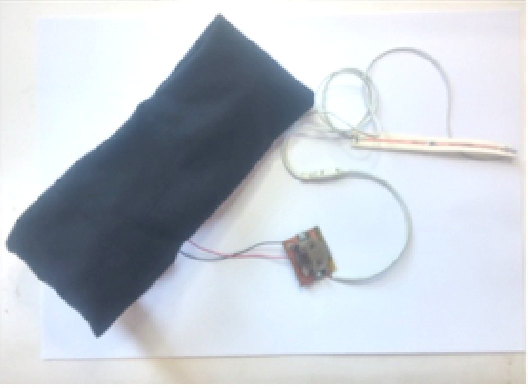

(a)

(b)

Figure 4.39: Breathing sensor prototype for the measurements (a) Photograph of the whole prototype (b) installed prototype for the measurement

The respiration rate is calculated at the same time. Fig. 4.38 shows the respiration fluctuation at a certain distance from the reader. Three apneas are shown with different time duration (12.4 s, 8.1 s, 9.7 s, respectively). During these time intervals, no ripple in the breathing signal is observed and the temperature decreases, gradually return to the ambient temperature. The apnea interval can be measured between a maximum and minimum when the interval (Δt) is larger than a threshold time. This threshold time is typically given as 10 seconds in the literature and it is considered as a dangerous apnea [105]. A variation in terms of angular rotation has also been performed. The rotation of the head changes the backscattering power of the signal. Some diverse positions were considered in order to check the robustness of the system. Fig. 4.40 shows the measured breathing signal for frontal and lateral head orientations. Fig. 4.41 shows the measured breathing signal as function of the head inclination. A rotation of 90° or change in the head inclination (see Fig. 4.41) does not affect the result, and it is correctly processed (Fig. 4.40c and Fig. 4.41c, respectively). The amplitude of the sampled signal at the output of the A/D depends on the distance to the reader (see Fig. 4.40a and Fig. 4.41a). However, the amplitude of the signal breathing (modulation frequency detected after the CZT) depends on the frequency shift due to temperature change that is a function of the distance between the sensor, nose and the airflow velocity; to avoid this effect, a distance between the nose and the sensor is fixed. Therefore, the normalized amplitude of the signal breathing (see Fig. 4.40b and Fig. 4.41b) remains approximately constant.

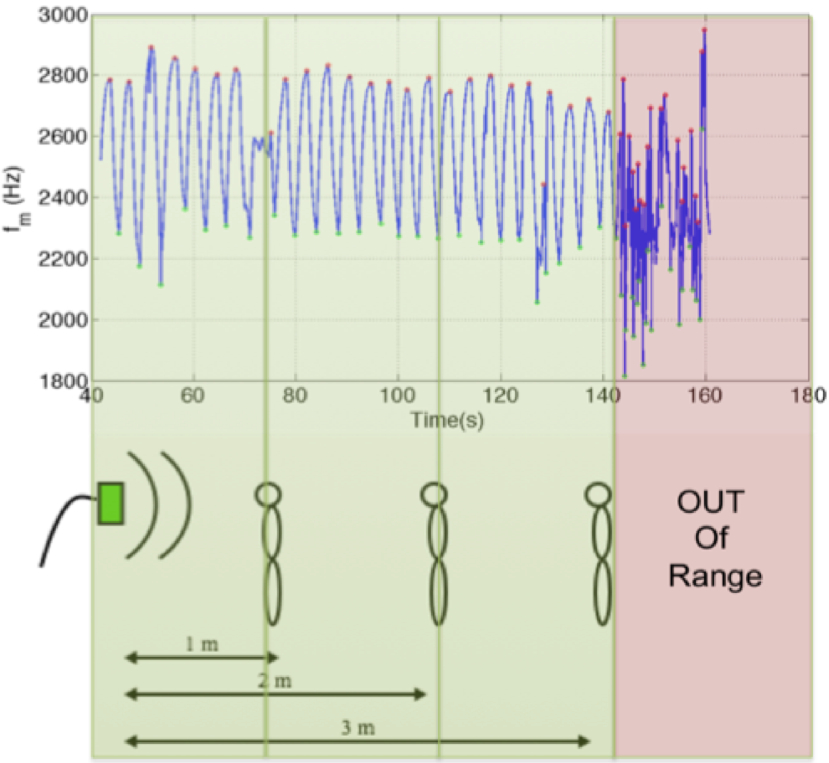

Figure 4.40: Reading distance for the FSS placed on body.

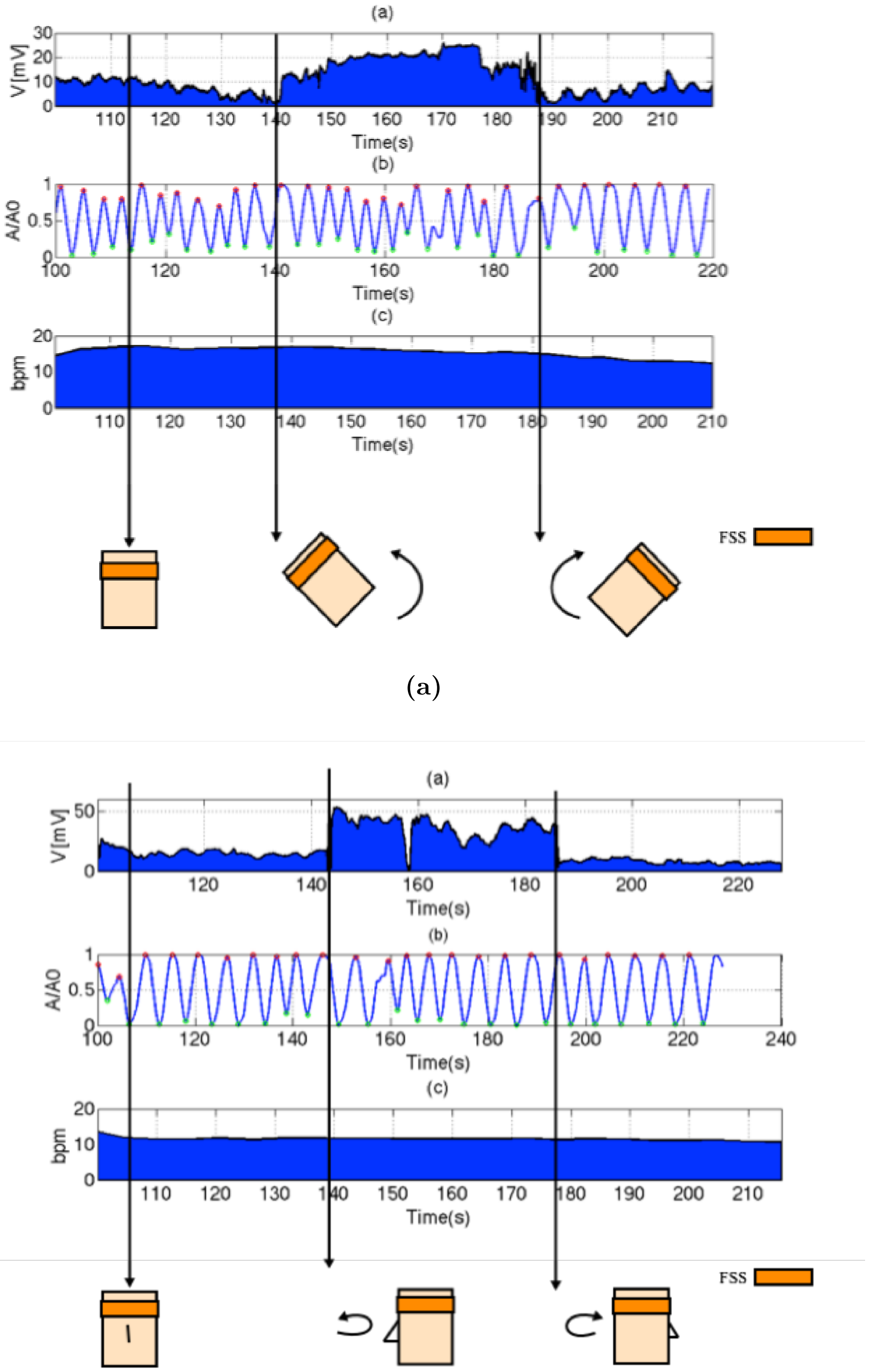

(a)

(b)

Figure 4.41: Breathing Sampled signal at the output of the A/D (a), normalized breathing signal (b) and breathing rate (c) for different head inclination.

4.6 Comparison between FSS and RFID-based sensors

In this section, a comparison between the presented technologies has been carrying on to determinate their proper field of application. Those two systems have many features in common as the complete passive transmission and the versatility due to their thin shape that makes them comfortable for on body application. On the other hand, these methods are different enough to define a rigid separation regarding their specific use. UHF RFID transmission is based on the EPC protocol that establishes a strict way of communication, while the FSS is a complete passive backscattering which makes the electromagnetic transfer lighter but also less safe. The entire passive nature and the lowest price of the RFID technology offer a wide range of spreading because it can be considered a disposable option. Therefore it can be efficient in case of tracking population behaviour for epidemics or mass market. Unfortunately, the sensors use the power given by the transceiver which is drastically decreased, in case of lossy material substrates (body-mass). Consequently, the reading range is reduced. For this reason, the FSS based sensors can find a more extensive field. First, sensors attached to the body do not use the electromagnetic power, and thanks to their low power, they can use alternative harvesting methods that are not deteriorated by the body mass. Moreover, the FSS is useful because the sensor, in the case of the temperature sensor, can be placed on separated position respect to the radiator on the body, allowing to lay the sensor in their suitable region, the body cavity (axillae, inside the ears)[100]. RFID result useful in case of many different users, thanks to the ID tracking that makes the user unique. The last generation of RFID can achieve to measure more than 40 users with a single interrogation slot. On the other hand, the readout in the FSS is analogue, therefore although each user can use different modulation frequencies, the number of simultaneous users will be small. A definite plus of the FSS sensor is its high-temperature resolution that can increase the healthcare in the home systems. Also, one of the bottlenecks of the RFID at the moment depends on the reader sensitivity. Despite the fact that the RFID tag can be able to wake up with a few amounts of energy, the reader cannot detect the backscattered signal. A commercial RFID reader, in fact, holds a sensitivity of about -80 dBm, while in the case of Reader for the FSS can detect the backscattered power of approximately -120 dBm

	RFID-UHF	FSS
Durability	∞ no battery needed	Depend on the battery if no other harvesting method is used
Reading distance	< 1 meter fully passive, Integrated temperature sensor	> 5 m The radiator can be displaced on some other place, reducing the interaction with the body.
Cost	< 2 €	> 10 €
Customizable	>20 device can be connected at the same	$<$ 10 device can be connected to the same reader
Sensibility	Low resolution (0.25 °C)	High resolution (0.01 °C)
Application	High distribution, not precise sensor, alert disposable sensors.	Light, home telemedicine based sensor, circadian body temperature variations detector.

Table 4.5: Comparison between FSS and UHF RFID based sensors

4.7 Conclusions

The backscattering technique has performed the communication between the transponder and the reader in the semi-passive connection. The RCS of the FSS-based transponder is modulated using low-cost reverse-biased varactors. The power consumption of the semi-passive FSS is, therefore, lowest compared to other alternatives. , and the frequency is controlled by a thermistor placed close to the nasal cavities which demonstrates good performances regarding sensing resolution, reading distances and reliability. The temperature at the sensor depends on the airflow during respiration with a variation of about 4 °C. The transponder contains several FSS's with different directions and is located around the head to improve the readability to around the circumference. This topology shows high robustness in front of fading due to non-line-of-sight (NLOS) situations, which might be caused when the path is partially blocked, either by objects or the body. A customized reader has also been developed using commercial components. Read ranges up to 3 m are typically obtained with the proof-of-concept prototype. A real-time algorithm that consists of determining the respiration peak and the measured modulated frequency is used to measure the breathing rate and detect the apnea intervals. The low power consumption enables long-term sessions of apnea monitoring for screening applications at home. These results open the door to more complex sensors based on FSS on-body applications, which integrate micro-controllers and more sophisticated sensors for other uses. A comparison between the RFID sensor and the FSS based monitoring device has been presented.

5

An active solution for a breathing sensing

Over the available energy and communication constrained technologies, Bluetooth Low Energy (BLE) is one of the most appealing alternative. BLE is a standardized communication technology designed for low-power systems and innovative sensor-based data acquisition frameworks. Also, it offers easy integration with most of existing personal devices (such as smartphones and tablets). The last bluetooth version provides no significant differences over its previews release (Bluetooth 4.0) that enable extensive use in new domains. In contrast, the new Bluetooth 4.2 has novel features that make Bluetooth LE an encouraging enabling technology for the wIoT [110]. In the field of medical and health devices, two main features make the BLE an appropriate solution: The improvement concerning the privacy of the users and enhancements in the security layer.

5.1 Implementing BLE for wIoT device

The concrete implementation of a Bluetooth LE device on a commercial *system-on-chip* (SoC) involves HW-SW trade-off to balances performance, power consumption and programmability. Whereas a controller API is usually provided along with host-side software to the developer as source code, the controller is implemented as firmware that has exclusive access to the radio. The stable integration of the firmware binary and the PHY layer is conducive to performance optimization and low power operation conducted by the chip vendor. The close-source nature of the firmware libraries provided by major vendors, however, becomes a disincentive to innovations by third parties. This trend has not stopped the active IoT community from integrating some of these chips with open-source embedded operating systems and tools. In spite of the binary form of the provided Bluetooth LE controller firmware, register-level details exposed in data-sheets by specific vendors leave the door open to ambitious developers who want to experiment with their own Bluetooth LE implementation [111, 63, 112, 113]. The low power and the low data rate nature of Bluetooth LE simplifies requirements for radio traffic monitoring, which in turn simplify protocol debugging and fault diagnosis. Those improvements are essential for continuous growth in the field of wearable medical devices, allowing a multitude of new body sensor for consumers but also for more critical applications.

5.2 Challenges

A regulated communication method is intrinsically more complicated than an unstandardized technology, which makes the power consumption a weakness of this devices. On the other hand, a rigorous standard allows a high-security level, the necessary condition for a wIoT that measure user health state. The challenge became to create a robust, secure and private prototype, able to handle physio-pathological parameters keeping a low power profile. In this chapter, a prototype, which uses the BLE communication method based on open-source code design, has been taken into account for a parallel with the previews mentioned techniques, which are based on analog not-standardized communication. A customized breathing sensor has been used as an example to demonstrate the feasibility of the proposed system. Standard breathing sensors based on the airflow are not accurate enough to guarantee a reliable result. The next section illustrates a method to make a breathing sensor most reliable. A tradeoff between the reliability and the power consumption has been addressed. First, a wearable device, based on the synergy between the airflow sensor and the skin conductance shows the opportunity to increase the breath volume for sleep apneas detection. Next, a correlation with a magnetometer sensor has been proposed to analyze the differences and the advantages of these solutions and evaluate the scenario of application that is adequate for the intended sensors.

5.3 Sensors for sleep disorder diseases

Monitoring the respiration conditions with the autonomous nervous system (ANS) activation during sleep could be a practical screening solution in the primary core-setting, thus increasing the number of patients identified. Many wearable systems propose monitor the respiration parameters during sleep but can't assess sleep quality. Galvanic skin response (GSR) and basal skin resistance (R) are often used as indicators of autonomic activity which has led to their widespread application in physiological and pharmacological investigations [114, 115]. GSR is also an indicator of many other sleep factors [16] and is directly related to sleep quality due to the connection with the sympathetic nerve [114]. A low-power and wearable integrated device that takes into account both the effect of respiration and the activation of ANS can be an efficient solution to detecting sleep disorders.

5.3.1 Architecture of the system

The prototype has been built using a small low energy Bluetooth module, attaching with two different sensors, a thermistor and a GSR sensor, to collect and manipulate information together. The transmitting line is capable of computing and sending pre-processed data to a client. The main hardware components of the prototype's current implementation have been presented below.

5.3.2 Breathing sensors based on NTC sensor

The breathing sensor uses a negative coefficient thermistor (NTC) placed close to the nose already discussed in Chapter 5. Fig. 5.1a. shows the signal conditioning circuit used for the temperature measurement. Fig. 5.3a shows the measured with a 10-bit A/D converter of the micro-controller connected to the output of a simple voltage divider. The detected signal is amplified using the circuit in Fig. 5.1a.

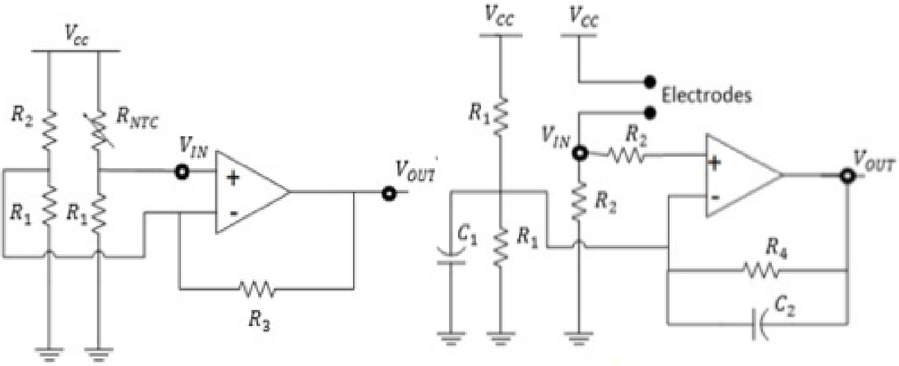

(a) **(b)**

Figure 5.1: a) Conditioning circuit for the airflow sensor b) Conditioning circuit for the GSR signal

Fig. 5.3b shows the output of the amplified signal after connecting the sensor close to the nose to reduce the effect of quantification noise due to the limited number of bits of the A/D. The effect of the warm body can be observed in Fig. 5.5. Since the temperature sensor is directly placed below the nose, the amplitude depends on the distance of the sensor by the nose (Fig. 5.2). Then, to guarantee the effectiveness of the algorithms, the sensor has been mechanically fixed at a certain distance to the nose. Consequently, a calibration is performed to clearly identify the correct parameters used for the calculations.

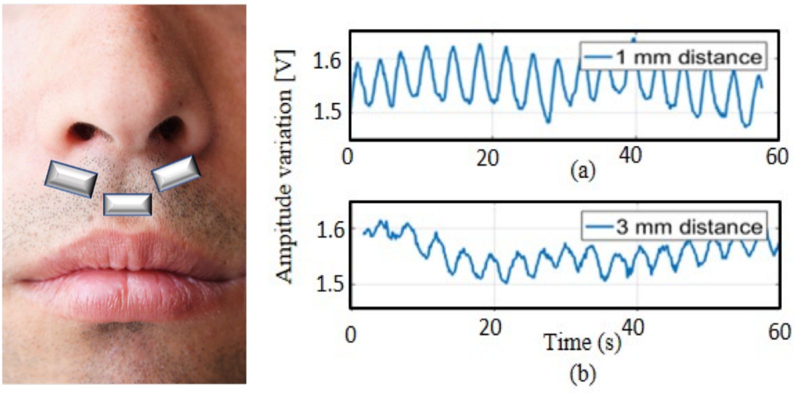

Figure 5.2: The temperature increase after sensor positioning

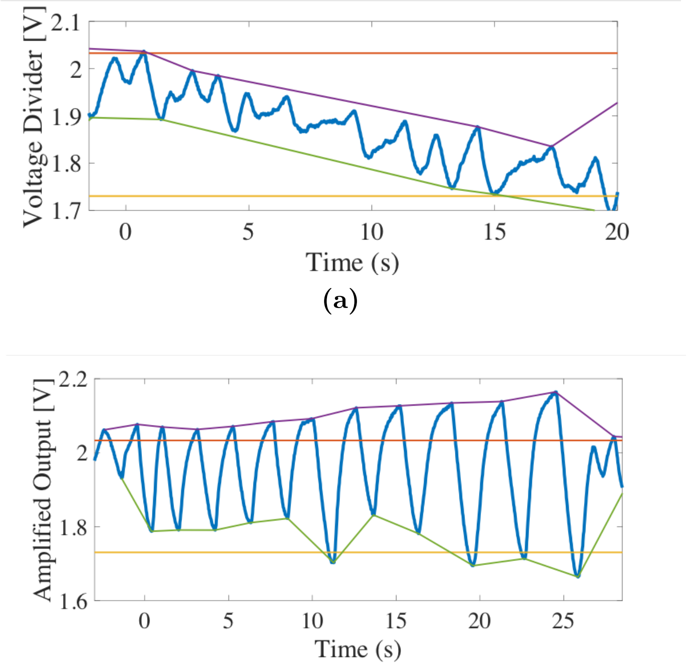

(a)

(b)

Figure 5.3: Raw voltage at the Input (VIN) and amplified output voltage (VOUT) a) Voltage divider, signal not processed, b) Conditioned signal

5.3.3 GSR sensor for ANS activity

An increased sympathetic activity (sympathetic arousal) elevates heart rate, blood pressure, and sweating, as well as redirects blood from the inner reservoir toward skeletal muscles, lungs, heart, and brain in preparation for motor action. Sympathetic postganglionic fibres consisting of nonmyelinated class C nerve fibres surround eccrine sweat glands, and their activity modulates sweat secretion [105]. Since sweat is a weak electrolyte and good conductor, the filling of sweat ducts results in many low-resistance parallel pathways, thereby increasing the conductance of an applied current. Changes in skin conductance at the surface, referred to as electrodermal activity (EDA), reflect activity within the sympathetic axis of the ANS and provide a sensitive and convenient measure of assessing alterations in sympathetic arousal associated with emotion, cognition, and attention [116]. Stress is defined as a disruption of the autonomic balance involving a state of high sympathetic activation. Since

EDA is solely determined by the activity of the sympathetic branch of the ANS, which is predominant in stress states, tonic EDA parameters may be regarded as suitable measures of ANS activity induced by stress [117]. Autonomic responses in the skin such as sweating, piloerection, and vasomotor changes can thus be elicited by various emotional states [118]. Also, it is widely recognized that attention-grabbing stimuli and attention-demanding tasks also evoke increased EDA responses. GSR can be obtained using a simple sensor that measures the resistance between two positions on the skin. The sensor consists of two electrodes, which are placed on two closed fingers and it regulates the activation of the gland cells after, sympathetic stimuli [116]. The signal is pre-filtered and amplified using the circuit shown in Fig. 5.1b. In comparison with the breathing sensor, the connection is not critical and is more conformable because it can be easily integrated into a glove[119]. Also, this application can be used as an alternative method for the detection of SDA's activation.

5.3.4 Conditioning methods

As the variation in time of the signals is slow (10-30 beat per minute), and the measurement takes a long time (one night), the amount of data use a lot of internal memory storage. Therefore, the signal should be processed to save storage space on the smartphone as well as its battery life. Fig. 5.5 shows an example of breathing just after installing the sensor close to the nose. After this period, the temperature variation is less than four Kelvin during the respiration cycle (Fig. 5.4a); The temperature detected by the sensor gradually increases due to its vicinity to the body, whereas the oscillation depends on the breathing. An increase and decrease in temperature are observed during the exhalation and inhalation time. The positioning of the sensor is a critical aspect because the amplitude of the temperature depends on the relative distance between the sensor and the nasal cavity (Fig. 5.2). A real-time peak detection algorithm has been developed to obtain peaks and troughs of the breathing signal. The breathing rate, expressed as breaths per minute (bpm) is estimated from the inverse of the interval between two consecutive peaks a discussed in the previews chapter, $1/\Delta$t (Fig. 5.4c).

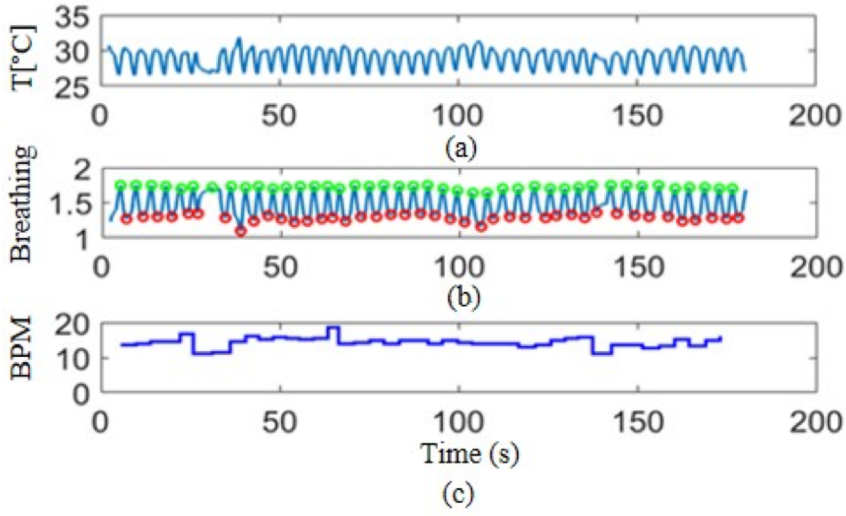

Figure 5.4: (a) Temperature of the airflow, (b) Peak detector applied (c) Istantaneous calculation for breaths per minute

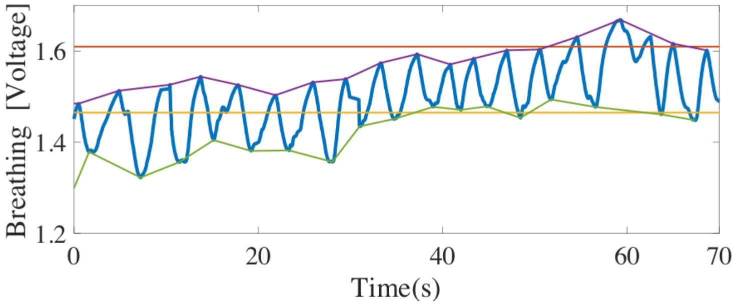

Figure 5.5: The voltage (linearly dependent on by the temperature) incresases after sensor positioning

5.3.5 Digital filtering for the GSR

GSR is a relatively slow signal because it measures the activation of gland cells located on the tip of the fingers. This activation is relatively delayed due to the persistence of ions on the skin. When the ANS is active, the gland cells on the fingertips open the ion channels, and the GSR sensor detects an increase in conductivity of the skin. For this reason, we are interested in the derivative of the signal. In this work, a robust algorithm for detecting the activation of the ANS is presented. At first, the algorithm filters the high frequencies, allowing that the gland cells need time to open and close the ion channels. Then, the derivative is calculated. The derivative of the signal gives useful information on the state of the ANS. Once the real-time derivative is obtained, a peak detector algorithm, described in Chapter 5, is applied to detect the highest relative variation in conductivity. Figure 5.7a shows GSR signal captured using two electrodes placed onto the skin. A low-pass IIR filter is applied to reject the noise as follows;

$$Y(t_i) = \alpha X(t_i) + (1 - \alpha)Y(t_i) \tag{5.1}$$

$$Y_{av}(t_i) = \alpha_2 X(t_i) + (1 - \alpha_2)Y_{av}(t_i) \tag{5.2}$$

$$GSR(t_i) = Y(t_i) - Y_{av}(t_i) \tag{5.3}$$

Where X(t_i) is the GSR samples, Y(t_i) is the low-pass IIR filter output and Y$_{av}$(t_i) is the moving average baseline of the GSR signal. Then the filtered GSR signal is obtained as the filtered samples less the baseline. The smoothing factors α and α_2 are between 0 and 1. In this work α and α_2 are set to 0.06 and 0.1 respectively. The filter cut-off frequency is given by:

$$f_c \approx \frac{\alpha}{2\pi T} \tag{5.4}$$

Where T is the sampling period. Figure 5.6b shows the filtered signal. This kind of filtering (filter IIR) avoids the usage of vectors to store many samples that is not possible in low power micro-controllers. The GSR signal carries information about the activation of the gland cells, so we are interested in the variation. Strong variations in terms of conductivity identify an activation of the ANS. Then, a numerical derivative is applied as follows:

$$\frac{dGSR(t_i)}{dT} \approx \frac{GST(t_i)\text{-GST}(t_{i-1})}{t_i - t_{i-1}} \tag{5.5}$$

The peak detector is then applied on the derivative function. Regarding the previous section, to find the peaks a calculation of a delta parameter is required. A delta parameter is a noise filter in the derivative, which is calculated during a previous calibration.

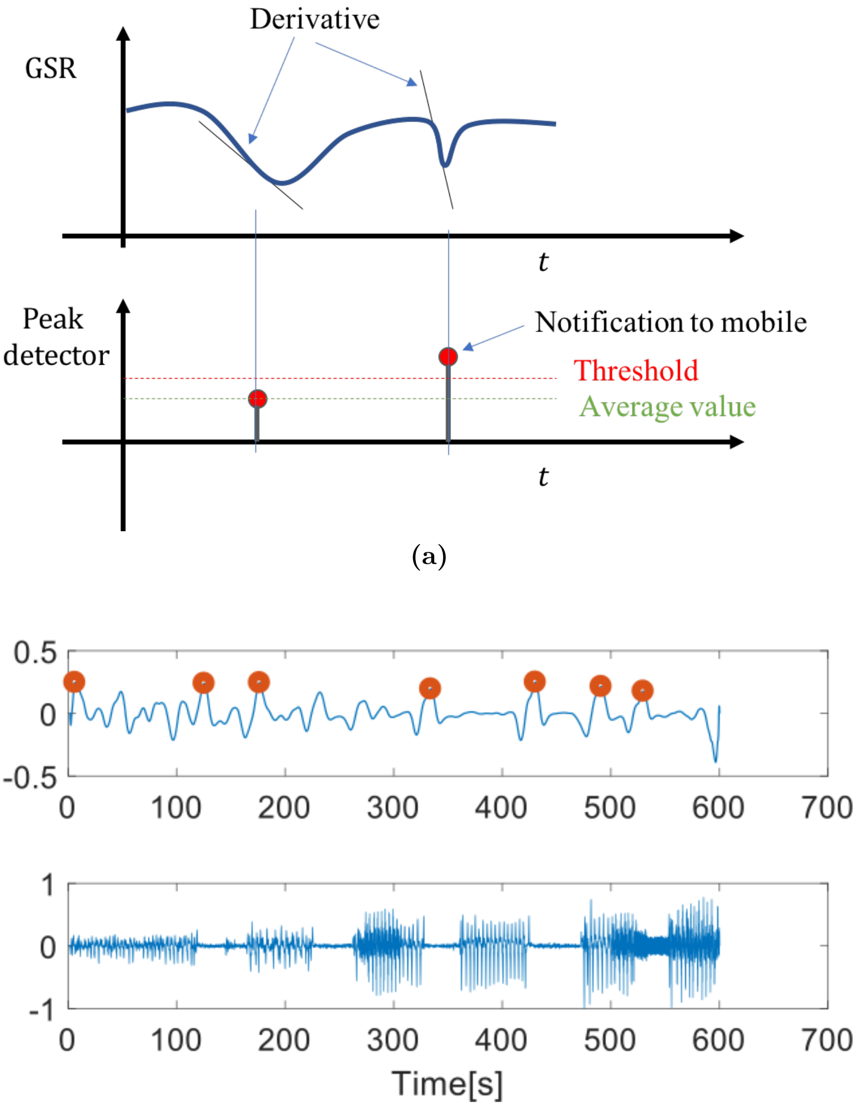

(a)

(b)

Figure 5.6: a) Signal GSR during an apnea event b)Example of breathing Derivative of the signal

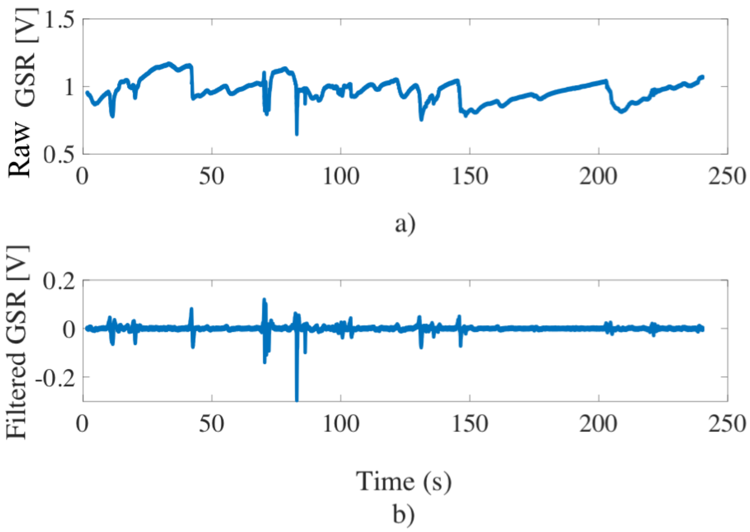

Figure 5.7: a) Raw GSR data, b) Filtered GSR

5.3.6 Calibration

The first minute of acquiring is considered as a calibration time. The low-pass band filter needs a few minutes to become operative. In the first minute, the user is awake and performs normal breathing. During this period the algorithm collects data. The filter expressed in 5.3 begins to work correctly once at least forty seconds has passed. Then, the device calculates the delta parameter as the percentage of the variation in the last twenty seconds as follows:

$$\Delta = \frac{1}{10}\left(\left(\frac{1}{n}\sum_{i=1}^{n}\max(Y(t_i))\right) - \left(\frac{1}{n}\sum_{i=1}^{n}\min(Y(t_i))\right)\right) \tag{5.6}$$

Where n is the number of the sample in the last twenty seconds of the measurement, and Y(t_i) is the filtered signal. So, the delta parameter is approximately 10% of the entire variation of the signal.

Algorithm 5.1 Algorithm for breathing and apnea detections

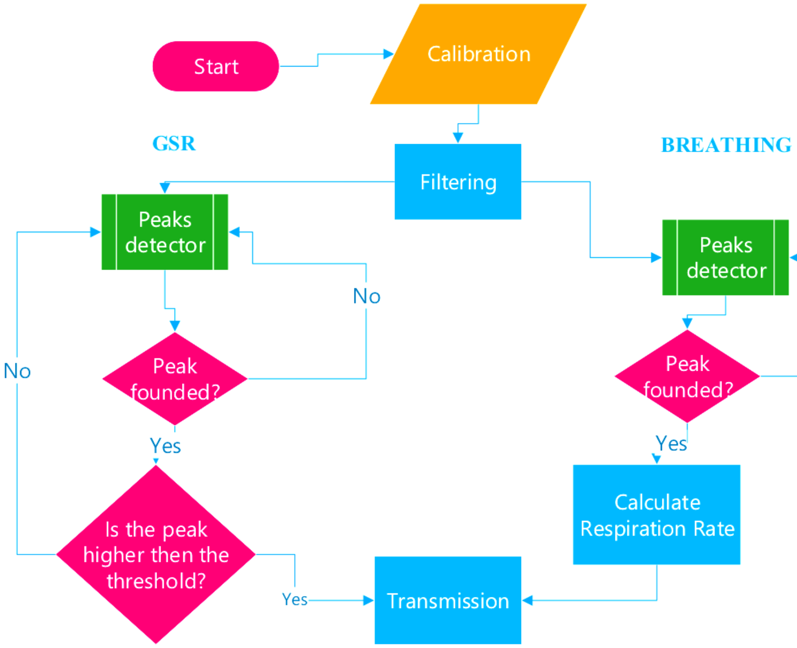

5.3.7 Results and discussion

The prototype has been built to study the robustness of the algorithms. An RFDUINO RFD22102 board is used to broadcast the signal and send the data to a smartphone. An application for the mobile phone has been built to show the results using the MIT app inventor. In this section, different measurements are presented to validate the algorithms. The measures involve;

- Normal breathing;
- Alternate breathing (deeper and slower);
- Alternate breathing with apneas.

Figure 5.8 shows three minutes of normal breathing. The GSR is quite regular, and there is not much variation in the derivative. Stimuli are not high enough to activate the sympathetic system. Then, the algorithm doesn't send information to the smartphone. Figure 5.10 shows variable respiration. When the breathing is more profound, it is possible to recognize peaks in the GSR signal. In this case, the device sends information to the smartphone. Figure 5.9 shows that apneas alternate with normal breathing. Just after an apneas, it is possible to recognize peaks in GSR measurement. The algorithm detects those peaks. Everyone gives different results since their cells behave differently, therefore the threshold cannot be defined before the test. So, during a calibration time, it is possible to define a threshold on the amplitude. It is calculated as a percentage in the deviation of the peaks detected:

$$S_{GSR} = (1+\gamma)\frac{1}{n}\sum_{i=1}^{n}|X_{p,i}| \tag{5.7}$$

Where γ is a percentage of the average values of the positive and negative peaks, $X_{p,i}$. Many peaks, during the first measurement, were not strongly connected to the ANS activation, as you can see in Fig. 5.8, because it depends on normal ventilation. When an apnea occurs, the recorded value is much higher than the average of the other peaks, therefore an activation of the ANS can be detected(Fig. 5.10).

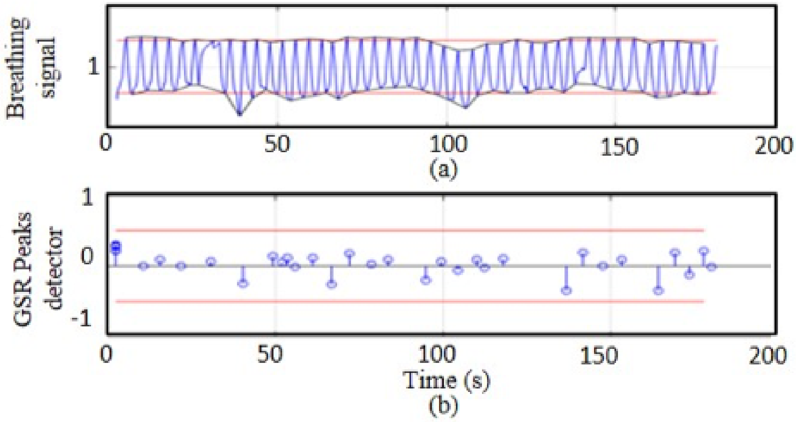

Figure 5.8: Normal breathing

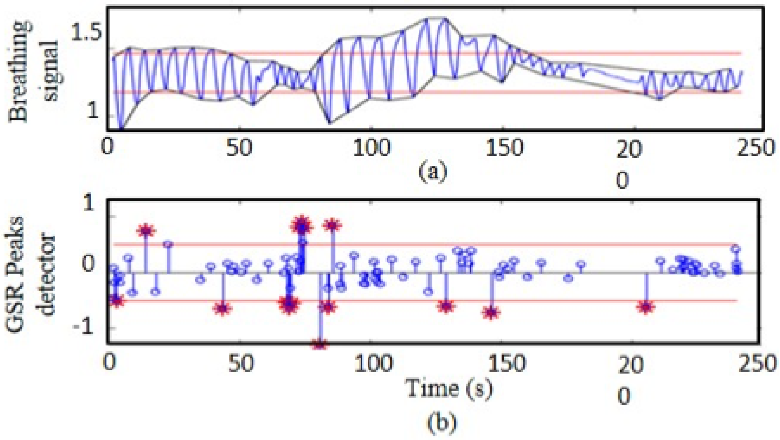

Figure 5.9: Output of the GSR algorithm for the case where there is changing in respiration. After 40 seconds, deeper breathing is performed. (a) Measured breathing signal, (b) Peaks of the GSR derivative (*) where a variation in ANS is detected by the algorithm.

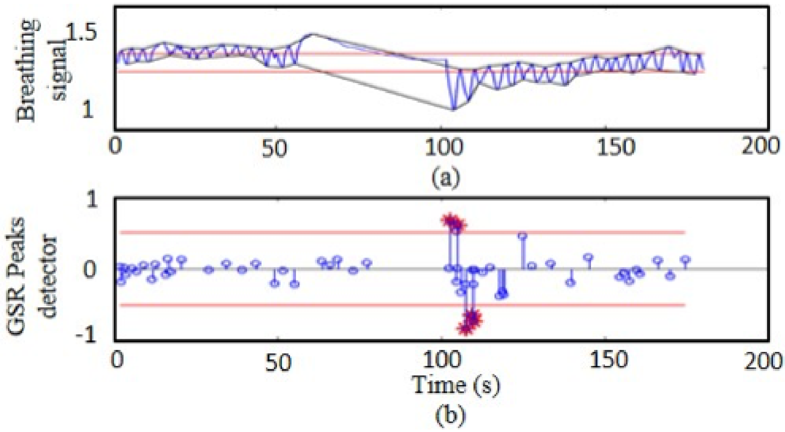

Figure 5.10: Output of the GSR algorithm for the normal breathing case. (a) Measured breathing signal. Red lines show an average of the maximum and minimum of the signal in the respiration. (b) Peaks of the GSR derivative. Red lines define the threshold GSR derivative signal. The algorithm detects every variation that is stronger.

5.3.8 Power consumption

The power consumption depends on the working time of any component. It can be possible estimate the lifetime of the device, considering the amount of energy used by each element, when a small, commercial coin battery is employed. The measured power consumption of each component is reported in Table 5.1. For this application, the primary dataset is presented as the respiration rate, which is estimated for each breath. The algorithm has been defined in the previews section. The module is an Arduino IDE based. The running time of the application is around 50 ms. Instead, the duration of a single breath is approximately 3 seconds for physiologic breathing. Therefore a sampling time of 100 ms can be acceptable to avoid artifacts. Accordingly, the micro-controller works at most for 50 ms every 100 ms to collect and elaborate data. A significant amount of energy is employed in transmission (Table 5.1). If the Bluetooth sent all samples to the mobile phone, the communication period would be 100 ms and the lifetime of the battery could decrease to approximately 24 hours. Since the consistent information is the respiration rate (RR), the amount of energy used for calculating on board is cheaper than the power for communicating with the mobile, hence a significant amount of energy, using this method is preserved.

A pie diagram reported in Figure 5.14 shows the amount of energy used in both cases, which are represented as a percentage of the energy of all components. Figure 5.14 shows a continuous transmitting. Figure 5.11 shows the improvement using calculation on board. Considering regular breathing, the lifetime of the battery increases of around 30 days (Figure 5.11). In the Figure is shown the lifetime of the battery compared to the period of communication of data by BLE. Figure 5.13 shows measurement of the time of calculation and power consumption of the device. A resistor of 100 Ω was used to measure the current.

Table 5.1: Power consumption of each used components

Component	Power Consumption	Working Time
Microprocessor cortex M0	~4 mA	22-100 ms
BLE module (transmission)	~15 mA	100/3000 ms
GSR sensor	~1 mA	100 ms
Respiration sensor (NTC)	~1 mA	100 ms

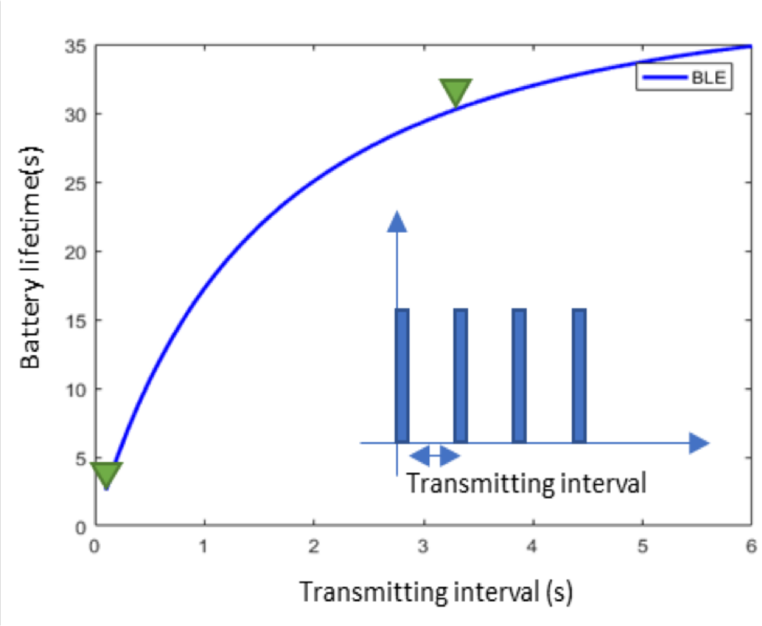

Figure 5.11: Improvement using calculation on board

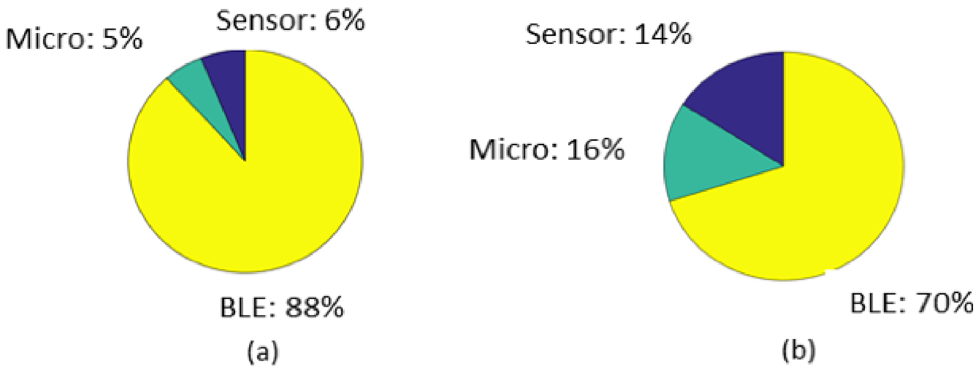

Figure 5.12: a continuous transmitting. 1) Most of the energy is used for the Bluetooth communication, therefore, the lifetime of the battery is reduced. 2) On the other hand, if the connection is focused on the most useful data, there is an balancing between the parts of the system.

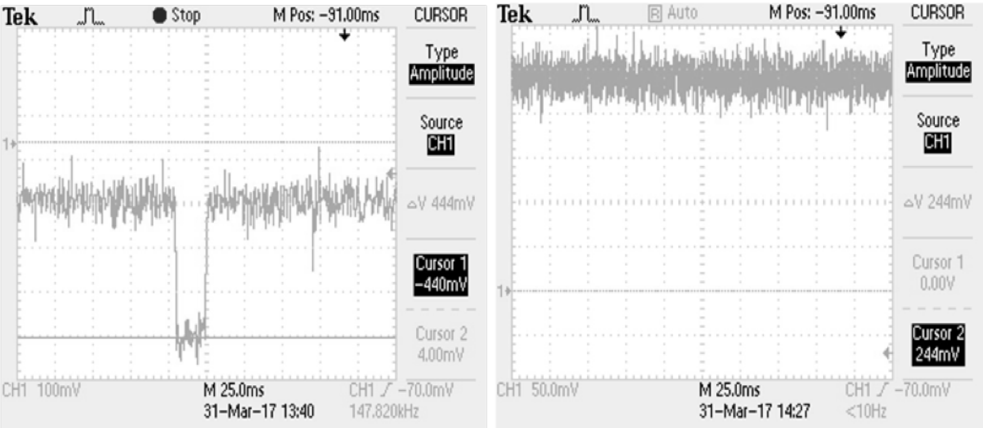

Figure 5.13: Oscilloscope measurement(a) Sleep mode for 25 ms. (b) Sensors always actives.

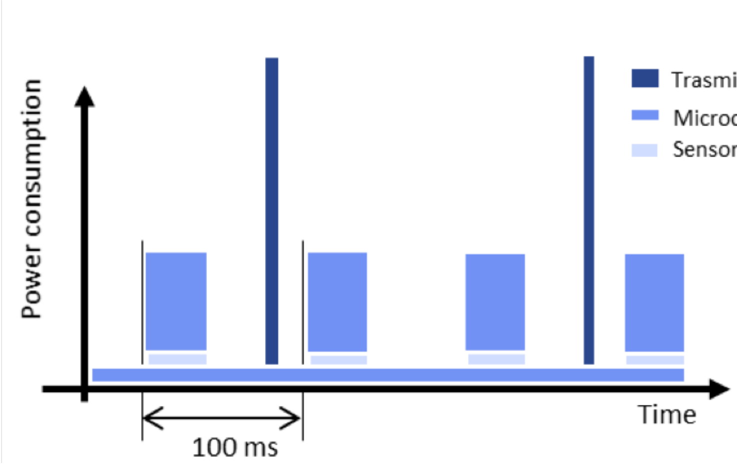

Figure 5.14: Device in different configuration.

5.3.9 Comments on results for breathing sensor with thermistors and GSR

A simple device to detect the correlation between respiration and activation of ANS has been proposed. While sleeping, the measurement of activation of the ANS is easy to identify because the body doesn't receive any external stimulus and risk of false negative detection is minimized. A strong correlation between apneas and the activation of the ANS can be noticed. A wearable GSR sensor can be used as a respiration sensor to detect apneas in the SBD. The GSR device is robust and comfortable and doesn't need to be stuck on to the skin. Efficient algorithms have been proposed to save energy and data storage. For three minute of recording, approximately 30 samples are transmitted by BLE after the calculation compared to the three thousand samples recorded. In addition to this data fusion improvement, at least 50% of battery is saved by calculating the peaks in GSR before transmitting the data.

5.4 Magnetometer-based respiration sensor for chest movement detection

Breathing is a prominent indicator of several problems such as sleep disorders and many devices have been designed to address the main parameters for this disease [107, 119]. Accelerometer-based sensors are designed to detect breathing and communicate through a gateway to a web service [64, 120]. Non-contact devices have been proposed to detect breathing [121, 61, 122]. Airflow sensors detect the breathing airflow measuring a temperature variation at nose level [106, 123, 46]. Capacitance variation sensors have been proposed for detecting respiration rate and time of apnea [107, 124]. These devices represent a good portion of a fast-growing world of wearable healthcare. However, steps forward can be made to overcome several typical problems such as battery lifetime, size, and comfort for the user. Indeed, complicated algorithms decrease battery lifetime, while long and bulky cables make devices uncomfortable.The use of accelerometers has recently emerged as an alternative method for monitoring the movement of the chest and abdomen [125]. Single or dual-axis accelerometers can only obtain an optimal breathing signal when appropriately aligned with the major axis of rotation, but it is not practicable for real-time application, using a low power microcontroller [62].

Other methods are based on the reconstruction of the angular movement induced by breathing, in periods when the patient is otherwise static, but it does not work for real-time applications yet [62, 126]. During a respiration cycle, breathing is characterized by an upper body activity, which involves a displacement of the thoracic rib cage. Especially during intense physical activities, the entire ventral cavity compresses and expands. Simultaneously, the abdominal cavity is pushed by the diaphragm contraction, moving the abdomen forward. A magnetometer is a simple sensor that measures magnetic fields and the magnetization of materials. This sensor is usually based on the electromagnetic property of the earth. The main advantage of using a magnetometer over accelerometer for breathing rate measurement is that movements of the chest can be obtained from the magnetometer data without complex processing. In the case of the accelerometer, the movement of the chest must be obtained from integration of the acceleration using sophisticated algorithms such as Kalman filters [64, 126]. This allows the magnetometer and signal-processing algorithm to be programmed in a low-power on-site micro-controller, instead of an external computational unit. Therefore, only real-time processed data are sent to a gateway (in this work a smartphone) for an IoT database, reducing the number of RF transmissions, improving its battery lifetime.

5.4.1 System architecture

Fig. 5.15 shows a block diagram of the entire wearable system used to detect respiration and compute respiration rate, apnea periods, and movement time. The system integrates an LM303DHLC sensor, an RFduino module that includes a micro-controller Cortex M0 and a nRF51822 Nordic Semiconductor Bluetooth low energy (BLE) module, Arduino compatible. The three computed parameters are sent to the cloud using a smartphone as a gateway.

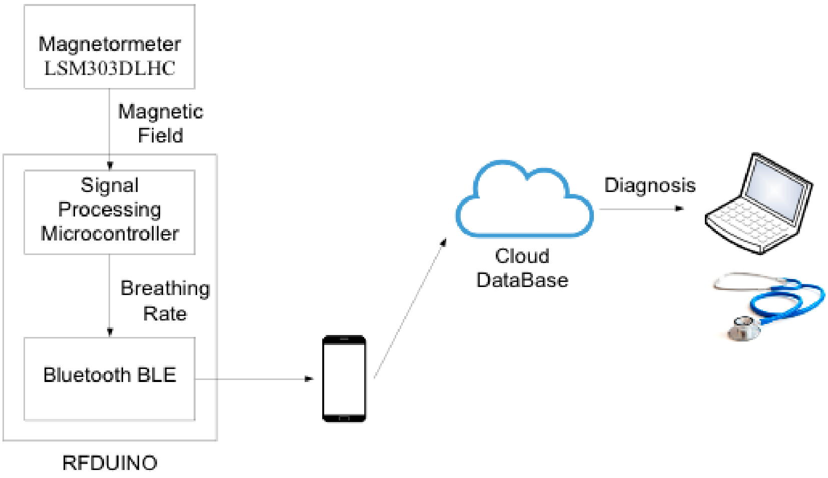

Figure 5.15: Block diagram of system

5.4.2 The sensor

An inertial measurement unit (LSM303DLHC from STMicroelectronics) measures the thoracic and abdominal cavity movements, by reading the corresponding variation in the magnetic vector in real-time. During breathing, this magnetic vector rotates due to the chest movement. This rotation changes one of the three magnetic vector components, which is detected by the sensor (Fig. 5.16). During regular breathing, the body movement moves the sensor, located on the chest, about 4 mm from its original position [127]. The average chest wall displacement is detected by the magnetometer sensor that shows a significant variation of the magnetic field, which allows distinguishing the waveform of breathing as described in section IV.

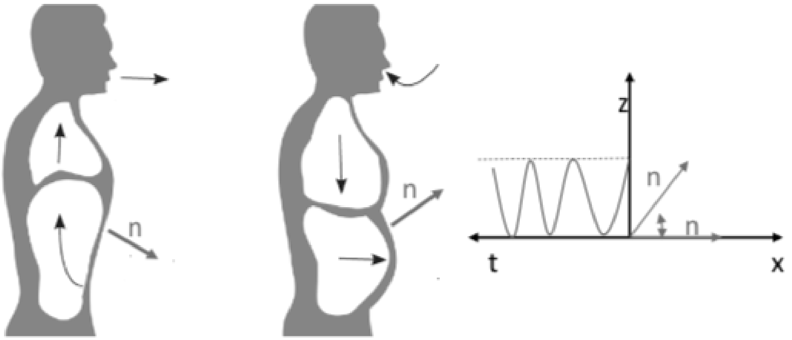

Figure 5.16: Vector magnetic field displacement.

LSM303DLHC contains a magnetic field full scale of ±1.3x104 to ±8.1x104 µT. According to previews works [127] , has been found that the Z-axis component of the magnetic field (perpendicular to the board) is the most sensitive to chest movement, as Fig. 5.17 shows. This displacement causes a changing of magnetic field power of around 0.2 µT in the direction of the shift, which is detected and recorded by the sensor. In addition, any different body movement is even easily identified, giving more information about the state of sleep.

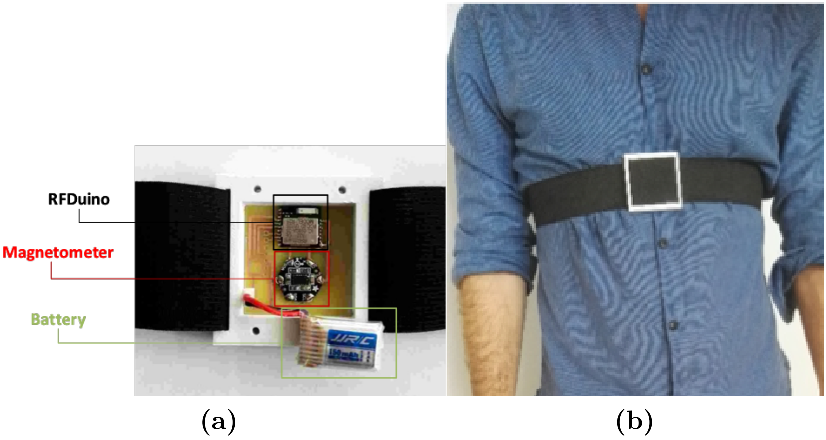

(a) (b)

Figure 5.17: (a) Photograph of prototype, (b) Magnetometer sensor setup. Sensor placed on the body using an elastic chest belt.

5.4.3 Transmitting and computing unit

RFduino [128] is an integrated system-on-chip (SoC), which can receive data from the magnetometer through the I2C bus and easily transmit it by using the bluetooth smart protocol to a smartphone. The RFduino module elaborates data, obtained from the breathing sensor, and extracts three sleep parameters: *respiration rate* (RR), *apnea periods* (AP) and *movement time* (MT). The smartphone receives these parameters and uploads them to a custom IoT database for analysis by a specialist. The smartphone can also display the data in a *custom made app*. A proof-of-concept prototype is shown in Fig. 5.17. The RFduino, the magnetometer sensor module and the Lite-on rechargeable battery are pointed out. The system is packaged in an ad-hoc box, manufactured using a 3D printer and made of *poly-lactic acid* (PLA), a wholly biocompatible material. An elastic chest belt is used to place the sensor on the body (5.17b). The Bluetooth communication has been implemented using *MIT app inventor®*. Data is recollected, and elaborated to be displayed on the phone and saved on an IoT analytics platform service (Fig. 5.18) that allows it to compile, visualize and analyze live data streams in the cloud (*ThingSpeak®*), which provides instant visualizations of data posted by a device.

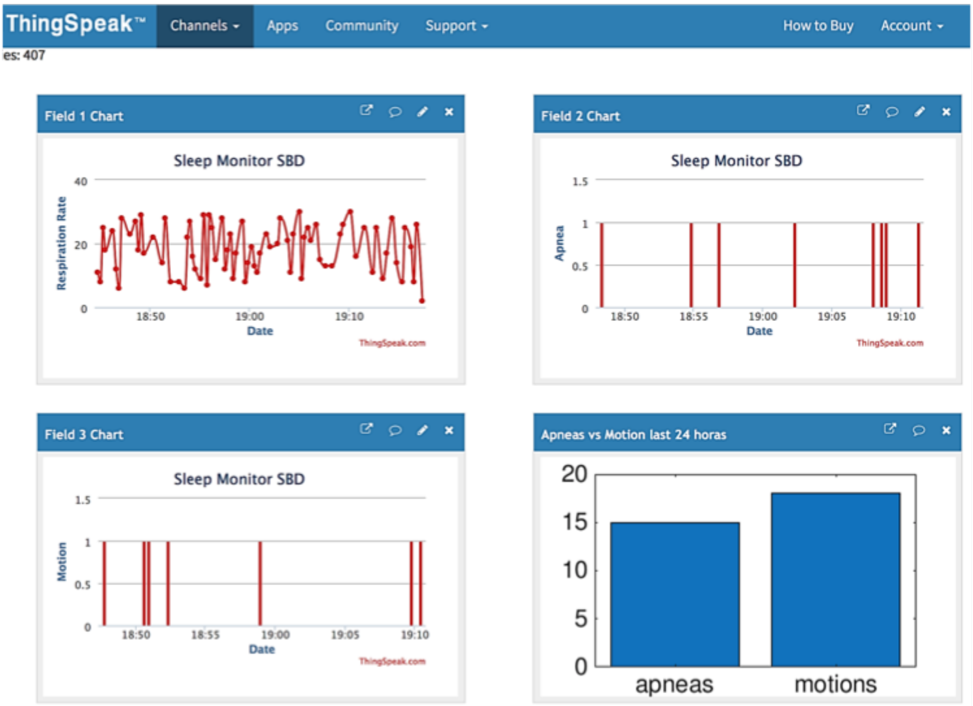

(a)

(b)

Figure 5.18: a) Thing-speak® screenshot, b) A phone"s screenshot of the app

5.4.4 Data processing

Sampled data are pre-treated by a *real-time filtering method*, which removes high- and low-frequency noise (as described in sec. 6). Therefore, an algorithm to detect peaks and troughs is applied, and consequently, the respiration rate is calculated for each breath. The same module can calculate time duration of apneas and detect body movements using the internal accelerometer available in the module.

Fig. 5.19 shows the block diagram of the signal processing applied to the breathing signal. This signal, which is weak and noisy, is superposed over a baseline value. Therefore, the average signal is subtracted, and the result is low-pass filtered to reduce noise. The used algorithm is explained in section 6, and is here reported for comparison. Since the filters must be implemented in a low-power micro-controller, exponential moving average filters are used to reduce the computational charge and memory. The average signal X_{av}[n] is estimated using the following recursive equations from the measured samples X[n]:

$$X_{av}[n] = \alpha_1 X[n] + (1-\alpha_1) X_{av}[n-1] \tag{5.8}$$

$$S[n] = X[n] - X_{av}[n-1] \tag{5.9}$$

Where S[n] is the breathing signal without the baseline signal. Then, the output breathing signal is obtained from a second exponential moving average filter:

$$Y[n] = \alpha_2 S[n] + (1-\alpha_2) S[n-1] \tag{5.10}$$

The smoothing factors α_i (i=1,2) are between 0 and 1 and are chosen as a function of the maximum and minimum physic-pathological breathing rate. The filters cut-off frequency can be approximated from the smoothing factors α_i (i=1,2) using:

$$f_c \approx \frac{\alpha}{2\pi T} \tag{5.11}$$

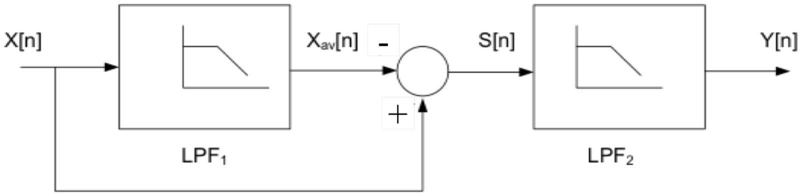

Figure 5.19: Block diagram of signal processing

Where T is the sampling period. In this work, α_1 and α_2 are set to 0.04 and 0.08, respectively.

Block diagram of signal processing Respiration rate and movement detector The breathing rate, usually expressed in breaths per minute (bpm), is estimated from the inverse of the interval between two consecutive peaks. At the same time, the readout of the accelerometer is used to detect movements applying a comparison with a threshold value. A peak detection algorithm has been developed to obtain the peaks and troughs of the filtered breathing signal Y[n]. Details about the implementation are explained in [8].

A suitable parameter allows calculating the respiration rate with minimal error. The peak detector is then applied to the filtered signal. When an interval between two consecutive breathings is longer than 10 seconds, it is considered as an apnea. In this case, an apnea index is activated to count the number of apneas during the measurement session. Every body movement introduces a substantial variation in the magnetometer signal that is detected by applying a threshold detector before the peak detection. The accelerometer integrated into the inertial unit can be used for this purpose. A movement index is defined as a counter which is uploaded as soon as movement is detected, then it can also be used as a sleep quality indicator. The breathing rate during this time interval is ignored.

5.4.5 Results

This section illustrates experiments to detect breathing signal using the proposed sensor performance . Measurements are compared with a temperature airflow sensor (Fig. 5.20). The temperature airflow sensor consists of a Negative Temperature Controlled (NTC) thermistor located under the nose. The same algorithm explained in Section 5.4.4 has been employed. In fact, by measuring the airflow under the nose, a comparable result is expected [67]. A thermistor placed under the nose measures the temperature of the airflow during a regular respiration act. This method is highly used in low-cost application but suffers from some disadvantages. Since it employs long thin cables for its movement, this sensor could, therefore, be uncomfortable for the users, especially during long recordings (for 6 hours at night). In addition, any displacement from the correct position can cause a weak measurement due to the modified distance between nose and sensor. An analogue signal amplifier is often used to overcome this problem even if power consumption is also increased. The NTC resistance (RNTC) can be measured using the Wheatstone resistive bridge followed by an inverting operational amplifier (Fig. 5.1a).

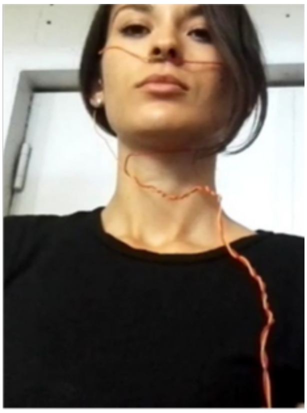

Figure 5.20: Experimental setup for the NTC thermistor sensor

The output voltage V_{out} is recorded using the analogue to digital converter (ADC) included into the microcontroller. However, this sensor is inadequate for people with OBC or nocturnal apnea, whose breath is often through the mouth during sleep. A wireless magnetometer, placed on the chest, can measure the breathing with a similar accuracy, in a more comfortable way, avoiding long, bulky cables. Both two sensors are simultaneously connected to the same micro-controller which has been used as a recording unit to obtain the results that are shown in this section. The sampling rate is the same for both sensors, 10 Hz=1/10 s. The algorithm, explained before, is applied in post-processing to evaluate three parameters: respiration rate, duration of apneas and movement events. A 3D accelerometer, which is embedded in the same module as the magnetometer, is also employed to validate the movement detection that is also captured by the magnetometer sensor. Measurement sections of 200 s have been performed to compare properties of these sensors. Subjects are asked to breathe through the nose and recreate apnea and movements randomly. The magnetometer signal shows a correlated waveform with the thermistor output for most of the acquiring time (Fig. 5.21).

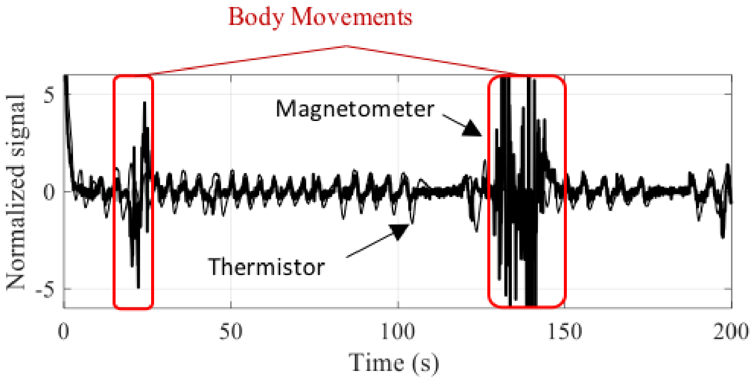

Figure 5.21: Normalized signal compared. Thermistor (thin line) vs magnetometer (thick line).

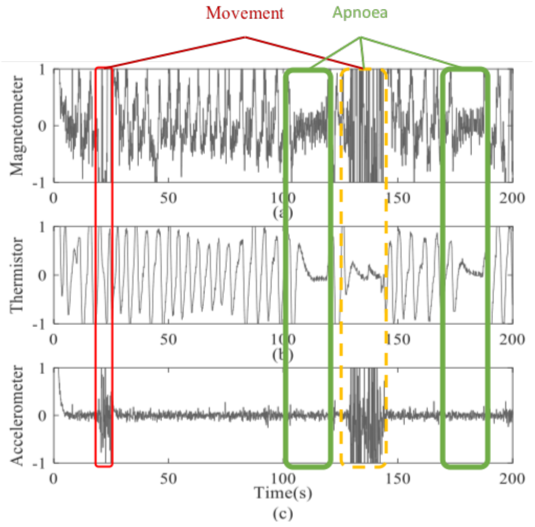

Figure 5.22: Normalized breathing detected with three different sensors. (a) Chest displacement sensor based on a magnetometer, (b) an airflow sensor based on thermistor (c) an accelerometer sensor.

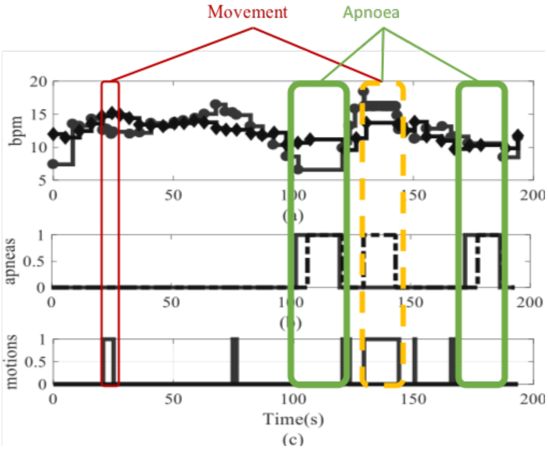

Figure 5.23: Comparison of the three extracted parameters, thermistor (red line), magnetometer (blue line) (a) bpm computed by the algorithm, (b) apnea and (c) movement detected.

The primary disagreement has been noticed during body movements. Indeed, the magnetometer is highly sensitive to the movement of the body, which can be used as a parameter for *Sleep Disorder Activity* (SDA). The signals are processed with the same filtering parameter α_1 and α_2 values. Consequently, the algorithm for peak detection has been applied to provide respiration rate with every breath. During the experimentation, it has been noticed that body activity is distinguished both by the accelerometer and the magnetometer (Fig. 5.22), while the airflow measurement does not show a relation with the body activity. Fig. 5.22 shows a comparison between the accelerometer sensor and the signal captured by the magnetometer during movements (thin rectangle), while the thermistor maintains stable behavior. Furthermore, a strong relationship between the thermistor and magnetometer signal can be appreciated during apnea (thick rectangle), while accelerometer does not show significant variations. The dotted line in Fig. 5.22 shows a case where apnea is recreated during a body changes. In this case, the magnetometer can detect body changes but not apneas, which is detected by the thermistor that is not able to identify body movement. As mentioned before, the highest mismatch in bpm calculation depends on the body activity. Thick rectangles in Fig. 5.22 show that applying the algorithm to detect apnea works correctly when no movement is performed. On the other hand, the dotted rectangles show missing apnea. Short time spikes are identified and reported in Fig. 5.23which depend on little drifts during the acquisition period, that doesn't modify bpm calculation. While sleeping, body repositioning is usually reduced, so that they cannot compromise the breathing measurements. In this case, results obtained by the airflow sensor and the magnetometer are very similar. As a result, the algorithm, applied to both signals, shows a maximum mismatch of around 0.5 bpm on the average error, measured continuously for 8 hours on a volunteer during sleeping. This result is acceptable for many applications. In summary, when the magnetometer detects a movement, it is not even able to catch the respiration rate, on the other hand, the thermistor is still able to measure breathing rate, but it cannot detect movements, and mouth breathing sensors show a good match. Since the algorithm estimates the breathing rate of each breath, the calculation shows some local errors due to the movement or a small variation (for instance, some breathing through the mouth). After passing the transient filter response at the start-up, the difference between waveforms is consistent for most of the recording time. Fig. 5.25a shows the correlation between respiration rate calculated from the thermistor and the same parameter derived from the magnetometer for a sampling. Despite some local error, the correlation coefficient remains over 0.85, and the average breathing value is also very similar (Fig. 5.25b shows the distribution of the average error).

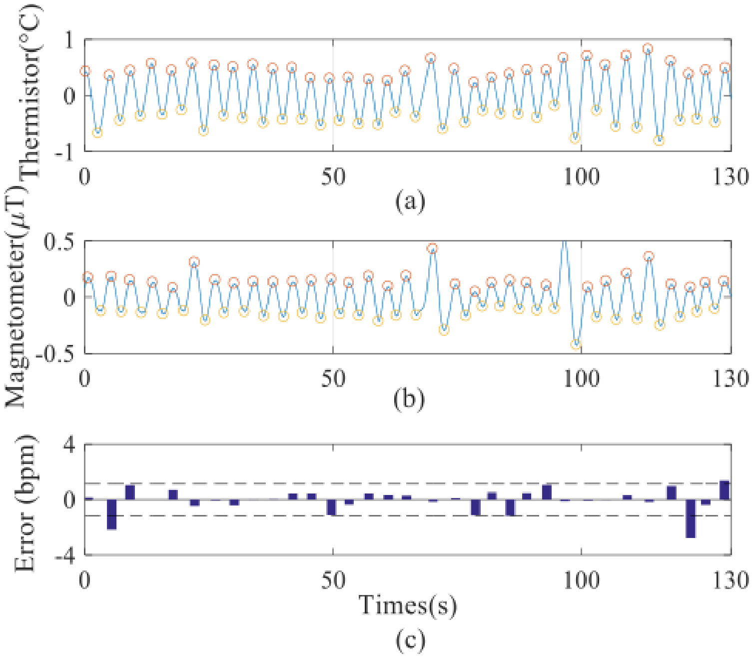

Figure 5.24: Comparison between thermistor and magnetometer sensor for 5 minute recording during a regular working activity. (a) Airflow at the level of the nose (b) Displacement (c) difference between thermistor and magnetometer measurements.

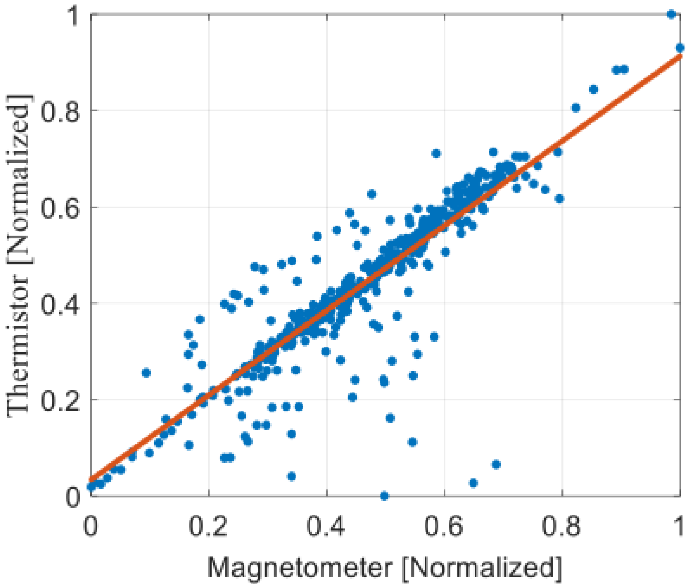

(a)

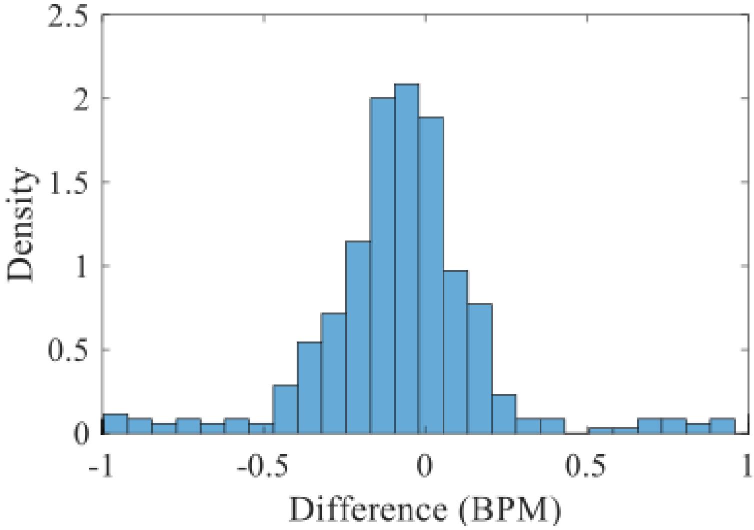

(b)

Figure 5.25: (a) Analysis of correlation between the normalized thermistor and magnetometer measurements, (b) histogram of the difference between the breathing rate obtained with the two sensors.

5.4.6 Power consumption

Breathing analysis for detecting major diseases may need several days, so a long-life battery is necessary. For each wearable device, the battery is a crucial issue due to its needs to be small enough to fit into the device while at the same time, it must deliver the right amount of energy to power the sensor for the entire period of measurement, avoiding a battery replacement. By a continuous recording and transmitting with one of the lowest power consumption technology available in the marketplace (a Bluetooth low energy based sensor [124]), a measurement for an entire night is not achievable if a small coin battery is considered. BLE is one of the most widely wireless communication technics used for sleep monitoring and body parameters monitoring for its low power and adaptability [125]. BLE allows the minimum power consumption by setting the sample rate to 100ms that guarantee a proper signal processing. Since RFduino needs only 3 ms to elaborate data and transmit it, a consistent amount of energy can be saved. A BLE module can manage the time of activity, going into a sleep mode state that is an ultra-low power state, reducing power consumption. The proposed algorithm also reduces transmissions since it updates data every breath (approximately every 4 seconds). Fig. 5.26 shows the current consumption of the device, considering the micro-controller in three different states. The measurement has been performed using an oscilloscope monitoring the supply current. Fig. 5.26a shows the BLE always on without considering sleep mode state; figure 5.26b shows the power consumption for 50% of the time in sleep mode. Since the sampling rate is 10Hz, it can remain in sleep mode for the entire period saving more than 85% of energy. Fig. 5.26c shows the amount of time spent in the calculation. Fig. 5.26b shows the event of transmitting that appears with every breath. The battery life in normal operating mode is around 25 hours, whereas by using the algorithm is more than 150 hours using a typical 3V Lite-on battery (150 man).

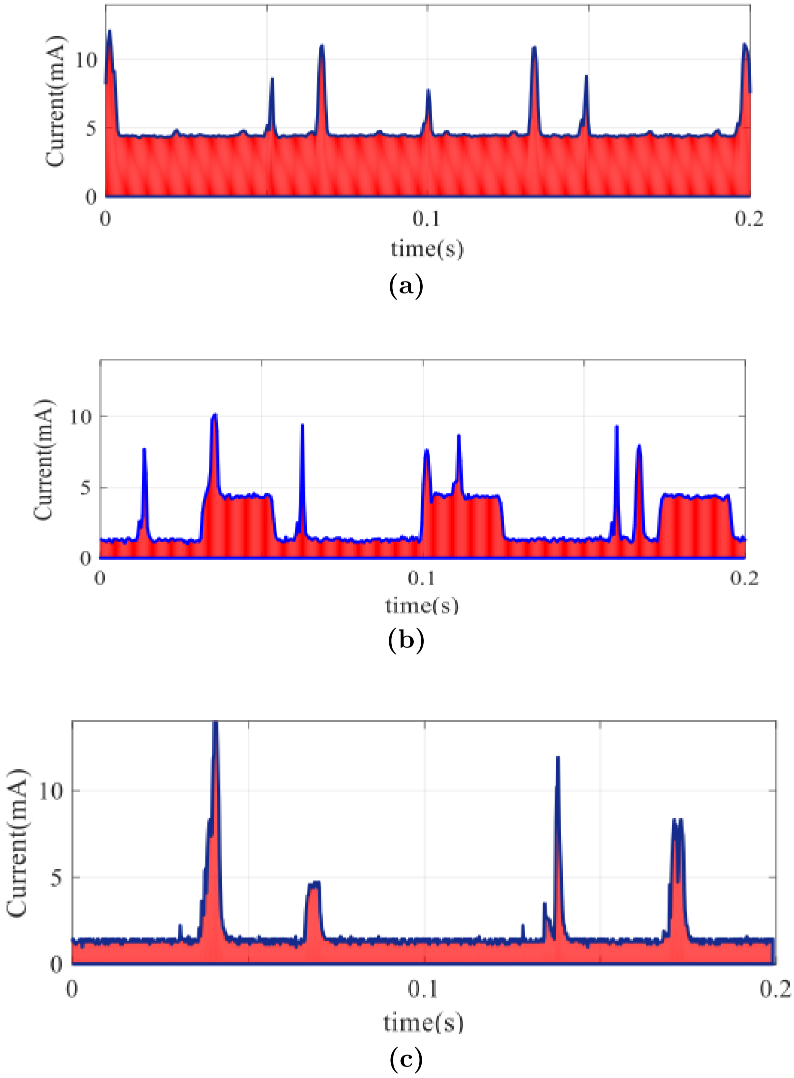

Figure 5.26: Power consumption (a) Microprocessor active 100% of the time (b) Microprocessor active 50% of the time (c) Microprocessor active 5% of the time

5.4.7 Discussion and comparison with other devices

Table 5.2 shows a comparison of different available works about breathing monitoring and sleeps quality, to demonstrate the potential application of the described sensor. Various sensor technologies are considered. Many wearable devices have been designed for sleep activity, but they can measure only some parameters. Commercial wristbands use the accelerometer as a pedometer and a sleep movement detector, but these devices cannot measure the breathing rate or apnea periods. Furthermore, many of the technologies analyses in Table 5.2 are sensible to the body movements. However, in sleep monitor applications, the duration of body movement events is small compared with the total analysis time. Also, a movement detector during sleep delivers useful information about the sleep quality or into detection of some types of epilepsies. On the other hands, these sensors are not appropriate for sports applications because the body is in constant movement. In these case, more invasive sensors such as based on thermistors [67, 129], spirometers or rip belts, which are often used in short time effort tests, can be used. In sleep applications an appropriate result is performed by no-contact devices like camera [130, 14, 131] and microphones [132] that do not need to be installed on the body. On the other hand, these sensors are not personal, and the presence of another user in the same environment can cause a weak measurement. In the case of a camera-based sensor, the body orientation is also critical and cannot be changed during the analysis, that is not practical for sleep monitoring. The portability and the low computational charge of the proposed sensor make it ideal for an extended period measurement, without any other device connected. Some personal breathing sensors [133] are based on accelerometers, but these techniques require complex processing techniques to obtain the chest movement that cannot be calculated on board, and it is performed on external computers after recording the data. Therefore, all the sampled data must be wirelessly transmitted reducing the battery life. Furthermore, breathing analysis may need several days to detect major diseases, so a long-life battery is necessary. BLE is one of the most widely wireless communication technics used for sleep and body parameters monitoring for its low power and adaptability [134, 135].

Table 5.2: Comparison with other breathing sensors

Ref	Sensor Type	Wearable	Communication Technology	Comments	Real-Time	Disadvantages
	Magnetometer	Yes	Low power (BLE), portable	Not invasive, sleep monitoring for new-borns (apnea detector)	Yes	Sensible to movements.
	Thermistor	Yes	Low power, portable analogue transmission [19] and BLE [20]	Breathing measured by the nose airflow	Yes	Not usable for mouth breathing. Quite uncomfortable.
	Camera	No-Contact	Wired, not portable	Breathing from image analysis	Yes	Not personal, sensible to movements and body orientation. Calibration is needed.
	Accelerometer Acc. + Gyro	Highly	Wireless (Bluetooth 2.0+EDR), portable	Respiration rate calculated by sensor fusion and integration	No	Sensible to movements. Processing not allowed on board, High power consumption
	Microphone	NO-Contact	Mobile phone, portable	Breathing and sleep monitor by recording sound	Yes	Not personal device. Sensible to sound interference.

5.5 Conclusions

The feasibility of a wearable device to detect apneas and breathing rate based on a magnetometer sensor has been presented and tested. A magnetometer has been fully integrated into a small wearable device with wireless capability. An algorithm for calculating respiration rate has been presented and applied to the data from the magnetometer and compared for verification to an airflow sensor based on a thermistor with excellent results. An increase of battery life has been demonstrated by applying an ad-hoc algorithm.

6

Conclusions

Inspired by the exponential growth of the IoT in biomedical fields, this Thesis has faced overall issues on multiple technologies which are nowadays accessible in the marketplace. The primary scientific contribution regarded a broad perspective for detecting well-being parameters using a non-invasive, light-weight, low-cost, and low-energy approach. By starting with a claimed RFID technology, the best-addressed challenge has been the reshaping of tags, which are not ideated to be placed on the body. The study was directed in the electromagnetic point of view at the hardware and the system level, but also on the sensing aspect of the whole design, taking into account a real environment. A good performance regarding conformability design, reading distance and temperature reliability have been achieved. The measured reading distance for epidermal tags allows monitoring the users while they are crossing a gate or around no-contact contactless barriers. Therefore, a real-life ability has been confirmed by the experiments, and a proper matching between requirements and achievements provides a step forward for the RFID in medical uses. The effectiveness of the RFID technology depends on its wholly passive nature that reduces its cost and enables disposable applications. Their performances have been demonstrated for real-time, spotted discontinuous cases. This approach is overall indicated for tracking and monitoring a significant amount of users in public areas likewise airports and stations. One of the most exciting alternatives to the passive RFID has been the FSS-based sensors that enable a better resolution and a high accuracy regarding sensing capability, still having a low price and a semi-passive behaviour. With top performances regarding wearability, battery life and reading distances, FSS-based are also very versatile, and high adaptability has been demonstrated by fabricating and testing various prototype for many frequency ranges. Furthermore, the FSSs are robust to the human body variability thanks to their wide frequency range, and the body presence and lossy substrates do not significantly reduce their performance. It has also been demonstrated they hold a longer reading distance than the RFID, introducing new scenarios. Moreover, the most accurate efficacy of the FSS-based allows measuring more complex body parameters, such as the respiration rate, by measuring the airflow temperature, that consequently also enable a wide range of new applications. Therefore, this property makes FSS-based sensing helpful in the continuous home measurement, where a combination of long-term recording and reliability are necessary. Despite RFID and FSS-based sensing are quite similar, an objective comparison emphasizes their differences regarding the usage permitted. Finally, a stable active alternative is also discussed here to indicate its advantages and disadvantages compared with the technologies above. This thesis demonstrates the usability of the BLE as a transmission method for breathing sensors based on a simple commercial magnetometer. The main benefits here discussed regard a smart onboard computation algorithm, which reduces consistently the amount of data transmitted, consequently decreasing the energy used in connections and also, the volume of the stored data. The possibility to arrange different sensors on the same board, increases the robustness of the calculation method, obtaining more reliable information which has been proved by adding the GSR information for detecting apnea and a deep breath. Another conferred advantage depends on its high compatibility with several consumer electronics which provide to use commercial smartphones as gateways to spread real-time details on web platform with any uses of other customized infrastructures. On the other hand, this more complex and rigid structure reduces the conformability on the body, forcing a redesign/reshaping that is not always achievable. The analogue mode is however considered a preferred choice also if the strategy to save energy can be implemented with structured technology or standardized protocols. The reduced amount of on body electronics is a benefit to reduce size, weight and dimension of batteries, enabling a not-invasive conformability on the human body.

6.1 Open issues and Future Research

Despite the significant achievements, various points are still open and attractive for future research aspects. The first aspect involves the RFID-based sensing. Notwithstanding a very low-energy activation threshold of the new generation of tags, the human body is still a visible obstacle to the radiation pattern, which deteriorates their performances. Research orientated on the reader design could increase its sensitivity, enabling a longer reading distance. New studies have demonstrated that an improvement in reader sensitivity can push forward the usability of the RFID in the medical field. Reading ranges can also be improved by including new materials capable of separating the body with satisfying electromagnetic performances. Furthermore, the RFID technology, as well as the FSS-based sensing, is highly versatile and reshapeable. That fact opens multiple possibilities for combination with biocompatible, biodegradable materials aligning these communication methods with the vision of the epidermal electronics. Moreover, FSS-based sensors are also more flexible because its semi-passive nature needs a few amounts of energy to power the sensors and alternative harvesting methods can be tested to eradicate the use of batteries. Peltier cells can be employed to exploit the body temperature to power up the sensors running in standalone mode. Wearable medical sensors are still far to be considered commercially available because this modern approach should be intensely tested and their reliability has to be validated. Therefore, many tests must be assessed by physicians and medical staff before becoming a new powerful toolbox. Finally, to implement the absolute idea of the “lab on skin”, the sensing functionalities of the epidermal radio-sensor must be expanded, and more applications for healthcare can be studied and tested.

Bibliography

[1] B. Abidi, A. Jilbab, and M. E. L. Haziti, “Wireless Sensor Networks in Biomedical: Wireless Body Area Networks,” in *Europe and MENA Cooperation Advances in Information and Communication Technologies*, ser. Advances in Intelligent Systems and Computing. Springer, Cham, 2017, pp. 321–329, dOI: 10.1007/978-3-319-46568-5_33. [Online]. Available: https://link.springer.com/chapter/10.1007/978-3-319-46568-5_33

[2] S. Hiremath, G. Yang, and K. Mankodiya, “Wearable Internet of Things: Concept, architectural components and promises for person-centered healthcare,” in *2014 4th International Conference on Wireless Mobile Communication and Healthcare - Transforming Healthcare Through Innovations in Mobile and Wireless Technologies (MOBIHEALTH)*, Nov. 2014, pp. 304–307.

[3] S. Siboni, A. Shabtai, N. O. Tippenhauer, J. Lee, and Y. Elovici, “Advanced Security Testbed Framework for Wearable IoT Devices,” *ACM Trans. Internet Technol.*, vol. 16, no. 4, pp. 26:1–26:25, Dec. 2016. [Online]. Available: http://doi.acm.org/10.1145/2981546

[4] R. Paradiso, G. Loriga, and N. Taccini, “A wearable health care system based on knitted integrated sensors,” *IEEE Transactions on Information Technology in Biomedicine*, vol. 9, no. 3, pp. 337–344, Sep. 2005.

[5] S. Amendola, S. Milici, and G. Marrocco, “Performance of Epidermal RFID Dual-loop Tag and On-Skin Retuning,” *IEEE Transactions on Antennas and Propagation*, vol. 63, no. 8, pp. 3672–3680, Aug. 2015.

[6] M. Raj, P. H. Wei, B. Morey, X. Wang, B. Keen, P. DePetrillo, Y. Y. Hsu, and R. Ghaffari, “Soft bio-integrated systems for continuous health monitoring,” vol. 9083, 2014, pp. 90 831M–

90 831M–6. [Online]. Available: http://dx.doi.org/10.1117/12.2051272

[7] R. Paradiso, "Wearable health care system for vital signs monitoring," in *4th International IEEE EMBS Special Topic Conference on Information Technology Applications in Biomedicine, 2003*, Apr. 2003, pp. 283–286.

[8] A. Ukil, S. Bandyoapdhyay, C. Puri, and A. Pal, "IoT Healthcare Analytics: The Importance of Anomaly Detection," in *2016 IEEE 30th International Conference on Advanced Information Networking and Applications (AINA)*, Mar. 2016, pp. 994–997.

[9] J. Andreu-Perez, D. R. Leff, H. M. D. Ip, and G. Z. Yang, "From Wearable Sensors to Smart Implants- #x2013;Toward Pervasive and Personalized Healthcare," *IEEE Transactions on Biomedical Engineering*, vol. 62, no. 12, pp. 2750–2762, Dec. 2015.

[10] G. Elhayatmy, N. Dey, and A. S. Ashour, "Internet of Things Based Wireless Body Area Network in Healthcare," in *Internet of Things and Big Data Analytics Toward Next-Generation Intelligence*, ser. Studies in Big Data. Springer, Cham, 2018, pp. 3–20, dOI: 10.1007/978-3-319-60435-0_1. [Online]. Available: https://link.springer.com/chapter/10.1007/978-3-319-60435-0_1

[11] O. D. Lara and M. A. Labrador, "A Survey on Human Activity Recognition using Wearable Sensors," *IEEE Communications Surveys Tutorials*, vol. 15, no. 3, pp. 1192–1209, 2013.

[12] F. Xu, Z. Qin, C. C. Tan, B. Wang, and Q. Li, "IMDGuard: Securing implantable medical devices with the external wearable guardian," in *2011 Proceedings IEEE INFOCOM*, Apr. 2011, pp. 1862–1870.

[13] J. M. Winters, Y. Wang, and J. M. Winters, "Wearable sensors and telerehabilitation," *IEEE Engineering in Medicine and Biology Magazine*, vol. 22, no. 3, pp. 56–65, May 2003.

[14] J. Alihanka, K. Vaahtoranta, and I. Saarikivi, "A new method for long-term monitoring of the ballistocardiogram, heart rate, and respiration," *American Journal of Physiology - Regulatory, Integrative and Comparative Physiology*, vol. 240, no. 5, pp. R384–R392, May 1981. [Online]. Available: http://ajpregu.physiology.org/content/240/5/R384

[15] G. Cf and S. A, "Sleep apnea & automobile crashes." *Sleep*,

vol. 22, no. 6, pp. 790–795, Sep. 1999. [Online]. Available: http://europepmc.org/abstract/med/10505825

[16] T. Coy, J. Dimsdale, S. Ancoli-Israel, and J. Clausen, “Sleep apnoea and sympathetic nervous system activity: a review,” *Journal of Sleep Research*, vol. 5, no. 1, pp. 42–50, Mar. 1996. [Online]. Available: http://onlinelibrary.wiley.com/doi/10.1046/j.1365-2869.1996.00006.x/abstract

[17] S. J. Crinion, B. D. Kent, S. Ryan, P. Boyle, M. Traynor, A. Zaffaroni, E. O’Hare, E. Doheny, D. Flanagan, V. Grace, C. Heneghan, and W. T. McNicholas, “Home Detection Of Obstructive Sleep Apnea Using The SleepMinder - A Novel Bio-Motion Sensor,” in *D30. NOVEL SCREENING APPROACHES AND THERAPIES FOR SLEEP DISORDERED BREATHING*, ser. American Thoracic Society International Conference Abstracts. American Thoracic Society, May 2014, pp. A5610–A5610, dOI: 10.1164/ajrccm-conference.2014.189.1_MeetingAbstracts.A5610. [Online]. Available: http://www.atsjournals.org/doi/abs/10.1164/ajrccm-conference.2014.189.1_MeetingAbstracts.A5610

[18] N. J. Douglas, D. P. White, C. K. Pickett, J. V. Weil, and C. W. Zwillich, “Respiration during sleep in normal man.” *Thorax*, vol. 37, no. 11, pp. 840–844, Nov. 1982. [Online]. Available: http://www.ncbi.nlm.nih.gov/pmc/articles/PMC459437/

[19] X. F. Teng, Y. T. Zhang, C. C. Y. Poon, and P. Bonato, “Wearable Medical Systems for p-Health,” *IEEE Reviews in Biomedical Engineering*, vol. 1, pp. 62–74, 2008.

[20] Q. Cao, H.-s. Kim, N. Pimparkar, J. P. Kulkarni, C. Wang, M. Shim, K. Roy, M. A. Alam, and J. A. Rogers, “Medium-scale carbon nanotube thin-film integrated circuits on flexible plastic substrates,” *Nature*, vol. 454, no. 7203, p. nature07110, Jul. 2008. [Online]. Available: https://www.nature.com/articles/nature07110

[21] S. Milici, S. Amendola, A. Bianco, and G. Marrocco, “Epidermal RFID passive sensor for body temperature measurements,” in *2014 IEEE RFID Technology and Applications Conference (RFID-TA)*, Sep. 2014, pp. 140–144.

[22] G. H. Gelinck, H. E. A. Huitema, E. v. Veenendaal, E. Cantatore, L. Schrijnemakers, J. B. P. H. v. d. Putten, T. C. T. Geuns, M. Beenhakkers, J. B. Giesbers, B.-H. Huisman, E. J. Meijer, E. M. Benito, F. J. Touwslager, A. W. Marsman, B. J. E. v.

Rens, and D. M. d. Leeuw, “Flexible active-matrix displays and shift registers based on solution-processed organic transistors,” *Nature Materials*, vol. 3, no. 2, p. nmat1061, Jan. 2004. [Online]. Available: https://www.nature.com/articles/nmat1061

[23] J. A. Rogers, Z. Bao, K. Baldwin, A. Dodabalapur, B. Crone, V. R. Raju, V. Kuck, H. Katz, K. Amundson, J. Ewing, and P. Drzaic, “Paper-like electronic displays: Large-area rubber-stamped plastic sheets of electronics and microencapsulated electrophoretic inks,” *Proceedings of the National Academy of Sciences*, vol. 98, no. 9, pp. 4835–4840, Apr. 2001. [Online]. Available: http://www.pnas.org/content/98/9/4835

[24] F. Merli, L. Bolomey, F. Gorostidi, B. Fuchs, J. F. Zurcher, Y. Barrandon, E. Meurville, J. R. Mosig, and A. K. Skrivervik, “Example of Data Telemetry for Biomedical Applications: An In Vivo Experiment,” *IEEE Antennas and Wireless Propagation Letters*, vol. 11, pp. 1650–1654, 2012.

[25] Y. H. Jung, H. Zhang, and Z. Ma, “Wireless Applications of Conformal Bioelectronics,” in *Stretchable Bioelectronics for Medical Devices and Systems*, J. A. Rogers, R. Ghaffari, and D.-H. Kim, Eds. Cham: Springer International Publishing, 2016, pp. 83–114, dOI: 10.1007/978-3-319-28694-5_5. [Online]. Available: http://link.springer.com/10.1007/978-3-319-28694-5_5

[26] D.-H. Kim, N. Lu, R. Ma, Y.-S. Kim, R.-H. Kim, S. Wang, J. Wu, S. M. Won, H. Tao, A. Islam, K. J. Yu, T.-i. Kim, R. Chowdhury, M. Ying, L. Xu, M. Li, H.-J. Chung, H. Keum, M. McCormick, P. Liu, Y.-W. Zhang, F. G. Omenetto, Y. Huang, T. Coleman, and J. A. Rogers, “Epidermal Electronics,” *Science*, vol. 333, no. 6044, pp. 838–843, Aug. 2011. [Online]. Available: http://science.sciencemag.org/content/333/6044/838

[27] S. Park, M. Vosguerichian, and Z. Bao, “A review of fabrication and applications of carbon nanotube film-based flexible electronics,” *Nanoscale*, vol. 5, no. 5, pp. 1727–1752, 2013. [Online]. Available: http://pubs.rsc.org/en/Content/ArticleLanding/2013/NR/C3NR33560G

[28] M. Magno, C. Spagnol, L. Benini, and E. Popovici, “A low power wireless node for contact and contactless heart monitoring,” *Microelectronics Journal*, vol. 45, no. 12, pp. 1656–1664, Dec. 2014. [Online]. Available: http://www.sciencedirect.com/science/

article/pii/S0026269214002213

[29] C. Medina, J. C. Segura, and Á. De la Torre, "Ultrasound Indoor Positioning System Based on a Low-Power Wireless Sensor Network Providing Sub-Centimeter Accuracy," *Sensors*, vol. 13, no. 3, pp. 3501–3526, Mar. 2013. [Online]. Available: http://www.mdpi.com/1424-8220/13/3/3501

[30] Y. J. Park, J. H. Park, H. J. Kim, H. Ryu, S. Kim, Y. Pu, K. C. Hwang, Y. Yang, M. Lee, and K. Y. Lee, "A Design of a 92.4% Efficiency Triple Mode Control DC #8211;DC Buck Converter With Low Power Retention Mode and Adaptive Zero Current Detector for IoT/Wearable Applications," *IEEE Transactions on Power Electronics*, vol. 32, no. 9, pp. 6946–6960, Sep. 2017.

[31] J. Park, H. Joshi, H. G. Lee, S. Kiaei, and U. Y. Ogras, "Flexible PV-cell Modeling for Energy Harvesting in Wearable IoT Applications," *ACM Trans. Embed. Comput. Syst.*, vol. 16, no. 5s, pp. 156:1–156:20, Sep. 2017. [Online]. Available: http://doi.acm.org/10.1145/3126568

[32] C. Park, P. H. Chou, Y. Bai, R. Matthews, and A. Hibbs, "An ultra-wearable, wireless, low power ECG monitoring system," in *2006 IEEE Biomedical Circuits and Systems Conference*, Nov. 2006, pp. 241–244.

[33] S.-D. Jang, B.-W. Kang, and J. Kim, "Frequency selective surface based passive wireless sensor for structural health monitoring," *Smart Materials and Structures*, vol. 22, no. 2, p. 025002, 2013. [Online]. Available: http://stacks.iop.org/0964-1726/22/i=2/a=025002

[34] D. J. Lipomi, B. C.-K. Tee, M. Vosgueritchian, and Z. Bao, "Stretchable Organic Solar Cells," *Advanced Materials*, vol. 23, no. 15, pp. 1771–1775, Apr. 2011. [Online]. Available: http://onlinelibrary.wiley.com/doi/10.1002/adma.201004426/abstract

[35] M. W. Woo, J. Lee, and K. Park, "A reliable IoT system for Personal Healthcare Devices," *Future Generation Computer Systems*, vol. 78, no. Part 2, pp. 626–640, Jan. 2018. [Online]. Available: http://www.sciencedirect.com/science/article/pii/S0167739X17305423

[36] S. K. Sood and I. Mahajan, "Wearable IoT sensor based healthcare system for identifying and controlling chikungunya virus," *Computers in Industry*, vol. 91, no. Supplement C, pp.

33–44, Oct. 2017. [Online]. Available: http://www.sciencedirect.com/science/article/pii/S0166361516303190

[37] C. Doukas and I. Maglogiannis, "Bringing IoT and Cloud Computing towards Pervasive Healthcare," in *2012 Sixth International Conference on Innovative Mobile and Internet Services in Ubiquitous Computing*, Jul. 2012, pp. 922–926.

[38] S. Amendola, R. Lodato, S. Manzari, C. Occhiuzzi, and G. Marrocco, "RFID Technology for IoT-Based Personal Healthcare in Smart Spaces," *IEEE Internet of Things Journal*, vol. 1, no. 2, pp. 144–152, Apr. 2014.

[39] E. D'Atri, C. M. Medaglia, A. Serbanati, U. B. Ceipidor, E. Panizzi, and A. D'Atri, "A system to aid blind people in the mobility: A usability test and its results," in *Second International Conference on Systems, 2007. ICONS '07*, Apr. 2007, pp. 35–35.

[40] M. Jung, J. Kim, J. Noh, N. Lim, C. Lim, G. Lee, J. Kim, H. Kang, K. Jung, A. D. Leonard, J. M. Tour, and G. Cho, "All-Printed and Roll-to-Roll-Printable 13.56-MHz-Operated 1-bit RF Tag on Plastic Foils," *IEEE Transactions on Electron Devices*, vol. 57, no. 3, pp. 571–580, Mar. 2010.

[41] T. Kellomaki, "On-Body Performance of a Wearable Single-Layer RFID Tag," *IEEE Antennas and Wireless Propagation Letters*, vol. 11, pp. 73–76, 2012.

[42] G. Marrocco, "Pervasive electromagnetics: sensing paradigms by passive RFID technology," *IEEE Wireless Communications*, vol. 17, no. 6, pp. 10–17, Dec. 2010.

[43] L. N. Allen and G. P. Christie, "The Emergence of Personalized Health Technology," *Journal of Medical Internet Research*, vol. 18, no. 5, May 2016. [Online]. Available: https://www.ncbi.nlm.nih.gov/pmc/articles/PMC4890734/

[44] S. Alzahrani, A. Giadedi, R. Lamberth, T. Lilja, O. Mbagwu, and E. Velez, "Wearable Technology: Diabetes Monitoring in the Healthcare Industry," *Engineering and Technology Management Student Projects*, Oct. 2016. [Online]. Available: http://pdxscholar.library.pdx.edu/etm_studentprojects/37

[45] R. R. Fletcher, M. Z. Poh, and H. Eydgahi, "Wearable sensors: Opportunities and challenges for low-cost health care," in *2010 Annual International Conference of the IEEE Engineering in Medicine and Biology*, 2010, pp. 1763–1766.

[46] S. Milici, J. Lorenzo, A. Làzaro, R. Villarino, and D. Girbau, "Wireless breathing sensor based on wearable modulated frequency selective surface," *EEE Sensors Journal*, vol. 17, no. 5, pp. 1285–1292, 2017.

[47] S. S. Intille, "A new research challenge: persuasive technology to motivate healthy aging," *IEEE Transactions on Information Technology in Biomedicine*, vol. 8, no. 3, pp. 235–237, Sep. 2004.

[48] A. Pantelopoulos and N. G. Bourbakis, "A Survey on Wearable Sensor-Based Systems for Health Monitoring and Prognosis," *IEEE Transactions on Systems, Man, and Cybernetics, Part C (Applications and Reviews)*, vol. 40, no. 1, pp. 1–12, Jan. 2010.

[49] ——, "A Survey on Wearable Sensor-Based Systems for Health Monitoring and Prognosis," *IEEE Transactions on Systems, Man, and Cybernetics, Part C (Applications and Reviews)*, vol. 40, no. 1, pp. 1–12, Jan. 2010.

[50] "Purchase | Wireless Temperature Monitoring System| TempTraq | TempTraq." [Online]. Available: https://www.temptraq.com/purchase

[51] "VivaLNK | Fever Monitor." [Online]. Available: http://www.vivalnk.com/fever-monitor/

[52] [Online]. Available: https://www.media.mit.edu/galvactivator/faq.html

[53] P. Kassal, J. Kim, R. Kumar, W. R. de Araujo, I. M. Steinberg, M. D. Steinberg, and J. Wang, "Smart bandage with wireless connectivity for uric acid biosensing as an indicator of wound status," *Electrochemistry Communications*, vol. 56, pp. 6–10, Jul. 2015. [Online]. Available: http://www.sciencedirect.com/science/article/pii/S1388248115000946

[54] "Wearable GSR Sensor | Shimmer Galvanic Skin Response Sensor | EDA sensor." [Online]. Available: http://www.shimmersensing.com/products/shimmer3-wireless-gsr-sensor

[55] "Prana Tech |." [Online]. Available: http://prana.co/

[56] "Apparatus." [Online]. Available: http://alumni.media.mit.edu/~carsonr/phd_thesis/ch03s03.html

[57] "E-TRACES, memories of dance - lesiatrubat." [Online]. Available: http://cargocollective.com/lesiatrubat/E-TRACES-memories-of-dance

[58] C. D. Katsis, N. Katertsidis, G. Ganiatsas, and D. I. Fotiadis, "Toward Emotion Recognition in Car-Racing Drivers: A Biosignal Processing Approach," *IEEE Transactions on Systems, Man, and Cybernetics - Part A: Systems and Humans*, vol. 38, no. 3, pp. 502–512, 2008.

[59] "#CES2016: De sensores para entrenamiento deportivo y zapatos inteligentes." [Online]. Available: https://www.unocero.com/coberturas/international_ces/ces2016-de-sensores-para-entrenamiento-deportivo-y-zapatos-inteligentes/

[60] S. F. Vissing, U. Scherrer, and R. G. Victor, "Stimulation of skin sympathetic nerve discharge by central command. Differential control of sympathetic outflow to skin and skeletal muscle during static exercise." *Circulation Research*, vol. 69, no. 1, pp. 228–238, Jul. 1991. [Online]. Available: http://circres.ahajournals.org/content/69/1/228

[61] F. Adib, H. Mao, Z. Kabelac, D. Katabi, and R. C. Miller, "Smart Homes That Monitor Breathing and Heart Rate," in *Proceedings of the 33rd Annual ACM Conference on Human Factors in Computing Systems*, ser. CHI '15. New York, NY, USA: ACM, 2015, pp. 837–846. [Online]. Available: http://doi.acm.org/10.1145/2702123.2702200

[62] A. Bates, M. J. Ling, J. Mann, and D. K. Arvind, "Respiratory Rate and Flow Waveform Estimation from Tri-axial Accelerometer Data," in *2010 International Conference on Body Sensor Networks*, Jun. 2010, pp. 144–150.

[63] A. M. Chan, N. Selvaraj, N. Ferdosi, and R. Narasimhan, "Wireless patch sensor for remote monitoring of heart rate, respiration, activity, and falls," *Conference proceedings: ... Annual International Conference of the IEEE Engineering in Medicine and Biology Society. IEEE Engineering in Medicine and Biology Society. Annual Conference*, vol. 2013, pp. 6115–6118, 2013.

[64] T. Elfaramawy, C. L. Fall, M. Morissette, F. Lellouche, and B. Gosselin, "Wireless respiratory monitoring and coughing detection using a wearable patch sensor network," in *2017 15th IEEE International New Circuits and Systems Conference (NEWCAS)*, Jun. 2017, pp. 197–200.

[65] A. R. Fekr, K. Radecka, and Z. Zilic, "Design and Evaluation of an Intelligent Remote Tidal Volume Variability Monitoring System in

E-Health Applications," *IEEE Journal of Biomedical and Health Informatics*, vol. 19, no. 5, pp. 1532–1548, Sep. 2015.

[66] J. F. Masa, M. Rubio, and L. J. Findley, "Habitually Sleepy Drivers Have a High Frequency of Automobile Crashes Associated with Respiratory Disorders during Sleep," *American Journal of Respiratory and Critical Care Medicine*, vol. 162, no. 4, pp. 1407–1412, 2000. [Online]. Available: http://www.atsjournals.org/doi/abs/10.1164/ajrccm.162.4.9907019

[67] S. Milici, J. Lorenzo, A. Lázaro, R. Villarino, and D. Girbau, "Wireless Breathing Sensor Based on Wearable Modulated Frequency Selective Surface," *IEEE Sensors Journal*, vol. 17, no. 5, pp. 1285–1292, Mar. 2017.

[68] S. Manzari, C. Occhiuzzi, and G. Marrocco, "Feasibility of Body-Centric Systems Using Passive Textile RFID Tags," *IEEE Antennas and Propagation Magazine*, vol. 54, no. 4, pp. 49–62, Aug. 2012.

[69] M.-C. Tsai, C.-W. Chiu, H.-C. Wang, and T.-F. Wu, "Inductively Coupled Loop Antenna Design for UHF RFID on - Body Applications," *Progress In Electromagnetics Research*, vol. 143, pp. 315–330, 2013. [Online]. Available: http://www.jpier.org/PIER/pier.php?paper=13080707

[70] D. M. Dobkin, *The RF in RFID: passive UHF RFID in Practice*, ELviser, Ed. Elviser, 2007.

[71] C. Occhiuzzi and G. Marrocco, "Precision and accuracy in uhf-rfid power measurements for passive sensing," vol. PP, no. 99, 2016.

[72] [Online]. Available: Available:EM4325,http://www.emmicroelectronic.com/products/rf-identification-security/epc-and-uhf-ics/em4325

[73] [Online]. Available: [Online].Available:SL900Achip,http://ams.com/eng/Products/UHF-RFID/UHF-Interface-and-Sensor-Tag/SL900A

[74] [Online]. Available: Available:ANDY100RFIDIC,http://www.farsens.com/en/products/andy100/

[75] [Online]. Available: [Online].Available:BlueSparkTechnologies, http://www.bluesparktechnologies.com/

[76] [Online]. Available: [Online].Available: FlexibleLithium-ionBatterybyPanasonic,http://news.panasonic.com/global/press/data/2016/09/en160929-8/en160929-8.html

[77] G. Marrocco, "RFID Antennas for the UHF Remote Monitoring of Human Subjects," *IEEE Transactions on Antennas and Propagation*, vol. 55, no. 6, pp. 1862–1870, Jun. 2007.

[78] S. Manzari, S. Pettinari, and G. Marrocco, "Miniaturised wearable UHF-RFID tag with tuning capability," *Electronics Letters*, vol. 48, no. 21, pp. 1325–1326, Oct. 2012.

[79] Z.-M. Huang, Y. Z. Zhang, M. Kotaki, and S. Ramakrishna, "A review on polymer nanofibers by electrospinning and their applications in nanocomposites," *Composites Science and Technology*, vol. 63, no. 15, pp. 2223–2253, Nov. 2003. [Online]. Available: http://www.sciencedirect.com/science/article/pii/S0266353803001787

[80] P. V. Nikitin and K. V. S. Rao, "Theory and measurement of backscattering from RFID tags," *IEEE Antennas and Propagation Magazine*, vol. 48, no. 6, pp. 212–218, Dec. 2006.

[81] N. Mehmood, A. Hariz, S. Templeton, and N. H. Voelcker, "An improved flexible telemetry system to autonomously monitor sub-bandage pressure and wound moisture," *Sensors (Basel, Switzerland)*, vol. 14, no. 11, pp. 21 770–21 790, Nov. 2014.

[82] X. Huang, Y. Liu, G. W. Kong, J. H. Seo, Y. Ma, K.-I. Jang, J. A. Fan, S. Mao, Q. Chen, D. Li, H. Liu, C. Wang, D. Patnaik, L. Tian, G. A. Salvatore, X. Feng, Z. Ma, Y. Huang, and J. A. Rogers, "Epidermal radio frequency electronics for wireless power transfer," *Microsystems & Nanoengineering*, vol. 2, p. 16052, Oct. 2016. [Online]. Available: https://www.nature.com/articles/micronano201652

[83] I. Ha, "Technologies and Research Trends in Wireless Body Area Networks for Healthcare: A Systematic Literature Review," *International Journal of Distributed Sensor Networks*, vol. 11, no. 6, p. 573538, Jun. 2015. [Online]. Available: https://doi.org/10.1155/2015/573538

[84] C. Occhiuzzi, S. Caizzone, and G. Marrocco, "Passive UHF RFID antennas for sensing applications: Principles, methods, and classifcations," *IEEE Antennas and Propagation Magazine*, vol. 55, no. 6, pp. 14–34, Dec. 2013.

[85] J. Kim, A. Banks, H. Cheng, Z. Xie, S. Xu, K.-I. Jang, J. W. Lee, Z. Liu, P. Gutruf, X. Huang, P. Wei, F. Liu, K. Li, M. Dalal, R. Ghaffari, X. Feng, Y. Huang, S. Gupta,

U. Paik, and J. A. Rogers, “Epidermal Electronics with Advanced Capabilities in Near-Field Communication,” *Small*, vol. 11, no. 8, pp. 906–912, Feb. 2015. [Online]. Available: http://onlinelibrary.wiley.com/doi/10.1002/smll.201402495/abstract

[86] D. P. Rose, M. E. Ratterman, D. K. Griffin, L. Hou, N. Kelley-Loughnane, R. R. Naik, J. A. Hagen, I. Papautsky, and J. C. Heikenfeld, “Adhesive RFID Sensor Patch for Monitoring of Sweat Electrolytes,” *IEEE Transactions on Biomedical Engineering*, vol. 62, no. 6, pp. 1457–1465, Jun. 2015.

[87] P. V. Nikitin, K. V. S. Rao, S. F. Lam, V. Pillai, R. Martinez, and H. Heinrich, “Power reflection coefficient analysis for complex impedances in RFID tag design,” *IEEE Transactions on Microwave Theory and Techniques*, vol. 53, no. 9, pp. 2721–2725, Sep. 2005.

[88] G. A. Conway and W. G. Scanlon, “Antennas for Over-Body-Surface Communication at 2.45 GHz,” *IEEE Transactions on Antennas and Propagation*, vol. 57, no. 4, pp. 844–855, Apr. 2009.

[89] A. Haj-Omar, W. L. Thompson, Y. S. Kim, and T. P. Coleman, “Adaptive flexible antennas for wireless biomedical applications,” in *2016 IEEE 17th Annual Wireless and Microwave Technology Conference (WAMICON)*, Apr. 2016, pp. 1–3.

[90] A. Lazaro, A. Ramos, D. Girbau, and R. Villarino, “A Novel UWB RFID Tag Using Active Frequency Selective Surface,” *IEEE Transactions on Antennas and Propagation*, vol. 61, no. 3, pp. 1155–1165, Mar. 2013.

[91] B. A. Munk, “General Overview,” in *Frequency Selective Surfaces*. John Wiley & Sons, Inc., 2000, pp. 1–25, dOI: 10.1002/0471723770.ch1. [Online]. Available: http://onlinelibrary.wiley.com/doi/10.1002/0471723770.ch1/summary

[92] ——, “Band-Pass Filter Designs: The Hybrid Radome,” in *Frequency Selective Surfaces*. John Wiley & Sons, Inc., 2000, pp. 227–278, dOI: 10.1002/0471723770.ch7. [Online]. Available: http://onlinelibrary.wiley.com/doi/10.1002/0471723770.ch7/summary

[93] ——, “References,” in *Frequency Selective Surfaces*. John Wiley & Sons, Inc., 2000, pp. 401–404, dOI: 10.1002/0471723770.refs. [Online]. Available: http://onlinelibrary.wiley.com/doi/10.1002/0471723770.refs/summary

[94] B. Sanz-Izquierdo, E. A. Parker, J.-B. Robertson, and J. C. Batchelor, “Tuning technique for active FSS arrays,” *Electronics*

Letters, vol. 45, no. 22, pp. 1107–1109, Oct. 2009. [Online]. Available: http://digital-library.theiet.org/content/journals/10.1049/el.2009.2264

[95] T. K. Chang, R. J. Langley, and E. A. Parker, "Active frequency-selective surfaces," *IEE Proceedings - Microwaves, Antennas and Propagation*, vol. 143, no. 1, pp. 62–66, Feb. 1996. [Online]. Available: http://digital-library.theiet.org/content/journals/10.1049/ip-map_19960115

[96] G. I. Kiani, T. S. Bird, and K. L. Ford, "60 GHz ASK modulator using switchable FSS," in *2010 IEEE Antennas and Propagation Society International Symposium*, Jul. 2010, pp. 1–4.

[97] G. I. Kiani and T. S. Bird, "ASK modulator based on switchable FSS for THz applications," *Radio Science*, vol. 46, no. 02, pp. 1–8, Apr. 2011.

[98] J. Lorenzo, A. Lazaro, D. Girbau, R. Villarino, and E. Gil, "Analysis of on-Body Transponders Based on Frequency Selective Surfaces," *Progress In Electromagnetics Research*, vol. 157, pp. 133–143, 2016. [Online]. Available: http://onlinewww.jpier.org/pier/pier.php?paper=16082501

[99] A.Lazaro, J.Lorenzo, R.Villarino, and D.Girbau, "Backscatter Transponder Based on Frequency Selective Surface for FMCW Radar Applications," *Radioengineering*, vol. 23, no. 2, pp. 632–641, Jan. 2014.

[100] J. Lorenzo, A. Lazaro, R. Villarino, and D. Girbau, "Diversity Study of a Frequency Selective Surface Transponder for Wearable Applications," *IEEE Transactions on Antennas and Propagation*, vol. 65, no. 5, pp. 2701–2706, May 2017.

[101] J. S. Steinhart and S. R. Hart, "Calibration curves for thermistors," *Deep Sea Research and Oceanographic Abstracts*, vol. 15, no. 4, pp. 497–503, Aug. 1968. [Online]. Available: http://www.sciencedirect.com/science/article/pii/0011747168900570

[102] T. Young, M. Palta, J. Dempsey, J. Skatrud, S. Weber, and S. Badr, "The occurrence of sleep-disordered breathing among middle-aged adults," *The New England Journal of Medicine*, vol. 328, no. 17, pp. 1230–1235, Apr. 1993.

[103] J. M. Parish and V. K. Somers, "Obstructive Sleep Apnea and Cardiovascular Disease," *Mayo Clinic Proceedings*, vol. 79,

no. 8, pp. 1036–1046, Aug. 2004. [Online]. Available: http://www.sciencedirect.com/science/article/pii/S0025619611625792

[104] C. L. Bassetti, M. Milanova, and M. Gugger, "Sleep-Disordered Breathing and Acute Ischemic Stroke," *Stroke*, vol. 37, no. 4, pp. 967–972, Apr. 2006. [Online]. Available: http://stroke.ahajournals.org/content/37/4/967

[105] H. K. Yaggi and K. P. Strohl, "Adult Obstructive Sleep Apnea/Hypopnea Syndrome: Definitions, Risk Factors, and Pathogenesis," *Clinics in Chest Medicine*, vol. 31, no. 2, pp. 179–186, 2010. [Online]. Available: http://www.sciencedirect.com/science/article/pii/S0272523110000341

[106] P. Corbishley and E. Rodriguez-Villegas, "Breathing Detection: Towards a Miniaturized, Wearable, Battery-Operated Monitoring System," *IEEE Transactions on Biomedical Engineering*, vol. 55, no. 1, pp. 196–204, Jan. 2008.

[107] C. R. Merritt, H. T. Nagle, and E. Grant, "Textile-Based Capacitive Sensors for Respiration Monitoring," *IEEE Sensors Journal*, vol. 9, no. 1, pp. 71–78, Jan. 2009.

[108] L. Rabiner, R. Schafer, and C. Rader, "The chirp z-transform algorithm," *IEEE Transactions on Audio and Electroacoustics*, vol. 17, no. 2, pp. 86–92, Jun. 1969.

[109] J. Pan and W. J. Tompkins, "A Real-Time QRS Detection Algorithm," *IEEE Transactions on Biomedical Engineering*, vol. BME-32, no. 3, pp. 230–236, Mar. 1985.

[110] S. Raza, P. Misra, Z. He, and T. Voigt, "Bluetooth smart: An enabling technology for the Internet of Things," in *2015 IEEE 11th International Conference on Wireless and Mobile Computing, Networking and Communications (WiMob)*, Oct. 2015, pp. 155–162.

[111] S. Bharathi, A. Ramesh, and S. Vivek, "Effective navigation for visually impaired by wearable obstacle avoidance system," in *2012 International Conference on Computing, Electronics and Electrical Technologies (ICCEET)*, Mar. 2012, pp. 956–958.

[112] N. Constant, O. Douglas-Prawl, S. Johnson, and K. Mankodiya, "Pulse-Glasses: An unobtrusive, wearable HR monitor with Internet-of-Things functionality," in *2015 IEEE 12th International Conference on Wearable and Implantable Body Sensor Networks (BSN)*, Jun. 2015, pp. 1–5.

[113] J. Decuir, "Bluetooth Smart Support for 6lobtle: Applications

and connection questions." *IEEE Consumer Electronics Magazine*, vol. 4, no. 2, pp. 67–70, Apr. 2015.

[114] R. Kobayashi, Y. Koike, M. Hirayama, H. Ito, and G. Sobue, "Skin sympathetic nerve function during sleep—a study with effector responses," *Autonomic Neuroscience*, vol. 103, no. 1–2, pp. 121–126, 2003. [Online]. Available: http://www.sciencedirect.com/science/article/pii/S1566070202002618

[115] M. Benedek and C. Kaernbach, "A continuous measure of phasic electrodermal activity," *Journal of Neuroscience Methods*, vol. 190, no. 1, pp. 80–91, 2010. [Online]. Available: http://www.sciencedirect.com/science/article/pii/S0165027010002335

[116] N. Nourbakhsh, F. Chen, Y. Wang, and R. A. Calvo, "Detecting Users' Cognitive Load by Galvanic Skin Response with Affective Interference," *ACM Trans. Interact. Intell. Syst.*, vol. 7, no. 3, pp. 12:1–12:20, Sep. 2017. [Online]. Available: http://doi.acm.org/10.1145/2960413

[117] P. H. Venables and I. Martin, "The Relation of Palmar Sweat Gland Activity to Level of Skin Potentialand Conductance," *Psychophysiology*, vol. 3, no. 3, pp. 302–311, Jan. 1967. [Online]. Available: http://onlinelibrary.wiley.com/doi/10.1111/j.1469-8986.1967.tb02710.x/abstract

[118] A. Alberdi, A. Aztiria, and A. Basarab, "Towards an automatic early stress recognition system for office environments based on multimodal measurements: A review," *Journal of Biomedical Informatics*, vol. 59, pp. 49–75, Feb. 2016. [Online]. Available: http://www.sciencedirect.com/science/article/pii/S1532046415002750

[119] Y. Lee, B. Lee, and M. Lee, "Wearable Sensor Glove Based on Conducting Fabric Using Electrodermal Activity and Pulse-Wave Sensors for e-Health Application," *Telemedicine and e-Health*, vol. 16, no. 2, pp. 209–217, 2010. [Online]. Available: http://online.liebertpub.com/doi/abs/10.1089/tmj.2009.0039

[120] J. Choi, B. Ahmed, and R. Gutierrez-Osuna, "Development and Evaluation of an Ambulatory Stress Monitor Based on Wearable Sensors," *IEEE Transactions on Information Technology in Biomedicine*, vol. 16, no. 2, pp. 279–286, Mar. 2012.

[121] Z. T. Beattie, T. L. Hayes, C. Guilleminault, and C. C. Hagen, "Accurate scoring of the apnea–hypopnea index using a simple non-contact breathing sensor," *Journal of Sleep Research*,

vol. 22, no. 3, pp. 356–362, Jun. 2013. [Online]. Available: http://onlinelibrary.wiley.com/doi/10.1111/jsr.12023/abstract

[122] D. Shao, Y. Yang, C. Liu, F. Tsow, H. Yu, and N. Tao, "Noncontact Monitoring Breathing Pattern, Exhalation Flow Rate and Pulse Transit Time," *IEEE Transactions on Biomedical Engineering*, vol. 61, no. 11, pp. 2760–2767, Nov. 2014.

[123] H. Nakano, T. Tanigawa, T. Furukawa, and S. Nishima, "Automatic detection of sleep-disordered breathing from a single-channel airflow record," *European Respiratory Journal*, vol. 29, no. 4, pp. 728–736, Apr. 2007. [Online]. Available: http://erj.ersjournals.com/content/29/4/728

[124] C. M. Yang, T. L. Yang, C. C. Wu, S. H. Hung, M. H. Liao, M. J. Su, and H. C. Hsieh, "Textile-based capacitive sensor for a wireless wearable breath monitoring system," in *2014 IEEE International Conference on Consumer Electronics (ICCE)*, Jan. 2014, pp. 232–233.

[125] P. S. P, A. Jeelani, P. Maniyar, J. Joseph, and M. Sivaprakasam, "Accelerometer based system for continuous respiratory rate monitoring," in *2017 IEEE International Symposium on Medical Measurements and Applications (MeMeA)*, May 2017, pp. 171–176.

[126] V. Aarts, K. H. Dellimore, R. Wijshoff, R. Derkx, J. v. d. Laar, and J. Muehlsteff, "Performance of an accelerometer-based pulse presence detection approach compared to a reference sensor," in *2017 IEEE 14th International Conference on Wearable and Implantable Body Sensor Networks (BSN)*, May 2017, pp. 165–168.

[127] A. De Groote, M. Wantier, G. Cheron, M. Estenne, and M. Paiva, "Chest wall motion during tidal breathing," *Journal of Applied Physiology*, vol. 83, no. 5, pp. 1531–1537, Nov. 1997. [Online]. Available: http://www.physiology.org/doi/abs/10.1152/jappl.1997.83.5.1531

[128] B. Yu, L. Xu, and Y. Li, "Bluetooth Low Energy (BLE) based mobile electrocardiogram monitoring system," in *2012 IEEE International Conference on Information and Automation*, Jun. 2012, pp. 763–767.

[129] P. Jiang, S. Zhao, and R. Zhu, "Smart Sensing Strip Using Monolithically Integrated Flexible Flow Sensor for Noninvasively Monitoring Respiratory Flow," *Sensors (Basel, Switzerland)*,

vol. 15, no. 12, pp. 31 738–31 750, Dec. 2015. [Online]. Available: https://www.ncbi.nlm.nih.gov/pmc/articles/PMC4721800/

[130] J. Penne, C. Schaller, J. Hornegger, and T. Kuwert, "Robust real-time 3d respiratory motion detection using time-of-flight cameras," *International Journal of Computer Assisted Radiology and Surgery*, vol. 3, no. 5, pp. 427–431, Nov. 2008. [Online]. Available: https://link.springer.com/article/10.1007/s11548-008-0245-2

[131] K. S. Tan, R. Saatchi, H. Elphick, and D. Burke, "Real-time vision based respiration monitoring system," in *2010 7th International Symposium on Communication Systems, Networks Digital Signal Processing (CSNDSP 2010)*, Jul. 2010, pp. 770–774.

[132] K. Watanabe, Y. Kurihara, T. Nakamura, and H. Tanaka, "Design of a Low-Frequency Microphone for Mobile Phones and Its Application to Ubiquitous Medical and Healthcare Monitoring," *IEEE Sensors Journal*, vol. 10, no. 5, pp. 934–941, May 2010.

[133] J.-W. Yoon, Y.-S. Noh, Y.-S. Kwon, W.-K. Kim, and H.-R. Yoon, "Improvement of Dynamic Respiration Monitoring Through Sensor Fusion of Accelerometer and Gyro-sensor," *Journal of Electrical Engineering and Technology*, vol. 9, no. 1, pp. 334–343, 2014. [Online]. Available: http://www.koreascience.or.kr/article/ArticleFullRecord.jsp?cn=E1EEFQ_2014_v9n1_334

[134] A. Dementyev, S. Hodges, S. Taylor, and J. Smith, "Power consumption analysis of Bluetooth Low Energy, ZigBee and ANT sensor nodes in a cyclic sleep scenario," in *2013 IEEE International Wireless Symposium (IWS)*, Apr. 2013, pp. 1–4.

[135] T. Suzuki, H. Tanaka, S. Minami, H. Yamada, and T. Miyata, "Wearable wireless vital monitoring technology for smart health care," in *2013 7th International Symposium on Medical Information and Communication Technology (ISMICT)*, Mar. 2013, pp. 1–4.

List of Publications

Journals

1. S. Milici, J. Lorenzo, A. Lazaro, R. Villarino, and D. Girbau. Wireless Breathing Sensor Based on Wearable Modulated Frequency Selective Surface. IEEE Sensors Journal, 17(5):1285–1292, March 2017. ISSN 1530-437X, 1558-1748, 2379-9153. doi: 10.1109/JSEN.2016.26457 URL http://ieeexplore.ieee.org/document/ 7801059/.
2. S. Milici, A. Lázaro, R. Villarino, D. Girbau, and M. Magnarosa. WirelessWearable Magnetometer-Based Sensor for Sleep Quality Monitoring. IEEE Sensors Journal, 18(5):2145–2152, March 2018. ISSN 1530-437X. doi: 10.1109/JSEN.2018.2791400.
3. S. Amendola, S. Milici, and G. Marrocco. Performance of Epidermal RFID Dualloop Tag and On-Skin Retuning. IEEE Transactions on Antennas and Propagation, 63 (8):3672–3680, August 2015. ISSN 0018-926X. doi: 10.1109/TAP.2015.2441211.

Conferences

1. S. Amendola, S. Milici, G. Marrocco, and C. OCChiuzzi. On-skin tunable RFID loop tag for epidermal applications. In 2015 IEEE International Symposium on Antennas and Propagation USNC/URSI National Radio Science Meeting, pages 202–203, July 2015. doi: 10.1109/APS.2015.7304487.

2. S. Milici, A. R. L. Guillen, R. M. Villarino, and D. G. Sala. A wearable, wireless, and long lifetime device to detect sleep disorder diseases. In 2017 40th International Conference on Telecommunications and Signal Processing (TSP), pages 444–447, July 2017. doi: 10.1109/TSP.2017.8076024.
3. S. Milici, A. Lazaro, J. Lorenzo, R. Villarino, and D. Girbau. Wearable sensors based on modulated frequency selective surfaces. In 2017 47th European Microwave Conference (EuMC), pages 942–945, October 2017. doi: 10.23919/EuMC. 2017.8231001.
4. S. Milici, S. Amendola, A. Bianco, and G. Marrocco. Epidermal RFID passive sensor for body temperature measurements. In 2014 IEEE RFID Technology and Applications Conference (RFID-TA), pages 140–144, September 2014. doi: 10.1109/ RFID-TA.2014.6934216.

UNIVERSITAT
ROVIRA i VIRGILI